الجـــــــــــــــــــــمهـوريـــــة الجـــــــــــــزائـريـة الديمـــــــقـراطيـة الشـــــــــعبيـة

REPUBLIQUE ALGERIENNE DEMOCRATIQUE ET POPULAIRE

وزارة التـــــــــــــــــــــــــــعليـم العـــــــالي و البـــــــــــحث العـــــلـمـــي

Ministère de l'Enseignement Supérieur et de la Recherche Scientifique

جـــــــــــــــامعة أبي بكـــر بـلـقـايـد – تـلمســـــــــــــــان –

Université Aboubakr Belkaïd – Tlemcen –
Faculté de TECHNOLOGIE

THESE

Présentée pour l'obtention du **grade** de **DOCTORAT 3ème Cycle**

En : Génie Civil

Spécialité : Matériaux en Génie Civil

Par: Hariz Samah

Sujet

Contribution to the study of mechanical strength and the thermo-diffusive effects on the durability of a cork bio-based concrete

Soutenue publiquement, le 23 / 06 /2026, devant le jury composé de :

M. BEZZAR Abdelillah	Professeur	Univ. Tlemcen	Président
M. TOUIL Brahim	MCA	Univ. Saida	Directeur de thèse
M. GHOMARI Fouad	Professeur	Univ. Tlemcen	Co- Directeur de thèse
M. MOULI Mohamed	Professeur	ENP Oran	Examinateur
M. AMZIANE Sofiane	Professeur	Univ. Clermont	Examinateur
M. TALEB Omar	MCA	Univ. Tlemcen	Examinateur
M. CHERIF Rachid	Maître de conférences	Univ. La Rochelle	Invité
M. TEDJDITI Ahmed Kamel	Maître de conférences	Univ. Strasbourg	Invité

بســـــــــم الله الرحمـن الرحيـم

﴿يَرْفَعِ اللَّهُ الَّذِينَ آمَنُوا مِنْكُمْ وَالَّذِينَ أُوتُوا الْعِلْمَ دَرَجَاتٍ﴾

سورة المجادلة، الآية 11

The Prophet Muhammad (peace be upon him) said: "Whoever treads a path in search of knowledge, Allah will make easy for him a path to Paradise." — Narrated by Muslim

" العلم مغرس كل فخر فافتخر، واحذر يفوتك فخر ذاك المغرس"

الإمام الشافعي

Praise be to Allah, by Whose grace righteous deeds are accomplished, and through Whose benevolence purposes are elevated and endeavors are perfected. Praise be to Allah Who taught by the pen, who taught mankind what they knew not, and Who made the pursuit of knowledge an act of worship and a responsibility, placing those who seek it in an exalted station.

Dedications

يا روائعَ الشعرِ حين الشعرُ يملؤنا

يا سلطانَ الحبِّ حين الحبُّ يغمرُنا

يا ظهراً، يا سنداً، يا كلَّ الهِبات

كم قلتُ إنَّ كلَّ جميلٍ آتٍ

وها قد أتى الفرحُ يا كلَّ المسرّات

كم سِرنا بين الممرّات

كم أصبْنا وأخطأنا

في دروبِ التجاربِ والأبحاث

وها نحن اليومَ نختمُ جميعَ المسيرات

يا قدَمَيَّ حين خانتني خُطُواتي

يا توازُني حين عصفتْ بي رياحُ الحياة

يا نوراً رافقَ سهري وأنارَ ظلُماتي

إليك أبي أُهدي كلَّ نجاحاتي

أبي، يا فخري، يا جنّةَ اللهِ في الأرض

والجنّةُ تحتَ أقدامِ الأمّهات

إليكِ أمّي أُهدي شهاداتي

يا يقيناً، يا دعاءً أزالَ كلَّ العثرات

يا جبر جُروحي، يا فجرَ طموحاتي

يا فؤاداً علّمني الصبرَ

وأنَّ كلَّ ما أرجوهُ بإذنِ اللهِ آتٍ

إليكما والديَّ أُهدي هذه الأبيات

إلى شقيقَيْ روحي إلياس وأيمن

Acknowledgements

The preparation of this dissertation was a transformative journey, both intellectually and personally. I am deeply grateful to Allah, and to the sincere individuals whose guidance, knowledge, and support made this work possible.

To My Esteemed Supervisors and Professors

*I extend my sincere gratitude to **Pr. Ghomari Fouad**, who served not only as a scientific mentor but also as a symbol of professionalism, guiding me through numerous challenges. His vision, patience, precise guidance, and extensive knowledge were an invaluable resource throughout this research. I also deeply thank **Dr. Touil Brahim** for his ethical conduct, scientific insight, and generous sharing of field experience, which greatly enriched this work. This research would not have reached its current level without your support.*

To the Distinguished Examination Committee

*It is my honor to express my deepest gratitude to **Pr. Bezzar Abdelillah** of Tlemcen University for kindly accepting the chairmanship of this committee and for the time and effort devoted to evaluating this work. I also extend my sincere appreciation to the esteemed members of the examination committee: **Pr. Mouli Mohamed**, ENP Oran; **Pr. Amziane Sofiane**, University of Clermont Auvergne; and **Dr. Taleb Omar**, Associate Professor at Tlemcen University. Your meticulous scientific observations and constructive contributions will have a profound impact on enhancing and developing the content of this dissertation, enriching this work. I am truly grateful for this valuable scientific contribution. I would also like to express my thanks to **Dr. Cherif Rachid**, Associate Professor at La Rochelle University, and **Dr. Tedjditi Ahmed Kamel**, Associate Professor at Strasbourg University, for accepting to evaluate this work and participate in the examination committee.*

*During my external training at the LaSIE Laboratory, I am grateful to **Pr. Aït Mokhtar Abdelkarim** for broadening my scientific perspective, and to **Dr. Cherif Rachid** for his constant guidance, support, and precise analysis, which greatly enriched this work. I also sincerely thank **Pr. Bezzar Abdellah**, Director of the EOLE Laboratory, for his continuous support, wise guidance, and facilitation of all experiments. My gratitude extends to **Pr. Azi Rachid**, **Pr. Bouhraoua Rachid Tarek**, **Pr. Selles Chaouki**, **Dr. Menni Younes**, and **Pr. Haddouch Idriss** for their exceptional support, advice, and guidance throughout this research.*

*To my laboratory colleagues, those who work silently and accomplish much. I extend special thanks to **Mr. Hannaoui Mustapha**, **Mr. Lehcel Hakim**, and Mr. **Benmostefa Houcine** for their warm welcome, continuous practical and advisory support, and generous sharing of expertise, which formed the backbone of the laboratory work and ensured the precise completion of the experiments.*

To my friends who offered moral and emotional support, shared the challenges and joys of research, and accompanied me through both difficult and rewarding moments. Thank you: Amina Harouat, Youssari Fatima, Berka Mohamed, Abdelmajid Aït Salem, Amina Belaidi, Hicham Bekhti.

To those who alleviated the pain: Pr. H. Boukli, Dr. M. A. Benmansour, Dr. I. Haddam, Dr. M. Benmansour, Dr. A. Saous, and Dr. A. Rahmouni. From the depths of my heart, you were an integral part of this journey, and its memory will never be recalled without you.

To My Family... Haven of Reassurance and Reason for Steadfastness

I owe everything to my father, whose perseverance and guidance ignited my dreams, and to my mother, whose prayers and support carried me through difficulties. To my siblings and extended family, your love and encouragement illuminated this journey.

To all mentioned above, I dedicate this dissertation, as it bears the marks of your hands, hearts, and support.

Samah Hariz

Abstract

Enhancing the mechanical and thermal performance of concrete structures has become a fundamental requirement in light of current trends emphasizing energy efficiency and carbon emission reduction in the construction sector. In this context, the present study aims to build upon previous research that investigated the mechanical and thermal properties of cork-modified concrete as a non-structural material, by developing improved bio-concrete formulations incorporating virgin cork granules, which are traditionally characterized by limited mechanical strength. The research focuses on enhancing the resistance and durability of this concrete under aggressive environments, particularly in chloride-rich marine conditions, which pose a serious threat to the integrity of steel reinforcement due to accelerated corrosion processes.

To achieve this objective, the cementitious matrix containing 450 kg/m³ of cement was reinforced with 10% finely ground limestone as a supplementary cementitious material, while the water-to-binder ratio was reduced to 0.38. Based on previous findings that indicated promising behavior when replacing 25% of the coarse aggregate with wet virgin cork, two experimental programs were designed to examine the influence of the wet-preconditioning method applied to cork aggregates. In the first program, dry cork was mixed with a quantity of water equivalent to its experimentally determined absorption capacity after two hours of immersion ($OC+HC_{2h\ AW}$). In the second program, cork granules were directly soaked in water for two hours prior to mixing ($OC+HC_{2h\ IW}$), in order to evaluate the differences between theoretical and actual water absorption and their effects on the final concrete properties.

The study investigated six concrete mixtures: reference concrete (OC); concrete with wet cork containing absorbed water ($OC+HC_{2h\ AW}$); concrete with water-immersed cork ($OC+HC_{2h\ IW}$); concrete with limestone filler (OC+F); concrete with limestone and wet cork containing absorbed water ($OC+F+HC_{2h\ AW}$); and concrete with limestone and water-immersed cork ($OC+F+HC_{2h\ IW}$).

Experimental results indicated that replacing 25% by volume of mineral aggregate with virgin cork granules, along with the addition of limestone filler, improved workability and reduced plastic viscosity. Furthermore, the dry density of the concrete decreased, ranging between 2008 and 2060 kg/m³. Although a reduction in mechanical

strength was expected due to cork incorporation, the addition of fine limestone resulted in compressive and tensile strengths comparable to those of the reference concrete, with a notable improvement observed in mixtures containing wet cork with absorbed water compared to those with immersed cork.

The results also revealed an inverse relationship between capillary absorption and porosity when limestone filler was used. Regarding chloride diffusion, higher diffusion coefficients were recorded for mixtures with wet cork containing absorbed water, whereas those with immersed cork exhibited reduced chloride diffusion rates, demonstrating superior resistance to chloride ingress and improved durability under marine exposure. The study concluded that the addition of limestone did not exert a significant influence on chloride diffusion behavior, as diffusion coefficients remained relatively close across all mixtures. This finding confirms that enhancing the durability of bio-concrete containing virgin cork primarily depends on the preconditioning method applied to the cork aggregates. Finally, these results highlight its potential for use in reinforced concrete horizontal structures exposed to aggressive conditions.

Keywords : Bio-based concrete, Virgin cork, Limestone, Mechanical properties, Diffusion coefficient, Thermo-diffusion, Microstructure, Durability.

Résumé

L'amélioration des performances mécaniques et thermiques des structures en béton est devenue une exigence fondamentale à la lumière des tendances actuelles mettant l'accent sur l'efficacité énergétique et la réduction des émissions de carbone dans le secteur de la construction. Dans ce contexte, la présente étude s'appuie sur des recherches antérieures ayant étudié les propriétés mécaniques et thermiques du béton à base de liège en tant que matériau non structurel, en développant des formulations d'éco-béton améliorées incorporant des granulats de liège vierge, traditionnellement caractérisés par une résistance mécanique limitée. La recherche se concentre sur l'amélioration de la résistance pour des applications structurel et de la durabilité de ce béton dans des environnements agressifs, notamment dans des conditions marines riches en chlorures, qui constituent une menace sérieuse pour l'intégrité des armatures en acier en raison de processus de corrosion accélérés.

Pour atteindre cet objectif, la matrice cimentaire contenant 450 kg/m³ de ciment a été renforcée avec 10 % de calcaire finement broyé en tant que matériau cimentaire supplémentaire, tandis que le rapport eau/liant a été réduit à 0,38. Sur la base des résultats antérieurs indiquant un comportement prometteur lors du remplacement de 25 % des granulats minéraux par du liège vierge humide, deux programmes expérimentaux ont été conçus pour examiner l'influence de la méthode de pré-conditionnement à l'eau appliquée aux granulats de liège. Dans le premier programme, le liège sec a été mélangé avec une quantité d'eau équivalente à sa capacité d'absorption déterminée expérimentalement après deux heures d'immersion ($OC+HC_{2h\ AW}$). Dans le second programme, les granulats de liège ont été directement immergés dans l'eau pendant deux heures avant le mélange ($OC+HC_{2h\ IW}$), afin d'évaluer les différences entre l'absorption théorique et réelle de l'eau et leurs effets sur les propriétés finales du béton.

L'étude a porté sur six mélanges de béton : béton de référence (OC) ; béton avec liège humide contenant de l'eau absorbée ($OC+HC_{2h\ AW}$) ; béton avec liège immergé dans l'eau ($OC+HC_{2h\ IW}$) ; béton avec calcaire comme filler (OC+F) ; béton avec calcaire et liège humide contenant de l'eau absorbée ($OC+F+HC_{2h\ AW}$) ; et béton avec calcaire et liège immergé dans l'eau ($OC+F+HC_{2h\ IW}$).

Les résultats expérimentaux ont indiqué que le remplacement de 25 % en volume du granulat minéral par des granulés de liège vierge, associé à l'ajout de calcaire, améliorait la maniabilité et réduisait la viscosité plastique. De plus, la densité sèche du béton a diminué, se situant entre 2008 et 2060 kg/m³. Bien qu'une réduction de la résistance mécanique ait été attendue en raison de l'incorporation du liège, l'ajout de calcaire fin a permis d'obtenir des résistances à la compression et à la traction comparables à celles du béton de référence, avec une amélioration notable pour les mélanges contenant du liège humide avec eau absorbée par rapport à ceux contenant du liège immergé.

Les résultats ont également révélé une relation inverse entre l'absorption capillaire et la porosité lorsque du calcaire était utilisé. Concernant la diffusion des chlorures, des coefficients de diffusion plus élevés ont été enregistrés pour les mélanges contenant du liège humide avec eau absorbée, tandis que ceux avec liège immergé présentaient des taux de diffusion réduits, démontrant une résistance supérieure à l'intrusion des chlorures et une durabilité améliorée en exposition marine. L'étude a conclu que l'ajout de calcaire n'exerçait pas d'influence significative sur le comportement de diffusion des chlorures, les coefficients de diffusion restant relativement proches pour tous les mélanges. Cette observation confirme que l'amélioration de la durabilité d'éco-béton contenant du liège vierge dépend principalement de la méthode de pré-conditionnement appliquée aux granulats de liège. Enfin, Les résultats obtenus ouvrent des perspectives prometteuses pour l'utilisation de ce type de matériau dans la construction de structures horizontales en béton armé exposées à des milieux agressifs.

Mots-clés : Béton biosourcé, Liège vierge, Calcaire, Propriétés mécaniques, Coefficient de diffusion, Thermo diffusion, Microstructure, Durabilité.

الملخص

أصبح تحسين الأداء الميكانيكي والحراري للهياكل الخرسانية متطلبًا أساسيًا في ضوء التوجهات الحالية التي تركز على كفاءة الطاقة وتقليل انبعاثات الكربون في قطاع البناء. في هذا السياق، وبناء على الأبحاث السابقة التي تناولت الخصائص الميكانيكية والحرارية للخرسانة المعدلة بالفلين كمادة غير هيكلية، من خلال تطوير صيغ محسنة للخرسانة الحيوية تحتوي على حبيبات الفلين الطبيعي الخام، والتي تتميز تقليديًا بقدرة ميكانيكية محدودة. يركز البحث على تعزيز مقاومة هذه الخرسانة وديمومتها في البيئات العدوانية، خصوصًا في الظروف البحرية الغنية بالكلوريد، والتي تشكل تهديدًا خطيرًا لسلامة التسليح الفولاذي نتيجة عمليات التآكل المتسارعة.

لتحقيق هذا الهدف، تم تعزيز المصفوفة الأسمنتية—التي تحتوي على 450 كجم/م^3 من الأسمنت—بإضافة 10٪ من الحجر الجيري المطحون ناعمًا كمادة مساعدة، بينما تم تقليل نسبة الماء إلى الرابط إلى 0.38. بناءً على النتائج السابقة التي أظهرت سلوكًا واعدًا عند استبدال 25٪ من الركام الخشن بالفلين الرطب، تم تصميم برنامجين تجريبيين لدراسة تأثير طريقة التحضير المسبق للفلين بالماء. في البرنامج الأول، تم خلط الفلين الجاف بكمية ماء تعادل قدرته التجريبية على الامتصاص بعد ساعتين من الغمر(OC+HC $_{2h\ AW}$) . أما في البرنامج الثاني، فقد تم نقع حبيبات الفلين مباشرة في الماء لمدة ساعتين قبل الخلط(OC+HC $_{2h\ IW}$) ، لتقييم الفروقات بين الامتصاص النظري والفعلي وتأثيرها على خصائص الخرسانة النهائية.

شملت الدراسة ستة خلائط خرسانية: الخرسانة المرجعية(OC) ؛ خرسانة الفلين الرطب مع الماء الممتص من طرف الفلين خلال ساعتين من الزمن (OC+HC $_{2h\ AW}$)، خرسانة الفلين المنقوع في الماء(OC+HC $_{2h\ IW}$) لمدة ساعتين، خرسانة مع الحجر الجيري كمضاف(OC+F) ؛ خرسانة مع الحجر الجيري والفلين الرطب مع الماء الممتص(OC+F+HC $_{2h\ AW}$) ، وخرسانة مع الحجر الجيري والفلين المنقوع في الماء OC+F+HC $_{2h\ IW}$) .

أظهرت النتائج التجريبية أن استبدال 25٪ من الركام المعدني بحبيبات الفلين الخام، مع إضافة الحجر الجيري، حسّن قابلية التشغيل وقلل اللزوجة البلاستيكية. كما انخفضت الكثافة الجافة للخرسانة لتتراوح بين 2008 و2060 كجم/م^3. وعلى الرغم من توقع انخفاض القوة الميكانيكية بسبب إدخال الفلين، فإن إضافة الحجر الجيري الناعم حققت مقاومة ضغط وشد مشابهة للخرسانة المرجعية، مع تحسن ملحوظ للخلائط التي تحتوي على الفلين الرطب مع الماء الممتص مقارنة بالفلين المنقوع.

كما أظهرت النتائج علاقة عكسية بين الامتصاص الشعري والمسامية عند استخدام الحجر الجيري. فيما يتعلق بانتشار الكلوريد، سجلت الخلائط التي تحتوي على الفلين الرطب مع الماء الممتص معاملات انتشار أعلى، في حين أظهرت الخلائط بالفلين المنقوع معدلات انتشار أقل، مما يدل على مقاومة أعلى لاختراق الكلوريد وتحسن الديمومة تحت التعرض البحري. واستنتجت الدراسة أن إضافة الحجر الجيري لم تؤثر بشكل كبير على سلوك انتشار الكلوريد، حيث بقيت معاملات الانتشار متقاربة نسبيًا بين جميع الخلائط. هذا يؤكد أن تعزيز ديمومة الخرسانة الحيوية المحتوية على الفلين الخام يعتمد أساسًا على طريقة التحضير المسبق للفلين. تُبرز هذه النتائج إمكانات استخدام هذا النوع من الخرسانة في الهياكل الأفقية من الخرسانة المسلحة المعرضة لظروف قاسية

الكلمات المفتاحية :الخرسانة الحيوية، الفلين الخام، الحجر الجيري، الخصائص الميكانيكية، معامل الانتشار، الانتشار الحراري، البنية المجهرية، الديمومة.

Table of Contents

Acknowledgements……...…… III

Abstract……. V

Résumé…….……. VII

الملخص…… IX

Table of Contents…….…… XI

List of Figures……... XV

List of Tables……. XIX

Nomenclature……...……. XX

General Introduction……. 1

Chapter 1: The Impact of Concrete Buildings on the Environment……...…. 4

1.1. Concrete as a Building Material…… 5

1.1.1. Historical Development and Technical Characteristics…….…. 5

1.1.2. Advancements in Concrete Technology……. 7

1.1.3. Challenges and Emerging Trends in the Concrete Industry…… 8

1.2. Environmental Impact of Concrete Production……. 9

1.2.1. Carbon Emissions in Cement Production……... 9

1.2.2. Water Usage and Pollution in Concrete Production…… 11

1.2.3. Air Pollution from Concrete Production……. 12

1.2.4. Solid Waste Generation and Management…….…. 13

1.2.5. Energy Efficiency and Thermal Performance of Concrete Buildings… 14

1.3. Environmental Performance of Concrete Structures……. 16

1.3.1. Environmental Impact of Concrete Structures…… 17

1.3.2. Strategies for Enhancing the Environmental Performance of Concrete Structures……...…... 18

1.4. Innovations in Sustainable Concrete Production……... 19

1.4.1. Alternative Binders……. 20

1.4.2. Recycled Aggregates……... 22

1.4.3. Carbon Capture and Storage……... 24

1.4.4. Renewable Energy and Materials……... 25

1.5. Conclusion……. 26

Chapter 2: Innovative Building Materials: Virgin Cork Concrete as a Structural Material…… 27

2.1. Green Concrete and Natural Plant-Based Additives……...…... 28

2.1.1. Diverse Plant-Based Materials in Concrete Enhancement……. 29
2.2. A Comprehensive Overview of Cork as a Material……... 33
2.2.1. Geographical Distribution……... 33
2.2.2. Cork Oak Forests in Algeria……... 37
2.2.3. Environmental Characteristics of Cork Oak Forests in Algeria…….…. 38
2.2.4. Cork Growth and Productivity in Algeria……... 39
2.2.5. Anatomical Structure…….…. 40
2.2.6. Morphological Characterization……. 42
2.2.7. Chemical Properties…… 44
2.2.8. Physical Properties…….…. 45
2.2.9. Mechanical Properties……. 46
2.2.10. Thermal Insulation and Fire Resistance…….…... 46
2.2.11. Hygroscopic Properties and Porosity…… 47
2.3. Cork Concrete: Composite Material Properties……. 48
2.4. Lime concrete: a versatile Building Material…….…. 54
2.5. Conclusion……. 56
Chapter 3: Characterization of Raw Materials and Experimental Methods… 57
3.1. Experimental study presentation…… 58
3.2. Materials…….……... 59
3.2.1. Cement…… 60
3.2.2. Limestone……..... 60
3.2.3. Mineral Aggregates……. 61
3.2.4. Virgin Cork Aggregate…… 62
3.2.5. Water……... 63
3.2.6. Superplasticizer……... 63
3.3. Mechanical Processing and Preparation…… 64
3.3.1. The particle size classification of virgin cork……. 65
3.3.2. Characterization of virgin cork: Density and absorption…… 66
3.3.3. Assessment of Virgin Cork Absorption Properties……. 68
3.4. Methodology for the composition of virgin cork-based concretes…… 73
3.4.1. Mixing Procedure and Sample Preparation…… 75
3.5. Concrete Characterization Methods……... 77
3.5.1. Workability and Visual Inspection…….…. 77
3.5.2. Plastic Viscosity Analysis……... 77

3.5.3. Density…… 78
3.5.4. Mechanical Properties……. 79
3.5.5. Water Porosity Measurement…….…..… 79
3.5.6. Pore size distribution…….……. 82
3.5.7. Capillary Absorption……... 83
3.5.8. Effective Diffusion Coefficient of Chloride Ions in Concrete……..….... 85
3.5.9. Scanning Electron Microscopy (SEM) Morphological Analysis…….... 88
3.5.10. Thermogravimetric Analysis (TGA)…….…… 90
3.5.11. Thermo-Diffusive Investigation…… 92
3.5.12. Chloride–Concrete Interactions…… 93
3.6. Conclusion……. 96
Chapter 4: Comprehensive Characterization of Male Cork Concrete Performance: Analysis of Mechanical Properties and Durability……... **97**
4.1. Performance assessment of cork-based concrete: An evaluation of its effectiveness…. 98
4.2. Workability……. 100
4.3. Viscosity……. 101
4.4. Density……... 102
4.5. Compressive strength……. 103
4.6. Flexural strength…… 105
4.7. Water porosity…… 106
4.8. Capillary water absorption……. 108
4.9. Chloride diffusion coefficient…… 110
4.10. Pore size distribution……... 115
4.11. Scanning Electron Microscopy (SEM) Morphological Analysis……. 116
4.12. Thermogravimetric Analysis (TGA)…… 119
4.13. The Derivative Thermogravimetric Analysis (DTG)……... 121
4.14. Thermo-Diffusive Investigation……... 124
4.15. Chloride–Concrete Interactions……... 127
4.16. Cork Interactions with Saline Solutions……. 135
4.17. Conclusion……... 139
General Conclusion……... 140
Future Perspectives……..... 142
Bibliographical References……... 143

List of Figures

Figure. 1.1. a. Historical Development and Technical Characteristics of Concrete…… 6

Figure 1.1. b. The Innovation Path in Concrete Materials Engineering…….……. 7

Figure .1.2. Market Share Projections by 2030……...… 8

Figure. 1.3. Building materials rank first in raw material consumption……. 10

Figure. 1.4. Carbon Emissions by Source…… 11

Figure. 1.5. Water Usage in Concrete Production…… 12

Figure. 1.6. Air Pollutants from Production……. 13

Figure. 1.7. Solid Waste Generation…… 14

Figure. 1.8a. Thermal Performance (U-values) …… 15

Figure. 1.8b. Embodied Energy Comparison……. 16

Figure. 1.9. Enhance and quantify the concrete environmental efficiency…….……. 17

Figure. 1.10. CO_2 Reduction Strategies……... 19

Figure. 1.11. Alternative Binders – Strength……... 22

Figure. 1.12. Recycled Aggregate Properties…….……. 23

Figure. 1.13. Photosynthesis process in wood……. 25

Figure. 1.14a. Renewable Energy Integration……...…… 26

Figure. 1.14b. Overall Sustainability Comparison…… 26

Figure. 2.1. Annual distribution of publications (2020–2026) ……... 28

Figure. 2.2. Global Plant Resources for Sustainable Concrete…… 29

Figure. 2.3. Classification and Diversity of Natural Fiber Sources……. 30

Figure. 2.4. Vegetation Zones of Algeria for Bio-Based Construction…… 32

Figure. 2.5. Global Distribution of Cork Production in Mediterranean basin….…… 35

Figure. 2.6. Cork oak tree after bark harvesting…….……. 37

Figure. 2.7. Distribution Map of Cork Oak Trees in Algeria……... 38

Figure. 2.8. Anatomical cross-section of a young cork oak stem depicting tissues before cork is harvesting…….…… 41

Figure. 2.9. Flowchart for the Production of Industrial Cork Products…..……. 42

Figure. 2.10. SEM images depicting the three principal anatomical planes of cork tangential (a), transverse (b), and radial (c) sections……...…… 43

Figure. 2.11. Chemical Composition of Cork…….…… 45

Figure. 2.12. Workability and density of the different mixtures…….……. 51

Figure. 2.13. Initial, secondary & water absorption coefficient of concretes…….…. 52

Figure. 2.14. Mechanical properties of concretes…… 52
Figure. 2.15. Physical and mechanical properties of cork concrete: a) Workability, b) Density, c) Mercury porosity, d) Compressive strength…….…. 53
Figure. 3.1. Blaine permeabilimeter…… 61
Figure. 3.2. SEM observation of limestone (x5000 enlargement) …….…… 61
Figure. 3.3. Adjuvant used & mini-cone spread test…….... 64
Figure. 3.4. Virgin Cork Preparation…….……..... 64
Figure. 3.5. Virgin Cork Classes…….……. 65
Figure. 3.6. Granulometric curves of mineral and virgin cork granules…….……. 66
Figure. 3.7. Absolute density test (a), 24 h virgin cork absorption (b)…… 67
Figure. 3.8. Virgin Cork Water Absorption Tests…….……... 68
Figure. 3.9. Mass variation after 24 days of immersion…….……. 69
Figure. 3.10. Mass variation of the three categories of cork after immersion to saturation..... 70
Figure. 3.11. Average volume calculated from dimensional measurements……..... 71
Figure. 3.12. Schematic Representation of Volume Measurement by Water Displacement…… 72
Figure. 3.13. Longitudinal section of immersed virgin cork for internal examination……. 73
Figure. 3.14. Immersion of virgin cork in water…….……. 74
Figure. 3.15. Cork concrete mixing process…….…... 76
Figure. 3.16. Casting fresh concrete into molds…….……. 77
Figure. 3.17. Moist curing of concrete…… 77
Figure. 3.18. Concrete saw…….……. 77
Figure. 3.19. Plastic viscosity test…… 78
Figure. 3.20. Cylindrical concrete specimen for testing…….……. 80
Figure. 3.21. Vacuum saturation device…….……. 81
Figure. 3.22. Mercury porosity measurement device (LaSIE Laboratory, La Rochelle University) …….……. 82
Figure. 3.23. Experimental measurement of capillarity……... 85
Figure. 3.24. Chloride migration test……... 86
Figure. 3.25. Evolution of Chloride Penetration: Transient to Steady State…… 87
Figure. 3.26. Chemical analysis of solution samples……... 87

Figure.3.27. Scanning Electron Microscopy test (Electron Microscopy Laboratory, Tlemcen University) ……... 89
Figure.3.28. Thermogravimetric Analysis Apparatus device (LaSIE Laboratory, La Rochelle University) ……... 91
Figure.3.29. Sample Grinding for TGA……... 91
Figure. 3.30. Thermo-Diffusive Apparatus device……..…... 93
Figure.3.31. Preparation of Cork Concrete Samples for Chloride Interaction…… 94
Figure. 3.32. Specimens Storage under Controlled Temperatures……... 95
Figure.4.1. Sectioning the cylindrical sample into various portions for testing…..……. 99
Figure.4.2. Sections used to assess the homogeneity of concrete mixtures……..… 100
Figure. 4.3. Workability of the different mixtures……... 100
Figure. 4.4. Various concretes plastic viscosity…….…….……. 102
Figure. 4.5. Density of reference and virgin cork concretes…… 103
Figure. 4.6. Evaluating the compressive strength of concretes at 28 & 90 days……. 104
Figure. 4.7. Compressive strength test……. 104
Figure. 4.8. Different concrete flexural strength…….……. 105
Figure. 4.9. flexural strength analysis…….……. 105
Figure. 4.10. Water accessible porosity of the different concretes…….……. 107
Figure. 4.11. Water uptake versus to square root of time……. 108
Figure. 4.12. Mixtures initial and secondary water absorption coefficient……. 109
Figure. 4.13. Concrete cumulative chloride concentration in downstream cell……... 110
Figure. 4.14. Concrete samples before and after chloride diffusion tests…… 113
Figure. 4.15. The deterioration of the ($OC+F+HC_{2HAW}$) specimens…….……... 114
Figure. 4.16. The pore size distribution of the concrete tested…… 115
Figure. 4.17. SEM and EDS analysis for the studied concretes……..…... 118
Figure. 4.18. TGA Results Analysis Diagram…….……. 120
Figure. 4.19. DTG Results Analysis Diagram……. 121
Figure. 4.20. Cumulative chloride content in the downstream compartment of concrete at 5°C…… 125
Figure. 4.21. Total chloride accumulation within the downstream cell of concrete at 20°C …… 126
Figure. 4.22. Total chloride accumulation within the downstream cell of concrete at 50°C……..... 126
Figure. 4.23. Chloride binding isotherms of concretes at 5°C…….…….. 129

Figure. 4.24. Chloride binding isotherms of concretes at 20°C…….. 131
Figure. 4.25. Chloride binding isotherms of concretes at 50°C……..... 132
Figure. 4.26. Virgin Cork Interaction with Saline Solutions……... 135
Figure. 4.27. Alterations in cork after 40 months of immersion…….……. 138

List of Tables

Table 2.1. Comprehensive Comparison Table of Previous Studies on Cork in Construction Materials……. 50
Table 2.2. Summary of Research Findings on Limestone-Based Concrete…….…… 55
Table 3.1. Cement & limestone physical properties…… 60
Table 3.2. Cement & limestone chemical properties……... 61
Table 3.3. Physical properties of mineral aggregates…….…. 62
Table 3.4. Chemical Composition and pH of the Mixing Water (mg/L) ……..... 63
Table 3.5. Virgin Cork Physical Characteristics…….……. 67
Table 3.6. Mass evolution after 24 days of continuous immersion……. 69
Table 3.7. Mass Differences in the Three Cork Types After Immersion Until Saturation……. 70
Table 3.8. Average volume of cork samples after 30 days of immersion…… 72
Table 3.9. The composition of the concretes prepared in the experimental campaign (kg/m^3) …… 75
Table 4.1. The diffusion coefficients and the lag times for all studied concrete types… 111
Table 4.2. Chemical Composition and $CaCO_3$ Content of Concrete Mixtures……... 123
Table 4.3. Diffusion coefficients, lag times of all studied concrete mixtures…….…. 127
Table 4.4. Effect of particle size on the efficiency of chloride ion adsorption by cork... 135

Nomenclature

Abbreviations

Abbreviation	Full Name
Alt Fuels	Alternative fuels
APCOR	Portuguese Cork Association
ATG	Thermogravimetric Analysis
BIM	Building Information Modeling
$CaCO_3$	Calcium Carbonate
C&D	Construction and demolition
CCS	Carbon Capture and Storage
CH	Calcium Hydroxide / Portlandite
CIC	Calcined illite clay
CO	Carbon monoxide
CO_2	Carbon dioxide
COP	Conference of the Parties
C-S-H	Calcium Silicate Hydrate
DC	Direct Current
DSC	Differential Scanning Calorimetry
DTA	Differential Thermal Analysis
DTG	Derivative Thermogravimetric Analysis
E/B	Water-to-binder mass ratio
E/C	Water-to-cement mass ratio
ECC	Engineered cementitious composites
EDS	Energy Dispersive X-ray Spectroscopy
ENG	National Aggregates Company
EOLE	Water and Structures in their Environment Laboratory
EPDs	Standardize Environmental Product Declarations

Abbreviation	Full Name
EPS	Expanded polystyrene / Extracellular polymeric substances
FA	Fly ash
GDP	Gross Domestic Product
Geo-MK	Geopolymer concrete
GGBS	Ground granulated blast-furnace slag
GWP	Global Warming Potential
ICF	Insulated concrete form walls
IEA	International Energy Agency
ITZ	Interfacial Transition Zone
LC	Limestone concrete
LC^3	Limestone-calcined-clay
LCA	Life Cycle Assessment
LP	Limestone powder
MBV	Moisture Buffer Value
MEB (E)	(Environmental) Scanning Electron Microscope
MIP	Mercury Intrusion Porosimetry
NAC	National Aggregates Company
NMR	Nuclear Magnetic Resonance
NO_x	Nitrogen oxides
PAHs	Polycyclic aromatic hydrocarbons
PCE	Polycarboxylate ether
PM_{10}	Fine particulate matter
PSE	Plunger Sand Equivalent
RCC	Raw cork concrete
RCP	Recycled concrete powder
RHA	Rice husk ash
SCC	Self-compacting concrete

Abbreviation	Full Name
SCMs	Supplementary cementitious materials
SCIBS	Béni Saf Cement Company
SEM	Scanning Electron Microscopy
SO_2	Sulfur dioxide
SS	Silica sand
TGA	Thermogravimetric analysis
THz	Terahertz Spectroscopy and Imaging
UHPC	Ultra-high performance concrete
VOCs	Volatile organic compounds
VSE	Visual Sand Equivalent
WB	Bound water
XPS	Extruded polystyrene

Latin Letters

Symbol	Physical Meaning	Unit
A	Sample surface area	m^2
Ab_{24h}	24-hour absorption	%
Ab_t	Absorption coefficient at time t	%
C	Concentration of chloride ions per unit volume	mol/l
$CaCO_3$	Calcium carbonate	-
CaO	Calcium oxide	-

Symbol	Physical Meaning	Unit
C_b	Bound chloride concentration per unit mass of material	g(Cl^-)/g concrete
C_0	Initial chloride concentration in concrete or upstream	mol/l
CCl^-	Concentration of free chlorides in solution	mol/l
$C_{Cl^-, upstream}$	Chloride concentration upstream	mol/l
C_f	Equilibrium chloride concentration	-
C_{Total}	Total chloride concentration in material	mol/g material
D_e	Effective diffusion coefficient	$m^2 \cdot s^{-1}$
D_{eff}	The effective diffusion coefficient	$m^2 \cdot s^{-1}$
E	Electric field	V/m
E_a	Activation energy	J/mol
F	Faraday constant	J/(V·mol)
J_e	Flux of chloride ions	mol/(m^2·s)
i	Current Density	(A/m^2)
L	Sample length	M
L_{dc}	Mass loss due to decarbonation of calcite	(%)

Symbol	Physical Meaning	Unit
L_{dh}	Mass loss due to dehydration of the hydrates	(%)
L_{dx}	Mass loss due to dehydroxylation of calcium hydroxide	(%)
M	Sample mass	kg
M_{air}	Mass of sample in air	G
M_d	Dry mass of sample	G
M_{eau}	Mass of sample in water	G
M_t	Wet mass at time t	G
P	Porosity	%
U	Voltage across the sample	V
R	Molar gas constant	$J \cdot K^{-1} \cdot mol^{-1}$
R	Measured Resistance	Ω
S	Cross-sectional area	m^2
t_0	Reference time	S
T	Absolute temperature	K
T_r	Lag time	S
V	Volume	m^3
Z	Chloride ion valency equal to 1	

Greek Letters

Symbol	Physical Meaning	Unit
α	Empirical coefficient / Retardation factor	-
β	Empirical coefficient	-
γ	Empirical coefficient	-
σ	Electrical conductivity	(S/m)
Δc	Concentration difference in downstream compartment	Mol/m^3
Δm	Mass change	G
ΔQ_{Cl}	Variation in chloride concentration in downstream compartment	Mol/m^3
Δt	Time interval required for measurement	S
ΔW	Mass Loss	mg
φ	Water porosity	M
(dφ/dx)	Electric potential gradient	(V/m)
ρ	Density	$kg \cdot m^{-3}$
ρ abs	Absolute density	kg/m^3
ρ app	Apparent density	kg/m^3
ρ s	Solid density	$kg \cdot m^{-3}$
ρ	Electrical Resistivity	Ω·m
rp	Pore radius	M

Subscripts

Subscript	Meaning
a	Apparent
cl	Chlorides
cr	Critical
diff	Diffusion
e	Effective
g	Gas
l	Liquid
mig	Migration

General Introduction

The construction industry constitutes one of the main pillars of the global economy; however, it simultaneously represents one of the largest sources of greenhouse gas emissions and a major consumer of energy and natural resources. Studies indicate that buildings constructed with conventional materials account for 30–50% of total global energy consumption and are responsible for nearly one-third of total greenhouse gas emissions during their operational life cycle. The cement industry alone contributes approximately 6% of anthropogenic greenhouse gas emissions annually, as the production of one ton of cement releases nearly one ton of carbon dioxide while consuming about two tons of raw materials such as limestone and shale.

With the continuous increase in urbanization across developing countries and the consequent rise in cement demand -which is projected to reach 4.83 billion metric tons by 2030, compared to 3.27 billion tons in 2010- the need for sustainable alternatives to conventional materials has become increasingly urgent. The 27th United Nations Climate Change Conference (COP27), held in Sharm El-Sheikh, emphasized the global commitment to limiting temperature rise to no more than 1.5°C and integrating green energy into all development sectors. This goal implies a substantial reduction in carbon emissions and the adoption of sustainable management practices for natural resources.

In recent years, research in construction materials has increasingly focused on the use of bio-based composites, recyclable by-products, and industrial wastes as sustainable alternatives to traditional materials. These biomaterials are locally available, exhibit excellent thermal and acoustic insulation properties compared to conventional materials, and significantly reduce heating and cooling energy demands in buildings, which represent nearly 40% of total energy consumption in the residential sector.

Virgin cork is among the most promising natural materials in this field. It is harvested from the outer bark of the cork oak tree without cutting it down, making it a renewable and environmentally friendly resource. The Mediterranean region encompasses approximately 2.275 million hectares of cork oak forests, with Algeria accounting for about 18% of this area. Cork possesses exceptional characteristics such as low density, excellent thermal and acoustic insulation, fire and corrosion resistance, high elasticity,

and stability under elevated temperatures. Nevertheless, its use in the construction sector remains limited, resulting in low economic value for raw cork.

Limestone, on the other hand, is a traditional and widely available material used in concrete production. It is abundant in cement plants and quarries, easy to extract, and resistant to frost and abrasion. Finely ground limestone can be used as a mineral additive in cement and concrete due to its technical, economic, and environmental advantages. It acts as a filler that improves certain mechanical properties of concrete, accelerates hydration, and promotes the formation of stable calcium carboaluminate hydrates.

This dissertation builds upon previous studies conducted in our laboratory on bio-concrete incorporating virgin cork aggregates. Preliminary results indicated that concrete containing 25% virgin cork demonstrated good homogeneity and enhanced thermal and mechanical performance, particularly when the cork aggregates were pre-soaked for two hours. Considering Algeria's extensive Mediterranean coastline of more than 1600 km and the importance of investigating chloride penetration in marine-exposed concrete structures, this research was extended to explore the effect of incorporating limestone as a reinforcement to cork-based concrete.

The main objectives of this study are to address the following questions:

- How does the addition of virgin cork, in both its dry and wet states, affect the mechanical properties and durability of concrete?
- Does combining limestone with virgin cork improve the overall performance of the concrete?
- How does the incorporation of limestone influence chloride diffusion in cork-based concrete under aggressive environmental conditions?

To answer these questions, a comprehensive experimental investigation was carried out on concrete mixtures containing 25% virgin cork aggregates (dry & wet) of graded particle sizes (0–4 mm, 4–8 mm, and 8–16 mm), supplemented with 10% limestone due to its local availability. The laboratory tests covered a range of properties, including workability, plastic viscosity, water-accessible porosity, capillary absorption, mechanical strength, and chloride diffusion.

This dissertation ultimately aims to contribute to the development of sustainable construction materials that combine technical efficiency with environmental responsibility, aligning with the principles of green construction and sustainable development.

To address the previously defined objectives of this thesis, the following structure has been adopted:

- The first chapter examines the environmental impact of concrete, highlighting technological developments, current challenges, circular economy solutions (recycling, waste valorization, recycled and bio-based materials), and future directions for sustainable concrete production.
- The second chapter presents innovative building materials and focuses on cork as a bio-based material. It examines the key properties of cork-based concrete, its potential applications, and current research aimed at enhancing its performance, exploring its use not only as an insulating material but also in structural elements for light construction projects.
- Chapter 3 provides a detailed description of the materials used (cement, aggregates, fillers, and cork) and their physicochemical characterization. It also outlines the experimental methods employed to achieve the thesis objectives, particularly for mechanical and durability assessment.
- Chapter 4 forms the core of the experimental work, focusing on the physical, rheological, mechanical, and durability properties of cork-based concrete. It concludes with a comparison to existing literature, providing a comprehensive analysis and critical discussion of the results.

The thesis ends with a general conclusion summarizing the main findings and outlining perspectives for future research.

Chapter 1

The Impact of Concrete Buildings on the Environment.

Introduction

This chapter addresses the environmental dimension of concrete in modern construction. It reviews technological developments and emerging environmental challenges, analyzes the environmental impacts of concrete production, and introduces the circular economy approach through recycling, waste valorization, and the use of recycled and bio-based materials. The chapter concludes by highlighting key challenges and future directions for sustainable concrete production.

1.1. Concrete as a Building Material

1.1.1. Historical Development and Technical Characteristics

The use of concrete as a construction material dates back to ancient civilizations (Fig.1.1a**)**, where the Egyptians, Greeks, and Romans were pioneers in developing early mixtures composed of lime, sand, and water. These primitive concretes were employed to construct durable architectural structures such as the Pyramids of Giza and the Pantheon. The modern evolution of concrete technology began in the 18th century with the discovery of Portland cement. In 1824, British craftsman Joseph Aspdin patented this material, which soon became the industrial standard for construction. From the late 19th to the early 20th century, a major advancement occurred with the emergence of reinforced concrete, an innovation attributed to the French builder François Coignet. By combining the compressive strength of concrete with the tensile strength of steel, this development revolutionized structural engineering and enabled the design of more resilient and versatile constructions. Contemporary concrete consists of cement as a binding agent, aggregates as inert fillers, water, and various chemical and mineral admixtures designed to enhance performance. Its composition can be adapted to achieve specific properties such as compressive strength, durability, workability, density, and thermal or acoustic efficiency. Concrete strength—particularly compressive strength—is a direct outcome of the continuous advancement in understanding the interaction mechanisms among its constituents and the control of its internal microstructure. Since the earliest applications of concrete, improving mechanical performance has been a central objective for researchers and engineers. This pursuit has driven the evolution of concrete formulations through enhancements in binder quality, optimization of aggregate grading, and precise control of the water-to-cement ratio.

Furthermore, progress in cement chemistry and admixture technology has significantly improved hydration reactions and densified the microstructure, resulting in enhanced strength development at both early and long ages. The incorporation of mineral admixtures and fine fillers has also played a crucial role in improving the interfacial transition zone between the cement paste and aggregates, which is widely recognized as one of the most mechanically vulnerable regions in concrete.

This gradual evolution highlights how concrete strength has become a controllable and design-oriented property rather than a mere by-product of composition, thereby

enabling its use in increasingly complex structural applications with higher performance requirements.

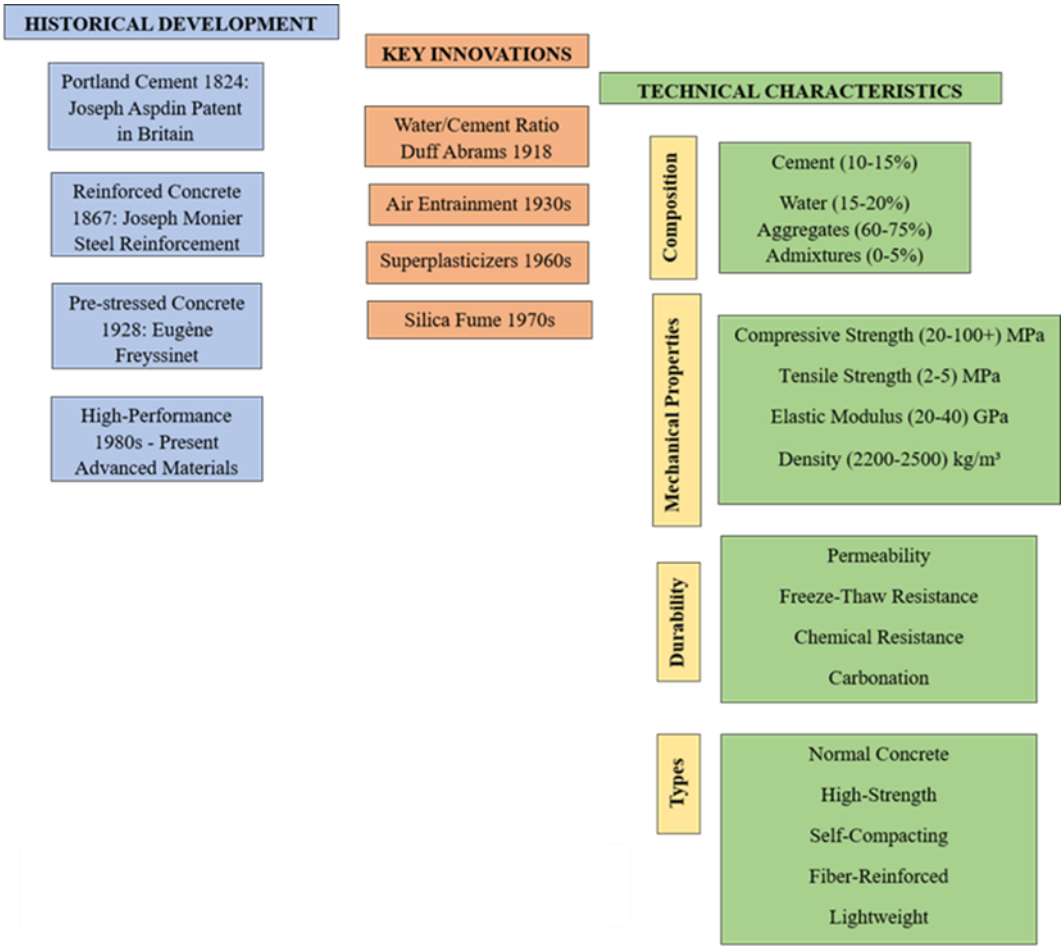


Fig. 1.1a. Historical Development and Technical Characteristics of Concrete (Portland Cement Association, 2021).

The chronological analysis in Fig.1.1b indicates a marked acceleration in the rate of innovation. Whereas the foundational phase extended over approximately 70 years, the subsequent decades have been characterized by multiple, concurrent advancements. This evolution underscores the growing integration of fundamental scientific knowledge with applied engineering practices, as well as a pronounced transition from an exclusive focus on mechanical performance toward increased consideration of sustainability and environmental efficiency in recent decades.

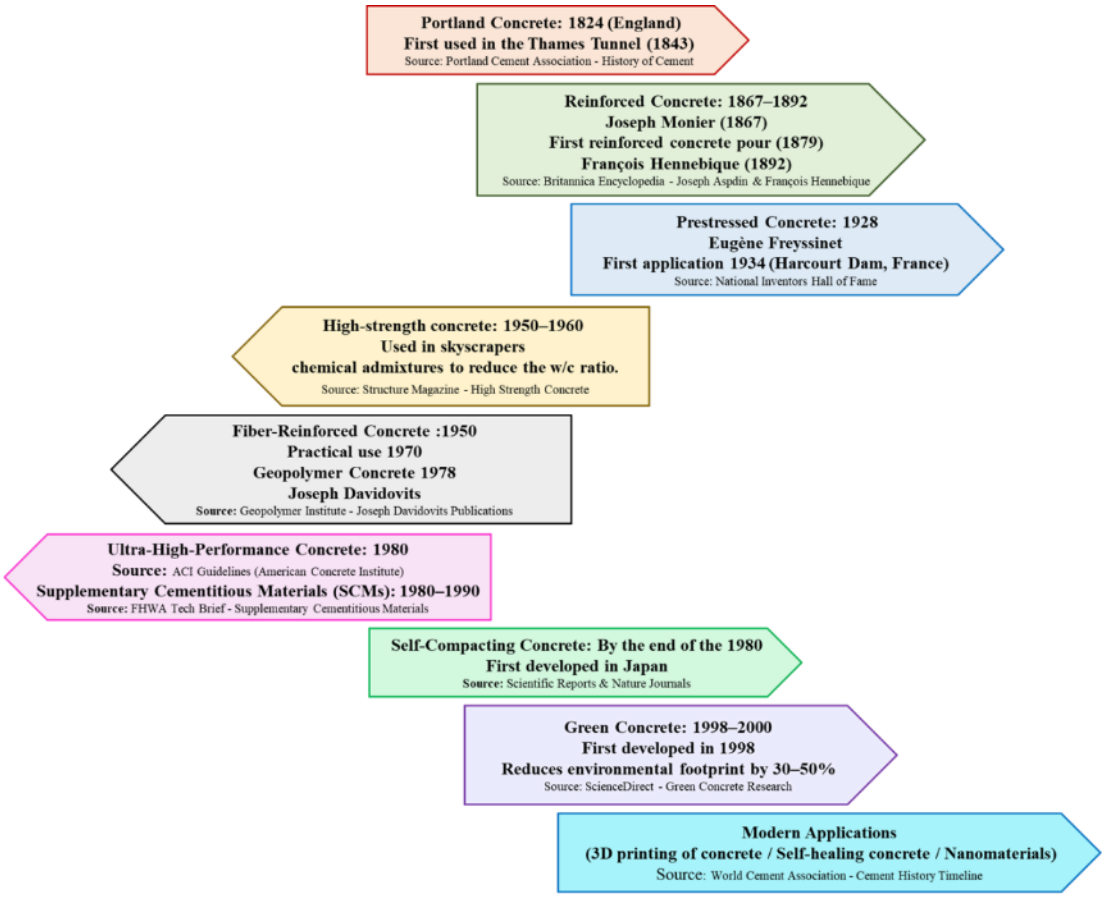


Fig. 1. 1b. The Innovation Path in Concrete Materials Engineering

Today, concrete is the most widely used construction material worldwide, with global cement consumption stabilizing at approximately 4.15 billion metric tons in 2025 (Volume Concrete, 2025; CSI, 2018). This prevalence is attributed to concrete's versatility, distinctive mechanical and physical properties, and the widespread availability of its constituent materials. These qualities make it the preferred choice for a broad spectrum of applications ranging from residential and commercial buildings to infrastructure, industrial facilities, and specialized engineering works.

1.1.2. Advancements in Concrete Technology

Concrete technology has evolved significantly in response to the growing demand for sustainable construction solutions. Key developments include the use of supplementary cementitious materials (SCMs), geopolymers, and recycled aggregates to reduce the environmental footprint of concrete. As shown in Fig. 1.2, conventional cement is projected to remain dominant by 2030 (45%), followed by blended cement (30%), while low-carbon alternatives such as carbon capture–based cement,

geopolymers, and recycled-content cement account for smaller but growing shares. This distribution reflects a gradual transition toward sustainability, constrained by challenges related to cost, standardization, supply chains, and long-term performance validation. At the same time, qualitative innovations have enhanced concrete performance through improved mechanical properties, smart functionalities, and durability, alongside environmental benefits such as pollution reduction and self-cleaning surfaces. These advancements underscore the role of continuous innovation in shaping the future of sustainable concrete technology.

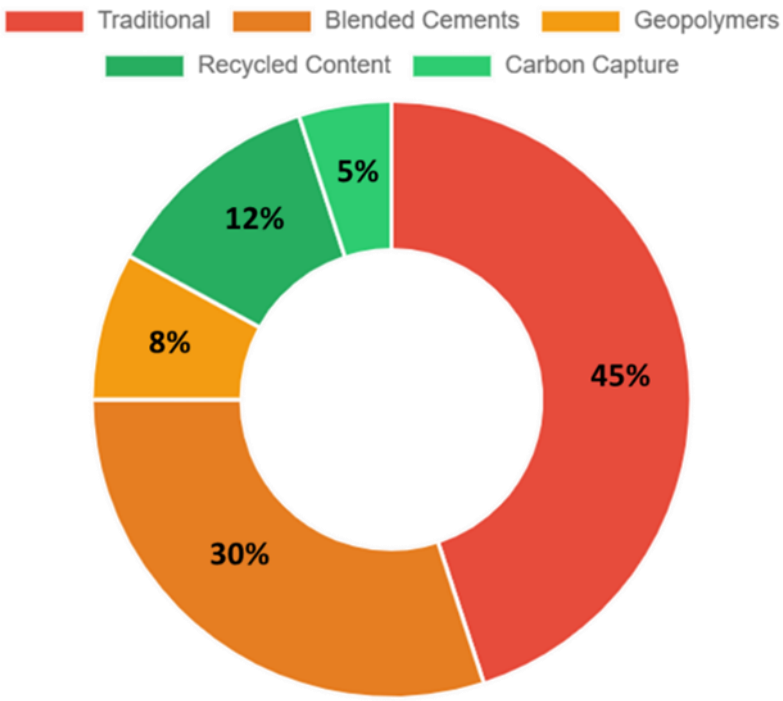


Fig .1.2. Market Share Projections by 2030

(Global Cement and Concrete Association, 2021).

1.1.3. Challenges and Emerging Trends in the Concrete Industry

Despite the significant technological progress achieved over recent decades, the concrete industry continues to face major challenges and evolving trends that will shape its future development. One of the most critical challenges is the substantial carbon footprint associated with cement production, as the cement industry remains one of the largest global contributors to greenhouse gas emissions. Addressing this issue requires the development of environmentally friendly concrete formulations through the incorporation of alternative binders and recycled materials in order to

significantly reduce the environmental impact of construction activities. In parallel, the intensive consumption of natural aggregates represents another major challenge, leading to the depletion of non-renewable natural resources. In response, recent research efforts have increasingly focused on the partial or total substitution of conventional aggregates with sustainable, bio-based materials. Within this context, the present research explores the use of cork as a bio-sourced aggregate, aiming to mitigate resource depletion while enhancing the environmental performance of concrete. The industry is also striving to enhance energy efficiency and reduce environmental impact throughout the entire life cycle of concrete structures. This includes extending the service life of infrastructure through improved durability and maintenance strategies, as well as increasing resistance to chemical attack**,** corrosion, and extreme weather conditions.

As the construction sector continues to evolve, the future of concrete will be defined by its ability to meet sustainability imperatives, improve long-term performance, and integrate with emerging technologies. The continued adoption of environmentally responsible practices, digital solutions, and material innovations will ensure that concrete remains a fundamental component of modern infrastructure and architecture.

1.2. Environmental Impact of Concrete Production

1.2.1. Carbon Emissions in Cement Production

The global raw material consumption is expected to change considerably over time, based on a comparison between 2017 data and projections up to 2060, as illustrated in Fig. 1.3. The results show that sand and gravel represent the most heavily consumed materials, with an expected increase of approximately 20%, while metal consumption is projected to rise sharply by nearly 75%. Coal consumption also exhibits moderate growth, despite the global transition toward renewable energy sources. Overall, these trends reveal the intensifying pressure exerted by construction materials on non-renewable natural resources and emphasize the growing environmental burden associated with their extraction, processing, and use. This context highlights the importance of assessing the carbon footprint of construction materials as a whole, in order to better understand their cumulative contribution to global emissions and resource depletion.

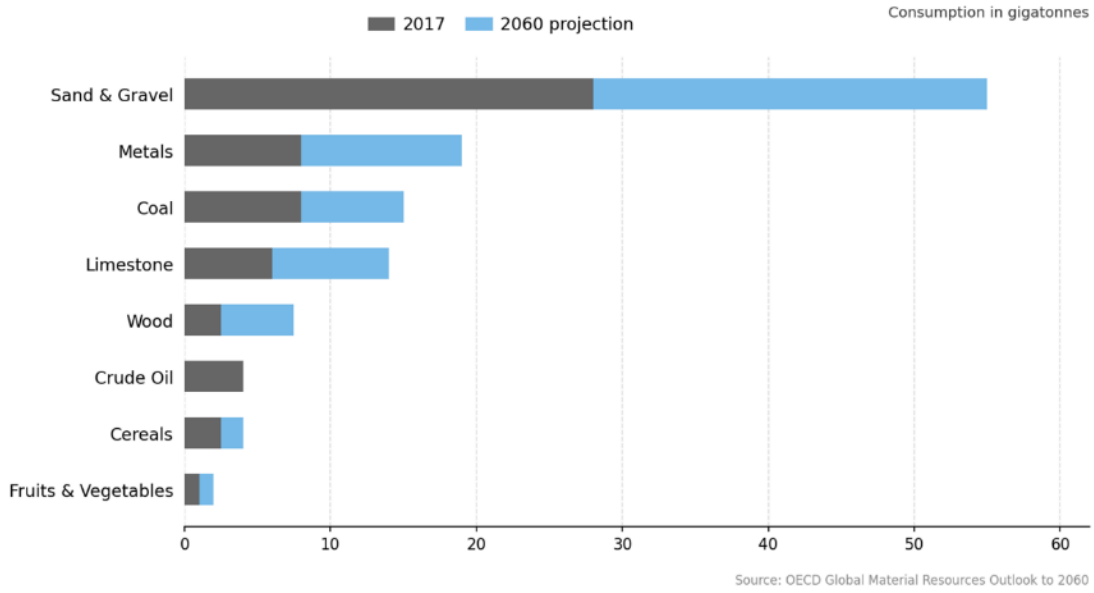


Fig. 1.3. Building materials rank first in raw material consumption (MECD, 2025).

Within this broader framework, cement emerges as one of the materials with a particularly high carbon intensity. Cement production is estimated to account for approximately 8% of global carbon dioxide (CO_2) emissions, positioning it as a critical contributor to the overall carbon footprint of the construction sector. These emissions arise from both energy-related processes—mainly the combustion of fossil fuels to heat raw materials, which accounts for around 40% of total emissions—and from process-related emissions associated with calcination, during which calcium carbonate decomposes into calcium oxide and releases CO_2, contributing nearly 60% of the total (Hasanbeigi et al., 2013 & Gartner et al., 2015). Additional indirect emissions stem from electricity consumption linked to grinding, material handling, and transportation operations, particularly when fossil-based energy sources are used (Madlool et al., 2011).

In response to the environmental challenges associated with construction materials, the industry has implemented several strategies aimed at reducing the overall carbon footprint while maintaining the required performance levels. These strategies include the diversification of energy sources through the use of biomass, waste-derived fuels, and hydrogen, as well as the partial substitution of conventional cement with supplementary cementitious materials (SCMs) such as fly ash, blast furnace slag, and natural pozzolan (Akhtar et al., 2018). Furthermore, circular economy approaches particularly the recycling of construction and demolition waste and the development

of innovative cement formulations incorporating industrial by-products are increasingly promoted to enhance resource efficiency and mitigate environmental impacts (IEA, 2018).

Fig. 1.4 illustrates the main sources of carbon dioxide emissions in the cement industry, totaling approximately 900 kg CO_2 per ton of cement. The majority of emissions (around 86%) stem from the calcination process and fuel combustion, highlighting the critical areas where mitigation strategies—such as using alternative low-carbon fuels, optimizing energy efficiency, and exploring alternative raw materials—can effectively reduce the sector's carbon footprint.

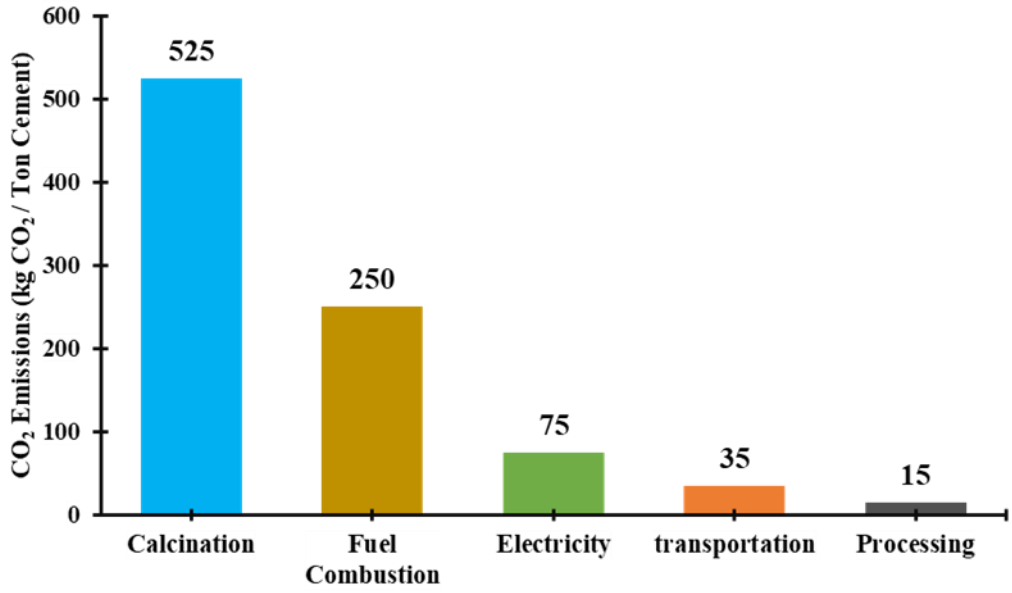


Fig. 1.4. Carbon Emissions by Source (IEA, 2020).

1.2.2. Water Usage and Pollution in Concrete Production

Concrete production is inherently water-intensive, as water is essential for cement hydration, workability, curing, and finishing. Average water consumption is estimated at approximately 165 liters per cubic meter, though this varies depending on mix design, cement type, aggregate characteristics, and the presence of chemical admixtures (Neville, 2011). Beyond mixing, water is also required for operational activities such as equipment cleaning, dust control, and cooling, generating wastewater that may contain suspended solids, chemical residues, and exhibit high

alkalinity. Improper management of this wastewater can lead to contamination of soil, groundwater, and nearby water bodies (WBCSD, 2018).

Fig.1.5 illustrates water consumption across the main stages of concrete production. Mixing represents the largest share, followed by washing, curing, dust control, and cleaning. This distribution highlights the key environmental concerns, including high alkalinity, suspended solids, chemical additives, and potential heavy metal residues. Addressing these challenges requires the implementation of sustainable water management strategies, such as recycling and reuse of treated process water, pH neutralization, and closed-loop systems to reduce total consumption and mitigate environmental impacts.

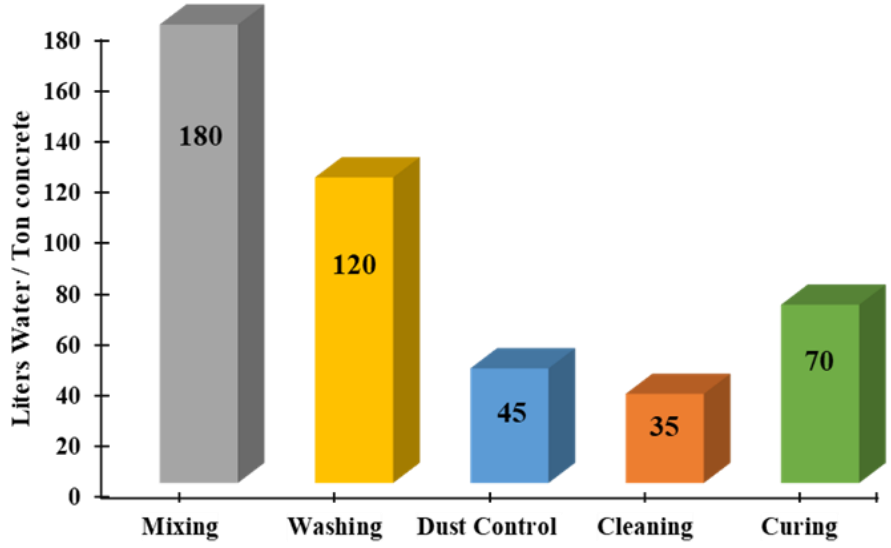


Fig. 1.5. Water Usage in Concrete Production (Miller et al., 2018).

1.2.3. Air Pollution from Concrete Production

Concrete production significantly contributes to air pollution through emissions of both particulate and gaseous pollutants, which have diverse environmental and health impacts. Particulate matter is generated during the handling and transportation of raw materials, while gaseous emissions include carbon dioxide (CO_2) from limestone calcination and fossil fuel combustion. Volatile organic compounds (VOCs) from chemical admixtures and solvents further affect air quality. Collectively, these emissions degrade air quality at local and regional scales and contribute to global

climate change, highlighting the need for effective emission mitigation strategies within the concrete industry (Szokolay, 2004).

Fig. 1.6 illustrates the emission rates of key air pollutants from cement production. Fine particulate matter (PM_{10}) exhibits the highest emission at 2.5 kg/ton, followed by nitrogen oxides (NO_x) at 0.8 kg/ton and sulfur dioxide (SO_2) at 0.5 kg/ton. Emissions of carbon monoxide (CO) and VOCs are lower but remain relevant due to their role in ground-level ozone formation. This distribution underscores the importance of implementing advanced air pollution control technologies to mitigate the environmental and health impacts of cement production.

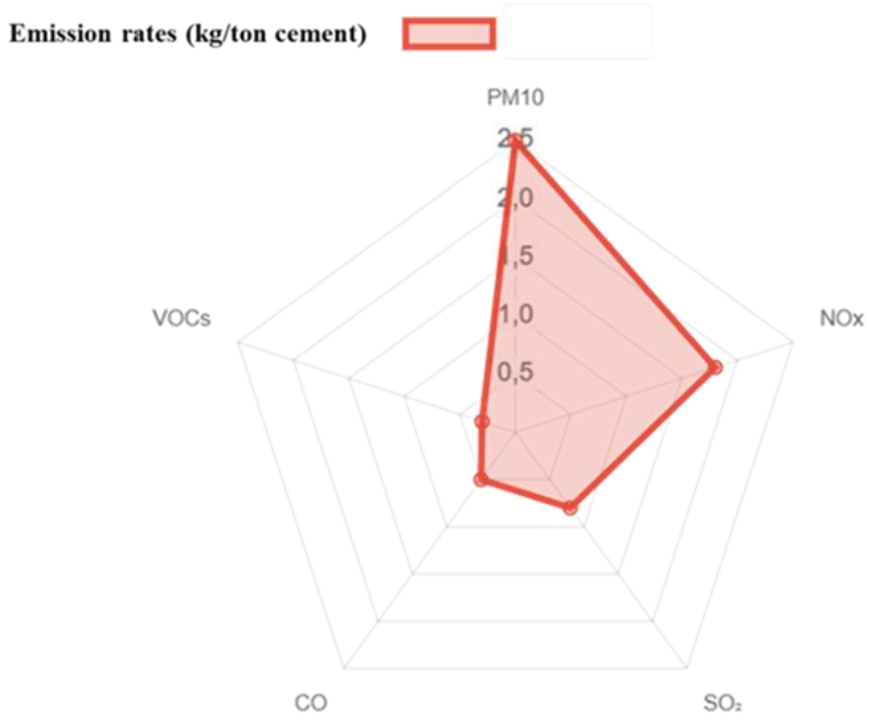


Fig. 1.6. Air Pollutants from Production (EPA, 2021).

1.2.4. Solid Waste Generation and Management

In addition to wastewater and air emissions, concrete production generates substantial amounts of solid waste, including unused or returned concrete from construction sites, residues from cement and raw material processing, and packaging waste such as bags, pallets, and barrels. Improper disposal of these wastes can cause environmental pollution and increase pressure on landfill capacities, emphasizing the need for sustainable waste management practices, including recycling, reuse, and safe disposal (WBCSD, 2018). Fig. 1.7, presents the distribution of solid waste generated by the

concrete industry, totaling approximately 1,328 million tons annually. Construction and demolition (C&D) waste represents the largest share (850 million tons, 64%), followed by concrete waste (320 million tons, 24%), recycled concrete (85 million tons, 6.4%), rejected molds (45 million tons, 3.4%), and washing residues (28 million tons, 2.1%). Although recycling rates currently range between 30–40%, most waste is still landfilled, highlighting the need to develop recycling infrastructure, utilize waste as recycled aggregates or road base materials, and implement regulatory frameworks that promote circular economy principles.

Addressing these challenges, alongside water and air pollution, requires coordinated strategies, technological innovations, and industry-wide adoption of sustainable practices. Such integrated efforts are essential for reducing the environmental footprint of concrete production and supporting the development of a more sustainable built environment.

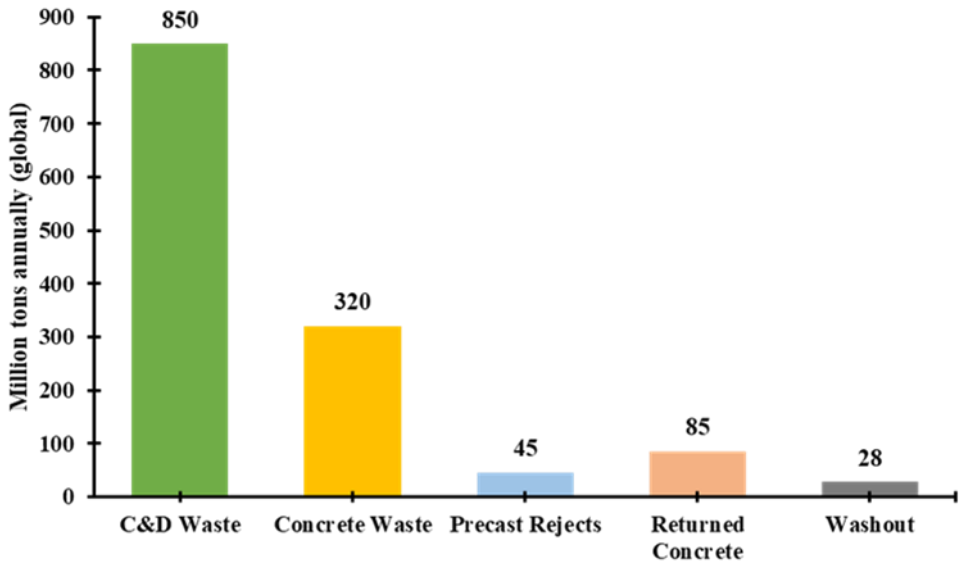


Fig. 1.7. Solid Waste Generation (European Commission, 2020).

1.2.5. Energy Efficiency and Thermal Performance of Concrete Buildings

Concrete remains one of the most widely used construction materials worldwide due to its strength, durability, and versatility. Its inherent thermal properties—thermal conductivity, specific heat capacity, thermal mass, and inertia—significantly influence building energy performance and occupant comfort. Thermal conductivity, typically ranging from 0.8 to 2.1 W/m·K depending on mix design and aggregates,

determines heat transfer, while the high thermal mass and specific heat capacity enable concrete to store and release substantial heat, stabilizing indoor temperatures and reducing energy demand for heating and cooling (Neville, 2011; Ozel, 2014).

Energy efficiency can be enhanced through architectural and material strategies. These include integrating thermal insulation (e.g., EPS, XPS, rock wool) within the building envelope, applying passive solar design principles, and addressing thermal bridges via insulated concrete forms (ICFs) or thermal breaks (Theodosiou et al., 2008; Sadineni et al., 2011). As shown in Fig. 1.8a, comparative U-values (Thermal Transmittance) for five types of concrete walls demonstrate the superior performance of insulated concrete, with U-values reduced by up to 89% compared to standard walls, indicating potential energy savings of 50–70% in heating and cooling systems.

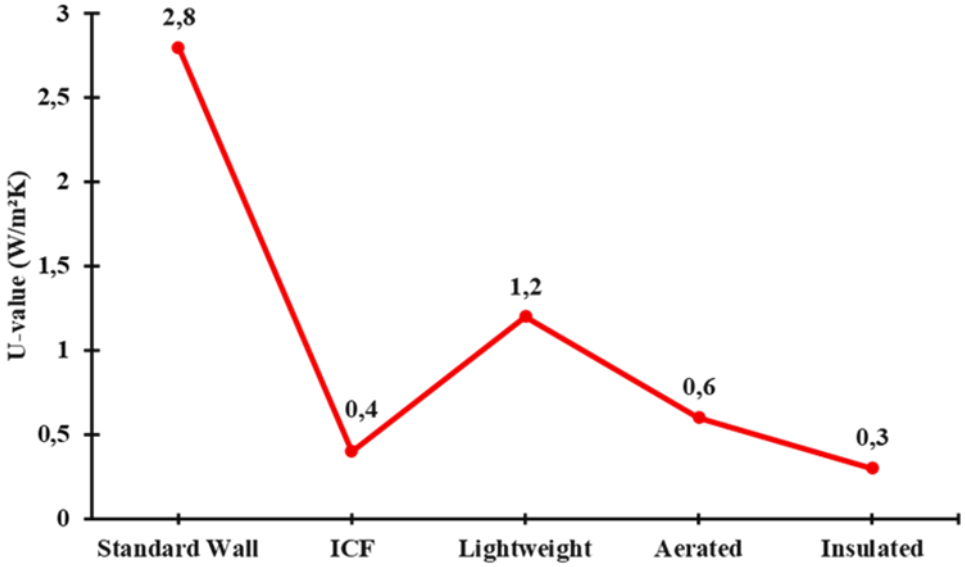


Fig. 1.8a. Thermal Performance (U-values) (ASHRAE, 2021).

Embodied energy analysis, presented in Fig. 1.8b, highlights that cement production accounts for 60–70% of total energy demand, while aggregates and transportation contribute 10–15% each. Ordinary Portland cement (OPC) concrete exhibits the highest embodied energy at 2400 MJ/m³, whereas geopolymer concrete demonstrates the lowest at 1400 MJ/m³, a 42% reduction. Ground granulated blast-furnace slag (GGBS) and recycled aggregate concretes also show substantial energy savings, confirming the effectiveness of alternative cementitious materials in reducing the carbon footprint and promoting sustainability.

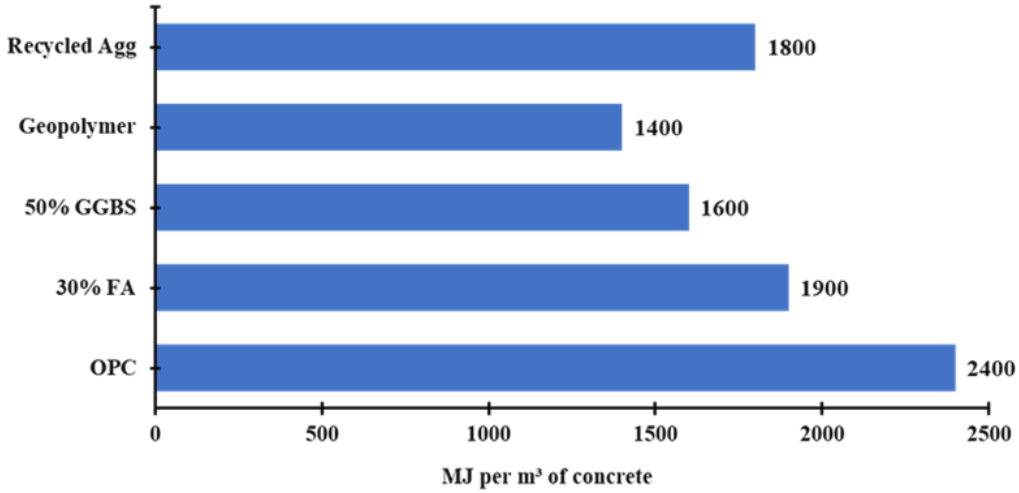


Fig. 1.8b. Embodied Energy Comparison (Hammond & Jones, 2011).

These findings emphasize the potential of combining innovative materials, energy-efficient design strategies, and advanced construction technologies to optimize thermal performance, reduce energy consumption, and enhance occupant comfort throughout the year. Furthermore, integrating bio-sourced materials can contribute to additional environmental benefits, aligning with contemporary regulatory frameworks such as RE2020 (RE2020, 2021), which prioritize energy efficiency, low carbon emissions, and improved indoor environmental quality.

1.3. Environmental Performance of Concrete Structures

The circular economy plays a pivotal role by promoting the reuse, recycling, and valorization of construction materials. Adopting alternative materials and strategies aimed at reducing waste generation and resource consumption is essential to achieving greater sustainability in concrete construction, as illustrated in Fig.1.9.

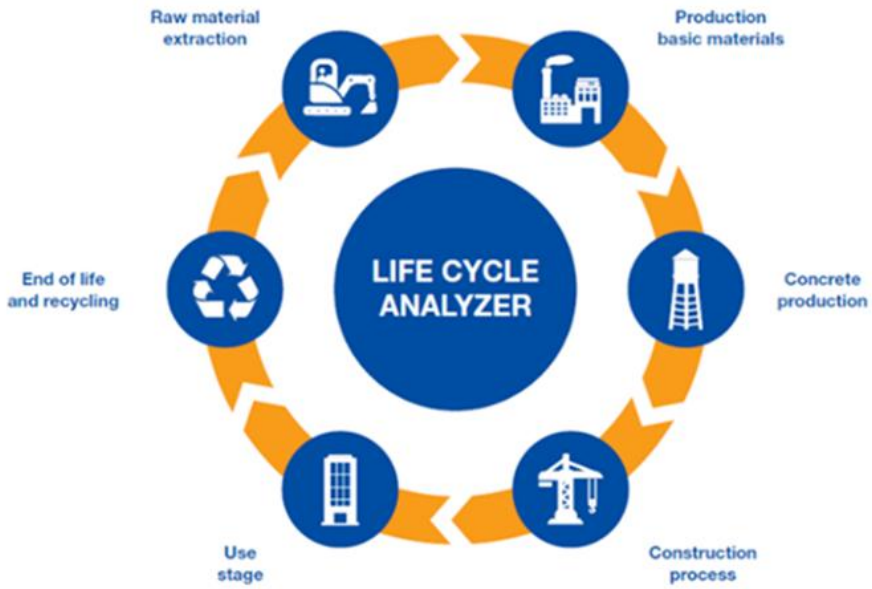


Fig. 1.9. Enhance and quantify the concrete environmental efficiency (SPHERE project, 2021).

1.3.1. Environmental Impact of Concrete Structures

The environmental impacts of concrete structures throughout their life cycle can be classified into several key categories that differ in nature and magnitude, each exerting distinct effects on ecosystems and natural resources. Foremost among these is the Global Warming Potential (GWP), which assesses the contribution of greenhouse gas emissions to climate change. These emissions play a critical role in intensifying global warming and altering atmospheric balance.

Another significant impact is the Non-Renewable Resource Depletion Potential, which evaluates the depletion of non-renewable natural resources, including fossil fuels and minerals consumed in concrete production. This process undermines the long-term availability of essential raw materials, posing sustainability challenges for future resource management.

The Eutrophication Potential also represents a major environmental concern, as the runoff of nutrients such as nitrogen and phosphorus from construction sites leads to excessive nutrient loading in aquatic systems. This results in algal blooms, oxygen depletion, and ecological imbalance within water bodies.

Furthermore, Toxicity effects arising from the use of chemical admixtures in concrete, along with the possible leaching of heavy metals from concrete structures, pose serious risks to both ecosystem health and human safety.

Finally, the extraction of raw materials—particularly aggregates—has direct consequences on biodiversity and land use, often resulting in habitat destruction and ecosystem disruption. Large-scale concrete construction activities further contribute to land-use change and surface sealing, which negatively affect soil functionality and the ecological services provided by natural systems.

1.3.2. Strategies for Enhancing the Environmental Performance of Concrete Structures

Reducing the environmental impact of cement production requires the implementation of integrated strategies, including the substitution of conventional cement with low-carbon alternatives, the development of novel cement types with reduced carbon footprints, and the increased use of recycled and secondary materials in production processes. In addition, the supply and transportation of raw materials—particularly aggregates—represent a significant source of environmental burden. Consequently, practices such as the use of recycled aggregates, optimization of concrete mix design, and prioritization of local sourcing play a crucial role in reducing emissions and energy consumption associated with material transport.

Improving transportation and construction efficiency further relies on optimized logistics, reduced distances between production and construction sites, effective waste management systems, and the promotion of prefabrication and modular construction techniques, which collectively enhance resource efficiency and limit on-site environmental disturbances. During the use and maintenance phase, environmental performance can be improved through energy-efficient design principles, including thermal insulation and passive design strategies, as well as the integration of renewable energy systems and sustainable maintenance practices. Extending the service life of concrete structures through durable, resilient, and adaptable design also reduces the need for frequent replacement or major rehabilitation, thereby limiting long-term environmental impacts.

At the end-of-life stage, environmentally responsible management requires the adoption of circular approaches such as selective demolition, concrete recycling, material dismantling and reuse, and diversion of waste from landfills. Numerous studies based on Life Cycle Assessment (LCA) have demonstrated that the effectiveness of these strategies varies across the concrete life cycle, with certain approaches offering greater emission reduction potential than others, as illustrated in Fig. 1.10. Overall, these findings highlight the importance of combining multiple complementary strategies within a unified framework to effectively reduce the environmental footprint of concrete structures and guide the construction sector toward lower-carbon practices.

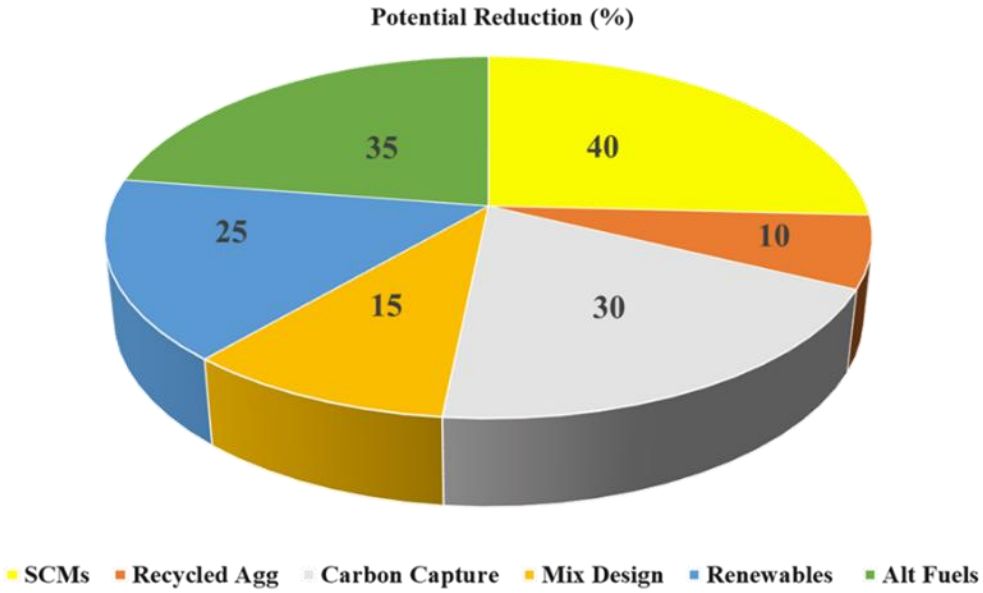


Fig. 1.10. CO_2 Reduction Strategies (Monteiro et al., 2017).

1.4. Innovations in Sustainable Concrete Production

Amid growing concerns over climate change and environmental sustainability, the construction sector is facing increasing pressure to adopt more sustainable alternatives in concrete production. The current environmental challenges underscore the urgent need to re-evaluate conventional practices in the concrete industry. Nevertheless, recent scientific and technological advancements have introduced innovative solutions that enhance the environmental sustainability of concrete manufacturing processes (Khan et al., 2011; Hasanbeigi et al., 2013).

1.4.1. Alternative Binders

Alternative materials constitute a major axis of innovation in sustainable concrete production, encompassing several categories, including supplementary cementitious materials (SCMs), recycled materials, geo-sourced materials, and bio-based materials. The integration of these alternatives aims to reduce reliance on conventional Portland cement, which is among the most energy-intensive components of concrete. Among promising bio-based materials, virgin cork represents an innovative solution aligned with modern architectural priorities, offering excellent thermal and acoustic insulation, moisture regulation, and fire resistance, making it a strategic option for projects emphasizing energy efficiency and reduced environmental impact (Khan et al., 2011).

Extensive research has demonstrated that the partial replacement of Portland cement with supplementary cementitious materials, typically at substitution levels ranging from 20% to 50%, is one of the most effective strategies for lowering the environmental footprint of concrete while maintaining—or even enhancing—its mechanical performance and durability (Khan et al., 2011). Among these materials, finely ground limestone plays a significant role due to its wide availability, low cost, and minimal environmental impact. Its partial replacement of clinker contributes to reductions in CO_2 emissions and energy consumption during cement production (Kim et al., 2018). From a physicochemical perspective, limestone acts as an active filler, improving the packing density of the cement matrix, reducing capillary porosity, and accelerating early-age hydration through a nucleation effect, thereby enhancing the development of mechanical strength (Ahmed et al., 2021). Moreover, studies have shown that limestone-containing cements can achieve satisfactory durability against aggressive agents when properly formulated, while adhering to circular economy principles and sustainable construction practices (Zhang et al., 2025).

Conversely, limestone concrete provides superior structural performance, long-term durability, and refined aesthetic qualities, making it a preferred choice for applications requiring strength, resilience, and architectural elegance. The combination of virgin cork and limestone in contemporary building design thus offers substantial potential to produce structures that integrate environmental sustainability, engineering

efficiency, and visual sophistication, reflecting the global trend toward advanced, eco-conscious construction practices.

In this context, national and international standards, such as (ASTM C618-19, 2019) and (EN 197-1:2011, 2011) provide regulatory frameworks for the use of supplementary cementitious materials by defining requirements related to chemical composition, physical properties, and appropriate replacement ratios. Beyond limestone and other SCMs, increasing attention has been directed toward the use of recycled materials, particularly industrial by-products, as well as geo-sourced and bio-based materials, in response to contemporary sustainability challenges. Widely adopted alternatives, such as fly ash and ground granulated blast furnace slag (GGBFS), can serve as partial substitutes for Portland cement, leading to significant reductions in the carbon footprint associated with concrete production (Damtoft et al., 2008). Other alternative binders, including silica fume and metakaolin, have also demonstrated their potential to improve mechanical performance and enhance long-term durability, thereby contributing to the extension of the service life of concrete structures (Mehta et al., 2014).

Overall, the adoption of alternative materials in concrete production reflects an integrated approach that combines environmental impact mitigation, enhanced engineering performance, economic feasibility, and effective waste valorization, in line with the principles of sustainable construction and the circular economy. As illustrated in Fig. 1.11, concretes incorporating alternative binders generally exhibit improved long-term compressive strength development compared to conventional Portland cement-based concrete, highlighting the mechanical potential of geopolymers, supplementary cementitious materials, and virgin cork as sustainable solutions for reducing carbon emissions while meeting structural performance requirements.

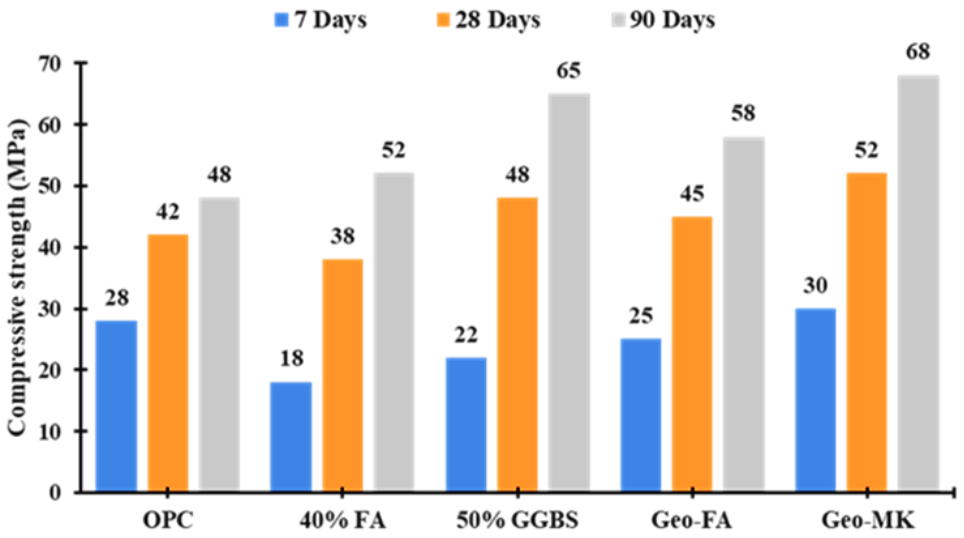


Fig. 1.11. Alternative Binders – Strength (Scrivener et al., 2018).

1.4.2. Recycled Aggregates

Recycled aggregates constitute one of the most prominent sustainable materials adopted in contemporary concrete manufacturing. They are derived from construction and demolition waste streams, including crushed concrete, bricks, and asphalt, and are employed as partial or total substitutes for natural aggregates in modern concrete mixtures (Tam et al., 2008). The incorporation of recycled aggregates contributes to reducing the demand for natural resources such as sand and gravel, while simultaneously diverting waste from landfill disposal. Previous studies have reported that their use can lead to a reduction in the carbon footprint of concrete of up to approximately 15% (Evangelista et al., 2005). The effective and durable use of recycled aggregates in concrete requires compliance with strict quality and performance criteria. This includes appropriate processing and cleaning procedures to remove contaminants, adjustments in mix design to account for the distinct physicochemical properties of recycled aggregates compared to natural aggregates, and adherence to relevant standards and regulatory frameworks to ensure consistent performance. As a result of extensive research efforts, several countries have developed specific guidelines governing the use of recycled aggregates in concrete. For example, the European standard (EN 206-1, 2013) permits the incorporation of recycled aggregates at limited substitution levels in structural concrete applications.

Beyond their use in concrete production, recycled aggregates are also widely applied in road construction and other civil engineering works, where they can fully replace natural aggregates without compromising functional performance. Overall, the adoption of recycled aggregates offers multiple benefits, including waste valorization through the recycling of construction and demolition waste, conservation of natural resources by reducing reliance on virgin aggregates, improved economic feasibility due to lower material costs, and enhanced environmental sustainability in line with circular economy principles. As illustrated in Fig. 1.12, concretes incorporating recycled aggregates generally retain a significant proportion of the engineering properties of natural aggregates, while exhibiting certain limitations related to workability, durability, and water absorption. These characteristics justify their controlled use in structural applications and highlight their suitability for non-structural and infrastructure-related applications, thereby achieving an effective balance between environmental sustainability and construction performance

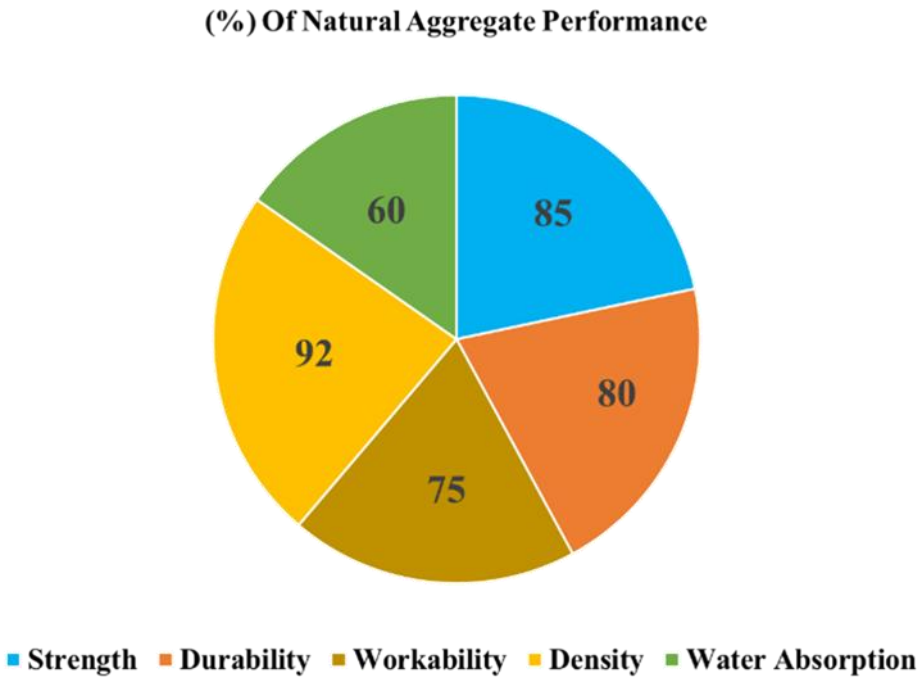


Fig. 1.12. Recycled Aggregate Properties (Tam et al., 2018).

1.4.3. Carbon Capture and Storage

Beyond alternative binders and recycled materials, successive developments in concrete manufacturing processes contribute to enhancing sustainability more profoundly, where Carbon Capture and Storage (CCS) technology represents one of

the most promising technological innovations in sustainable concrete production. This technology captures carbon dioxide emissions generated during cement production processes and stores them underground or redeploys them in diverse industrial applications (Leeson et al., 2017), with scientific estimates indicating that CCS technology is capable of achieving reductions in greenhouse gas emissions from cement production by rates potentially reaching 80% (Kuramochi et al., 2012). The implementation of CCS technology in the cement industry represents a paradigm shift toward mitigating the substantial environmental impact associated with traditional production methods, offering a viable pathway for the sector to achieve significant carbon neutrality goals while maintaining production efficiency and meeting global construction demands.

In parallel with industrial carbon capture technologies, bio-based materials offer a complementary approach to carbon sequestration through natural photosynthesis processes. Plants play a fundamental role in capturing atmospheric CO_2 during their growth cycle, converting it into organic matter through photosynthetic reactions (Fig.1.13). The photosynthesis equation demonstrates that $6CO_2 + 6H_2O$ yields $C_6H_{12}O_6$ (glucose) + $6O_2$, wherein carbon dioxide is biochemically transformed and stored within plant tissues. Quantitatively, the carbon storage capacity of plant-based materials is remarkable: 1000 kg of wood biomass represents the sequestration of approximately 1851 kg of CO_2 from the atmosphere during the tree's growth period (MECD, 2025). When bio-based materials such as cork bark are incorporated into concrete formulations, the carbon previously captured through photosynthesis remains sequestered within the building structure for decades, effectively transforming the constructed environment into a long-term carbon storage medium. This approach transcends conventional carbon capture methodologies by utilizing materials that have already performed natural CO_2 removal, thereby contributing to both embodied carbon reduction and extended carbon storage in the built environment.

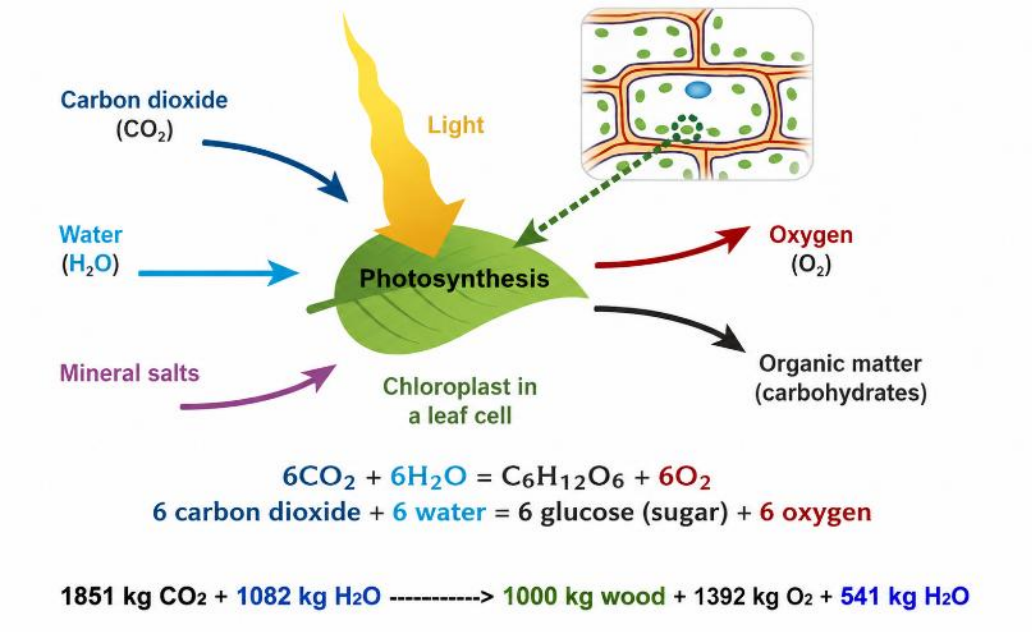


Fig. 1.13. Photosynthesis process in wood (MECD, 2025).

1.4.4. Renewable Energy and Materials

The integration of renewable energy sources into concrete production systems plays a crucial role in reducing dependence on fossil fuels and mitigating carbon emissions. Solar and wind energy are among the most effective solutions for supplying power to various stages of concrete production, from cement manufacturing to mixing and curing processes, thereby significantly reducing the environmental footprint of the industry (Hossain et al., 2016). As illustrated in Fig. 1.14a, waste heat recovery and solar energy exhibit the highest feasibility levels, whereas wind and geothermal energy show lower applicability due to technical and geographical constraints. These findings support the adoption of a hybrid energy strategy capable of achieving energy savings of approximately 20–30%. In parallel with the energy transition, the incorporation of recycled materials into concrete mixtures represents a fundamental pillar of sustainable development. The use of recycled plastic as a partial replacement for natural aggregates contributes to waste reduction while enhancing the thermal insulation properties and durability of concrete (Saikia et al., 2012; Frigione, 2010). Similarly, the utilization of recycled rubber derived from end-of-life tires improves impact resistance and reduces the volume of industrial waste directed to landfills (Siddique et al., 2004). Furthermore, Fig. 1.14b highlights the substantial variation in the environmental performance of cement alternatives. Conventional Portland cement satisfies only about 30% of sustainability criteria, whereas blended cements

demonstrate progressive improvement, reaching up to 70% compliance. In contrast, geopolymer cements and carbon-neutral concrete exhibit significantly higher alignment with circular economy principles and long-term carbon neutrality objectives (Habert et al., 2020). Overall, these findings emphasize the necessity of a clear, phased roadmap to guide the transition from transitional solutions toward transformative technologies, ensuring that the concrete industry effectively reduces its environmental impact while maintaining its essential role in economic and social development.

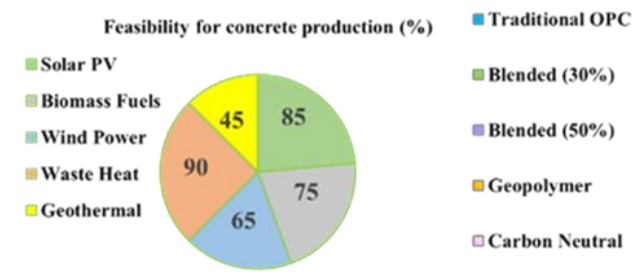


Fig. 1.14a. Renewable Energy Integration (IEA, 2018)

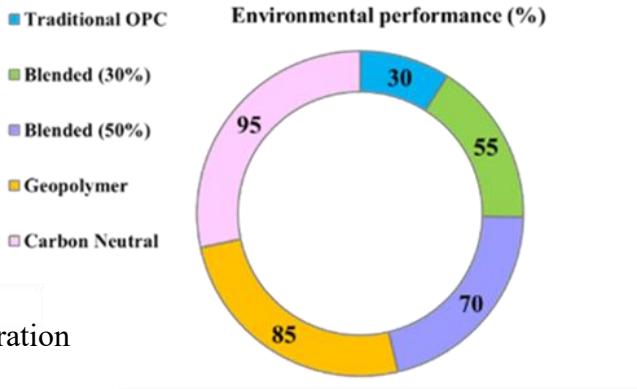


Fig. 1.14b. Overall Sustainability Comparison. (Habert et al., 2020).

1.5. Conclusion

The first chapter establishes the general framework of the research by examining concrete as a fundamental construction material, its historical development, and the major environmental challenges associated with its production, including high carbon emissions, energy consumption, pollution, and waste generation. It also addresses energy efficiency and thermal performance in concrete buildings, while reviewing key innovations in sustainable concrete production, such as alternative binders, geopolymer concrete, recycled aggregates, carbon capture technologies, and the integration of renewable energy sources. Based on the need to explore sustainable solutions relying on natural, renewable, and locally available materials, the second chapter is devoted to an in-depth investigation of concrete additives, with particular emphasis on virgin cork as a promising bio-based material for developing concrete with enhanced thermal efficiency and environmental performance.

Chapter 2

Innovative Building Materials: Virgin Cork Concrete as a structural material

Introduction

Innovative building materials have advanced sustainable construction by combining superior physical properties with improved environmental performance, enhancing insulation, durability, and reducing reliance on conventional resources.

Virgin cork concrete has emerged as a promising sustainable material, offering excellent thermal and acoustic insulation and renewability. However, its low density limits mechanical strength in structural applications. This chapter reviews the key properties of raw cork concrete, its potential applications, and current research focused on optimizing its performance, exploring its use not only as an insulating material but also in structural elements in low-load or individual construction projects.

2.1. Green Concrete and Natural Plant-Based Additives

With escalating global concern regarding environmental challenges, green concrete has emerged as a promising alternative through the integration of recycled materials and advanced production technologies aimed at minimizing environmental impact throughout its lifecycle. This innovative material relies on recycled aggregates, industrial by-products, and plant-based materials to reduce dependence on natural resources while promoting waste recycling, including fly ash and blast furnace slag. Consequently, green concrete not only reduces the environmental footprint of the construction sector and enhances structural performance but also contributes to the development of more resilient and energy-efficient urban environments.

The rapid growth of green and alternative construction materials, particularly bio-based building materials, is mainly driven by the urgent need to mitigate global warming. The construction sector contributes significantly to climate change due to its substantial environmental footprint (Amziane et al., 2017).

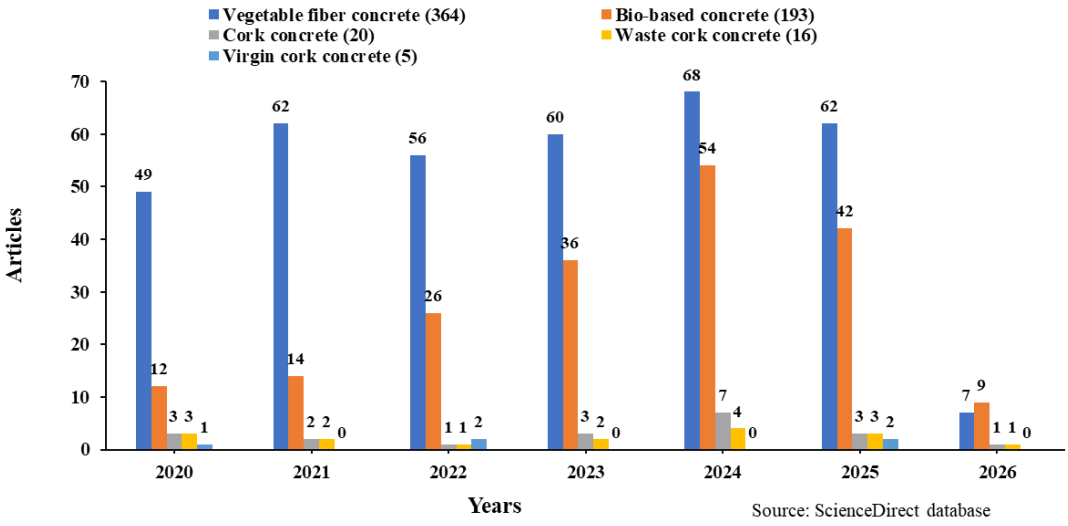


Fig. 2.1. Annual distribution of publications (2020–2026) (ScienceDirect database).

Bio-based materials are widely acknowledged as environmentally friendly, sustainable, and multifunctional solutions. While the hygrothermal and insulation performance of bio-based concrete has been extensively investigated, its mechanical performance in compression remains comparatively underdeveloped.

2.1.1. Diverse Plant-Based Materials in Concrete Enhancement

Research has demonstrated that the incorporation of plant-based natural fibers and bio-derived additives into concrete can significantly enhance its mechanical performance and overall functionality, offering a sustainable alternative to conventional reinforcements such as steel or synthetic fibers (Jahami et al., 2024). These bio-based materials, often derived from agricultural and industrial by-products, contribute to reducing the environmental footprint of concrete by preserving non-renewable natural resources such as sand and gravel, while also lowering carbon dioxide emissions associated with cement production (Younes et al., 2024).

Within this context, the global vegetation map in Fig. 2.2 illustrating plant resources suitable for concrete applications provides a comprehensive overview of the geographical distribution of bio-based materials across different continents. The map highlights that each climatic region possesses specific plant resources that can be valorized in sustainable construction. Asia and Africa are particularly rich in agricultural residues and fibrous plants such as rice husk, banana fibers, and date palm (Amin et al., 2022) while Europe and the Americas predominantly rely on well-studied fibers such as flax, hemp, and wood-based materials.

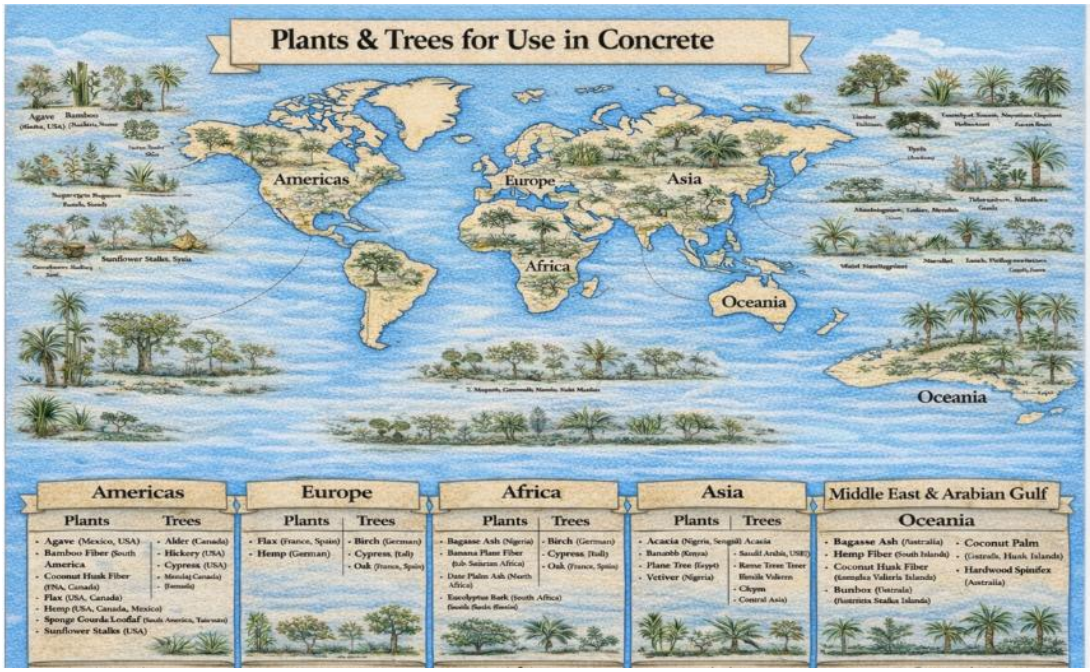


Fig. 2.2. Global Plant Resources for Sustainable Concrete

(Amin et al., 2022 ; Joachim et Oettel., 2024).

Oceania, in contrast, is characterized by plant species adapted to harsh environmental conditions, which are mainly exploited for lightweight and insulating applications. This global distribution confirms that the use of plant-based materials in concrete is not a localized approach, but rather a worldwide strategy aligned with sustainability and circular economy principles (Oettel, 2024).

Complementing this global perspective, Fig. 2.3 presents a systematic classification of natural fiber sources derived from plants, categorized according to the plant part utilized, including seeds, leaves, bast fibers, grasses, stalks, wood, and fruits (Hamza et al., 2023). This classification emphasizes the remarkable diversity of plant-based fibers available for concrete applications and demonstrates that the botanical origin of the fiber strongly influences its physical and mechanical characteristics, which in turn affect the behavior of fiber-reinforced concrete in terms of strength, ductility, and durability (Bazan et al., 2020; Flores-Nicolás et al., 2025).

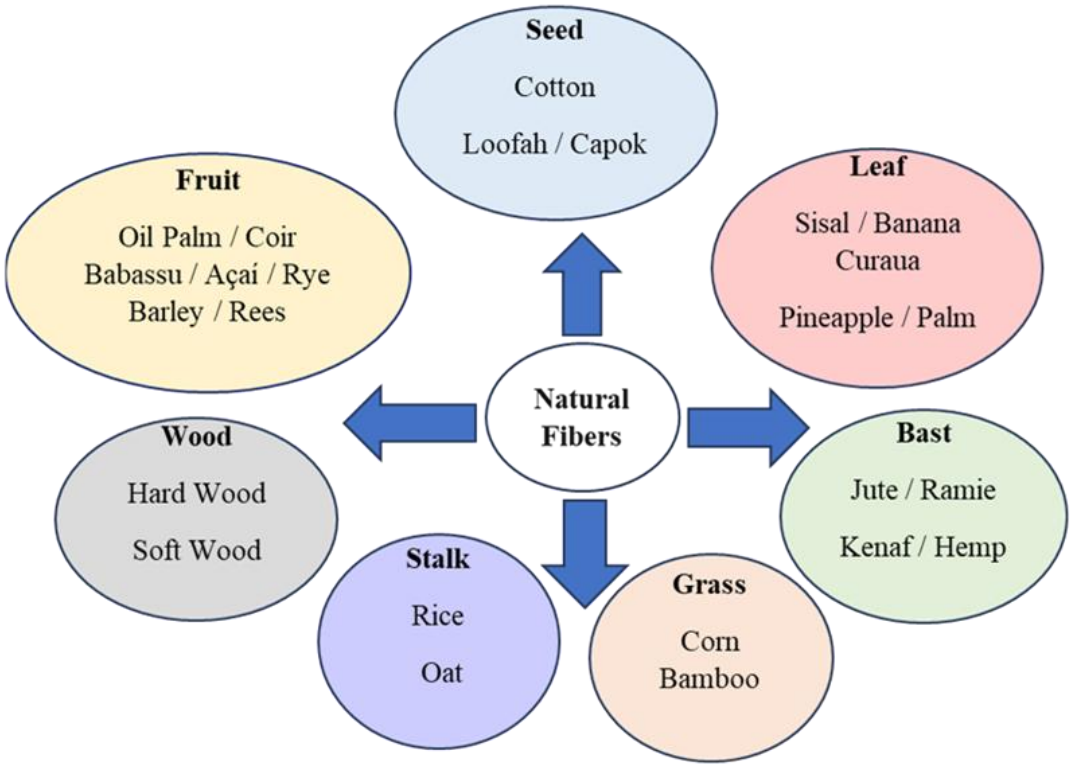


Fig. 2.3. Classification and Diversity of Natural Fiber Sources (Hamza et al., 2023).

Natural plant additives demonstrate significant capacity to enhance concrete resistance and durability when utilized in studied proportions. (Barco Tocto et al., 2025) indicated that a mixture comprising 2% prickly pear cactus and 0.5% aloe vera increased compressive strength from 245 to 443.4 kg/cm² (an 81% increase) while

reducing corrosion rates in saline environments. Miscanthus fibers (Acikel, 2011) improved compressive strength by 4–28%, tensile strength by 9–25%, and flexural strength by 2–9%. Euphorbia tortilis extract (Mohanraj et al., 2024) increased compressive strength by 29%, while utilizing 15% prickly pear cactus mucilage (Opuntia ficus-indica) as a partial water replacement resulted in a slight increase in compressive strength, alongside a 39% reduction in liquid permeability and improved freeze-thaw cycle resistance.

Other plant additives have shown tangible benefits, as nanocellulose fibers at 0.05% concentration (Kolour et al., 2024) improved compressive strength by up to 28% and reduced shrinkage by 13%. Straw or husk ash (Kumar et al., 2022) used at 10–20% as a partial cement replacement enhanced compressive, tensile, and flexural strength while increasing resistance to acidic, sulfate, and chloride attacks. Bambusa arundinacea extract (Ismail, 2014) demonstrated compressive strength superior to that provided by synthetic inhibitors. In composite systems, such as combining Phragmites australis fibers at low dosages with waste glass (Ramadan et al., 2023), results demonstrated that dosage is a critical factor; low dosages improve ductility and bearing capacity, while excessive dosages lead to decreased compressive strength.

Transitioning from the global scale to the regional context, Algeria represents a particularly relevant case study, as illustrated by the vegetation zone map of Algeria (Fig. 2.4). This map reveals a pronounced climatic and ecological gradient extending from the Mediterranean coastal zone to the Saharan regions. The northern areas are dominated by tree species such as cork oak, Atlas cedar, Aleppo pine, and olive trees, which are of significant interest for bio-based construction materials and insulation purposes. The Tell Atlas and High Plateaus are characterized by steppe vegetation rich in fibrous plants such as esparto grass, diss grass, and sagebrush, while the southern regions host drought-adapted species including date palm, acacia, and tamarisk, alongside abundant agricultural residues such as wheat and barley straw. This spatial distribution demonstrates that Algeria possesses a wide range of plant resources providing substantial potential for the development of locally sourced, bio-based concrete materials (Meddour et al., 2021).

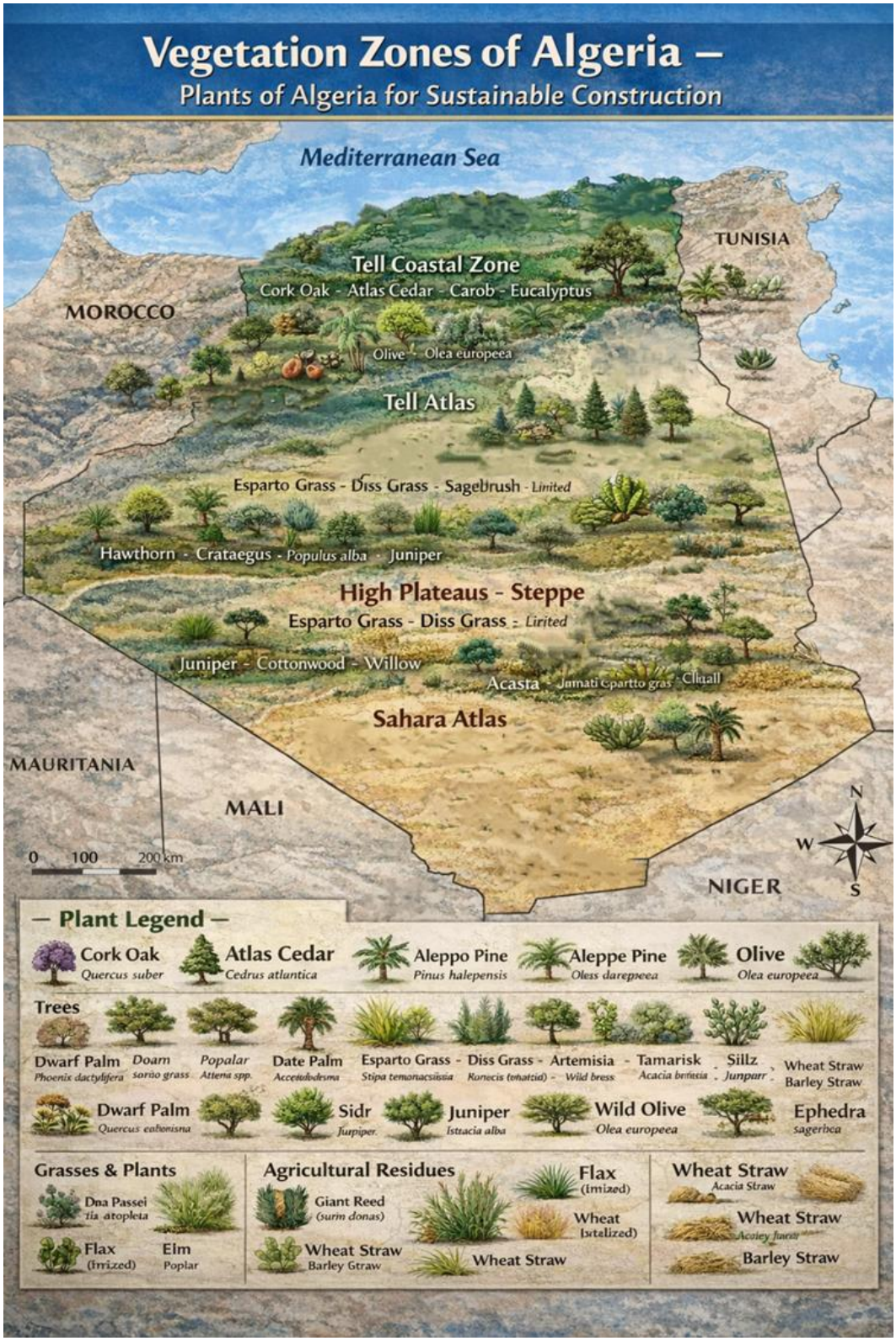


Fig. 2. 4. Vegetation Zones of Algeria for Bio-Based Construction (Meddour et al., 2021).

Numerous studies have confirmed that the incorporation of such plant-derived materials, both globally and locally, can lead to significant improvements in concrete performance when used in optimized proportions, including enhanced compressive,

tensile, and flexural strengths, as well as improved durability and resistance to permeability and corrosion (Chaitanya et al., 2023; Antony et al., 2024). Within this framework, cork, which is abundantly available in northern Algeria, emerges as a strategic bio-based material due to its exceptional thermal and acoustic insulation properties, low density, and environmental compatibility. Cork has already been extensively investigated within our laboratory, forming the scientific basis for its detailed presentation and performance evaluation in cork-based concrete systems in the following section.

2.2. A Comprehensive Overview of Cork as a Material

2.2.1. Geographical Distribution

Cork is a natural, renewable, non-toxic, and biodegradable raw material that has been utilized by humans for over 5000 years across various sectors (Petlitckaia et al., 2024). It exhibits an exceptional combination of properties—including thermal and acoustic insulation, abrasion resistance, and durability—that make it particularly suitable for applications in construction and infrastructure. These intrinsic characteristics, along with its low environmental footprint, enable cork to meet key criteria for green building practices, sustainability standards, and energy efficiency regulations.

Cork is derived from the outer bark of the cork oak tree (*Quercus suber L.*), a species belonging to the *Fagaceae* family. Widely recognized as an environmentally friendly material, cork is harvested cyclically without harming the tree, allowing for continuous production throughout the tree's lifespan. The cork oak, native to the Mediterranean region, is a long-lived species that sequesters atmospheric CO_2 and demonstrates remarkable resilience to harsh climatic conditions—attributes largely attributed to the protective nature of its bark. The quality and thickness of cork bark are influenced by the specific environmental conditions in which the tree grows. Cork oak is an evergreen, slow-growing species that thrives only in select regions where it can receive abundant sunlight and a rare combination of low annual rainfall with relatively high humidity (Silva et al., 2005).

Cork oak forests are primarily distributed across the western Mediterranean basin, encompassing parts of Southern Europe and North Africa, including Portugal, Spain, Morocco, Algeria, Tunisia, southern France, and specific regions of Italy (notably Sicily and Sardinia) **(**Fig.2.5**)**. These areas provide the distinct climatic conditions—

dry summers and mild winters—necessary for the growth and sustainability of the species. Beyond their economic value, these forests play a vital ecological role by combating desertification and supporting rich biodiversity. The majority of cork oak trees are integrated into multifunctional agroforestry systems that combine cork harvesting with livestock grazing, hunting, and the collection of other non-timber forest products. This land-use system, known as Montado, has been recognized by the European Environment Agency as a High Nature Value farming system and is included in the EU Habitats Directive as a conservation-priority habitat. Nevertheless, this ecosystem faces increasing threats from both biotic and abiotic stressors, including insect infestations and wildfires (Pereira, 2007; Machado et al., 2016; Alexandre Ricardo, 2019).

Cork oak forests span an estimated 2.2 million hectares worldwide, with approximately 700 000 hectares located in North Africa and 1.5 million hectares in Europe. Notably, Portugal accounts for nearly one-third of the global total—approximately 737 000 hectares—representing 23% of its national forest area and 34% of the world's cork oak forest coverage. Europe, as a whole, is home to about 60% of the total cork-producing forest area.

The global annual cork production is approximately 201 000 tons, predominantly sourced from cork oak trees in Portugal and Spain, which contribute 49.6% and 30.5% of the raw material supply, respectively. According to (Lopes et al., 2000), over 67% of the world's cork oak forests are concentrated in Portugal, Spain, France, and Italy—countries that collectively produce more than 85% of global cork output.

Portugal leads the global cork industry, where cork products represent around 1% of the national GDP and are largely export-driven. According to the Portuguese Cork Association (APCOR, 2015), annual cork exports exceed €1.346 billion. In 2018, Portugal exported 201 000 tons of cork—over 90% of its total production—representing 62.5% of the global market. Consequently, the European Union accounts for approximately 80% of worldwide cork production (Chorana et al., 2019; Costa et al., 2019; Cunha et al., 2020).

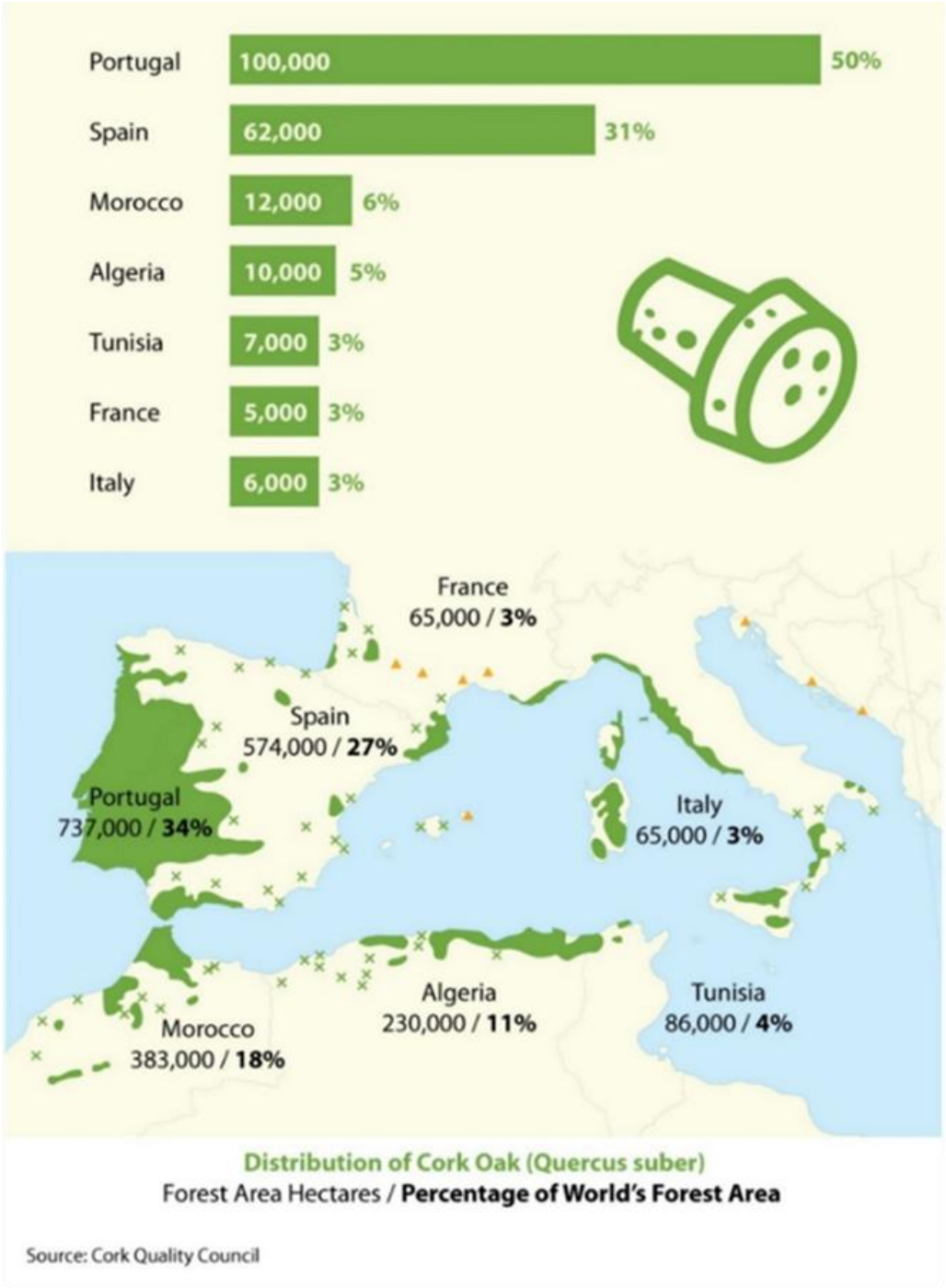


Fig. 2.5. Global Distribution of Cork Production in Mediterranean basin (Reddit, 2021).

Globally, cork production is estimated at 340 000 tons per year. Natural cork stoppers are the industry's most valuable product, forming the backbone of the cork sector, with an estimated market value of USD 1.3 billion annually. Cork is used in a broad range of applications, including flotation devices, insulation, and energy absorption systems such as thermal shielding for space shuttles. More recently, cork has been studied as a biosorbent material for removing heavy metals, polycyclic aromatic hydrocarbons (PAHs), and oil from contaminated environments (Chorana et al., 2019).

Cork's unique combination of properties—including low density, elasticity, durability, impermeability to liquids, low thermal and electrical conductivity, sound insulation, abrasion resistance, fire retardance, hypoallergenic qualities, and longevity—distinguishes it from other natural materials such as wood or stone (Pereira, 2007). These characteristics make cork an attractive material across various sectors, from construction to aerospace. Nevertheless, cork is globally recognized for its use as a sealing material, with approximately 70% of global cork production dedicated to wine bottle stoppers. The production of cork stoppers generates around 50 000 tons of cork waste annually—equivalent to 25–30% of the input material (Jové et al., 2011).

In the construction sector, cork is increasingly valued for its sustainability and natural origin (Gomes, 2016). Rising market demand for environmentally friendly materials has contributed to cork's appeal, particularly in high-value and distant markets such as Asia, the United States, and Australia. Its applications in flooring, wall cladding, and insulation have grown significantly, driven by innovation in design and product development. High-profile architectural projects—such as the use of cork in façade cladding—have also boosted public awareness, as seen in the Portuguese Pavilions at the World Expos in Hannover (2000) and Shanghai (2010) (Machado et al., 2016).

Several cork-based materials are used in the construction industry, including: untreated cork boards stripped directly from tree trunks; granulated cork; cork composites (made from granules and resin); rubber–cork blends; and expanded cork agglomerates without resin. In addition, advanced cork products combine cork with other materials, typically for customized technical solutions.

A major byproduct of the cork industry is cork granules, derived from the trimming and cutting residues during stopper production. These granules are subjected to heat and pressure in sterilization chambers to form either expanded agglomerates (produced without synthetic binders) or composite agglomerates (produced with synthetic resins). Both stopper production and agglomerate manufacturing generate waste, with rejected materials accounting for 20–30% of the raw cork input. Cork dust—the most abundant form of waste—is usually incinerated for energy recovery, while rejected granules are often recycled into new production cycles. Although much of the cork waste is reused, it is still considered a byproduct of relatively low commercial value (Cunha et al., 2020).

Cork formation is closely associated with specific physiological processes occurring in the bark of the cork oak tree (Quercus suber L.) **(**Fig.2.6**)**. In plant anatomy, cork—referred to as phellem—is a protective tissue that constitutes a key component of the periderm (outer bark). This layer encases the trunk, branches, and roots of the tree, serving as a natural barrier that safeguards the internal tissues from environmental stressors (Machado et al., 2016).



Fig. 2.6. Cork oak tree after bark harvesting (Gibson, 2016).

2.2.2. Cork Oak Forests in Algeria

Cork oak forests (Quercus suber) are naturally distributed across Algeria's Mediterranean coastal and mountainous zones (Fig.2.7). Notably, these forests are well-documented in the Tell Atlas range in northwestern Algeria. For example, Tlemcen National Park contains cork oak stands situated at elevations between approximately 1084 and 1418 m, with an average annual rainfall of around 483 mm.
In the Kabylie region (Tizi Ouzou), cork oak forests extend from the coastal lowlands to mountain slopes exceeding 1000 m in elevation, thriving under humid to semi-humid Mediterranean conditions with annual precipitation ranging from 700 to 1500 mm.
Further occurrences are recorded in El Kala National Park, the Akfadou Mountains (700–860 m), and the Séraïdi Forest within the Edough range in Annaba. Across these regions, cork oaks are typically found on humus-rich soils developed over sandy or

sandstone substrates, occupying a broad altitudinal range and demonstrating their adaptability to diverse ecological conditions.



Fig. 2.7. Distribution Map of Cork Oak Trees in Algeria (Dehane et al., 2014).

2.2.3. Environmental Characteristics of Cork Oak Forests in Algeria

Algerian cork oak forests demonstrate remarkable ecological consistency across multiple study sites, characterized by several distinctive patterns. These forests show a clear preference for sandy or sandstone-derived soils enriched with humus, reflecting their adaptation to well-drained substrates with mildly acidic conditions. Their resilience to variable precipitation is particularly notable, as research indicates they can flourish across a wide annual rainfall gradient spanning from approximately 500 mm to 1 500 mm. This precipitation tolerance explains their extensive distribution throughout diverse ecological zones, ranging from coastal lowlands to mountainous terrain. A defining feature of these ecosystems is the ubiquitous presence of Erica arborea (heath tree) alongside cork oak across different geographical locations, which points to shared environmental preferences or potentially beneficial ecological interactions between these species. Furthermore, the altitudinal distribution of cork oak forests extends from sea-level coastal areas to elevations surpassing 1,400 meters, underscoring their considerable adaptability to varied altitude conditions within the broader Mediterranean climatic context.

These environmental characteristics offer valuable insights into the habitat requirements and community structure of cork oak forests in Algeria. Variations in certain factors, such as rainfall and elevation, across different sites highlight the cork

oak's ecological flexibility, which may play a key role in its resilience to environmental changes.

2.2.4. Cork Growth and Productivity in Algeria

Cork oak forests are of high cultural and environmental value, supporting a rich diversity of plant and animal species. The management of cork oak forests is primarily focused on cork production, particularly on preserving cork growth and ensuring its quality. Several factors influence cork growth, including genetic diversity, site quality, stand conditions, individual tree characteristics, and the cork stripping process. The quality of cork is determined by three main factors: cork thickness, porosity, and the presence of defects such as insect channels or wood inclusions. To achieve high-quality cork, low porosity and high density are essential. In Algeria, cork oak forests cover approximately 450 000 hectares. The current state of these forests is considered unstable, with challenges such as tree degradation, frequent fires, and a lack of skilled labor for cork extraction. Over the past two decades, the productivity and ecological integrity of cork oak forests in Algeria have significantly declined. Studies indicate that annual cork production has fallen from around 20 000 tons to less than 10 000 tons between 2000 and 2010. This decline is attributed to changes in forest structure, from dense to less dense forests, and a reduction in ecosystem services (Chorana et al., 2019).

Additionally, poor management practices, land conversion, overgrazing, and climate change have led to a sharp decrease in the productivity and sustainability of cork oak forests in Algeria since 2000. The economic viability of cork harvesting has been undermined by inadequate harvesting techniques, land conversion to housing and agriculture, and poor forest management. From an environmental perspective, the pressures include widespread overgrazing, reduced rainfall, rising temperatures, recurring droughts, and soil degradation, with projections suggesting a decline in suitable habitats by 1.1% to 4.2%.

While cork oak trees demonstrate resilience, with a survival rate of up to 92.74% after fires and active regeneration, the decline in cork quality and the weakening of mycorrhizal root connections highlight the ongoing challenges to the sustainability of these forests.

2.2.5 Anatomical Structure

Fig. 2.8 presents the cross-sectional analysis of Quercus suber trunk reveals a stratified organization comprising internal xylem and external bark, developing through

continuous activity of two specialized cambial tissues: the vascular cambium, which differentiates bidirectionally producing secondary xylem centripetally and phloem centrifugally, and the cork cambium (phellogen), which generates phloem elements inward and phellem (cork tissue) outward (Machado et al., 2016). The cork oak exhibits unique periderm properties distinguishing it from other species, including a continuous circumferential phellogen forming homogeneous cork layers, exceptional meristematic longevity, and remarkable regenerative capacity following extraction through traumatic phellogen formation within residual phloem tissue. Periderm development initiates during the first year, with initial radial expansion inducing longitudinal stresses causing characteristic virgin cork fissuring; upon debarking, regenerated cork demonstrates superior structural integrity due to reduced mechanical stress from increased stem diameter. Cork production follows seasonal rhythms with phellogen dormancy during winter (November-March) and active growth in spring-summer (April-October), with annual increments demarcated by dark bands representing late-season cell production; maximum accumulation occurs immediately post-extraction, declining gradually until subsequent harvest (Costa et al., 2019). Cork tissue contains radially-oriented lenticular channels formed by specialized lenticular cambium, facilitating vital gas exchange (O_2, CO_2) and moisture transfer between internal living tissues and external environment; these channels exhibit variable density and diameter, with porosity decreasing progressively from trunk base to apex primarily through diameter reduction rather than numerical decrease, representing a genetic adaptation to environmental fluctuations (Silva et al., 2005; Costa et al., 2021). Annual cork accumulation averages 4.1 mm (range: 1.7-6.0 mm), and following standard 9-year production cycles, harvested planks are classified by thickness from very thin (<22 mm) to very thick (>54 mm), determining industrial applications. Cork extraction is performed manually during peak physiological activity (late spring-early summer) when phellogen fragility facilitates separation; initial virgin cork harvest occurs at (~20-25) years when trunk circumference reaches 70 cm at 1.3 m height, with subsequent 9-year cycle extractions throughout the tree's (170-200) year lifespan, enabling 15-18 harvests (Machado et al., 2016). Post-extraction processing involves boiling (~1 hour at 100°C) to enhance flexibility, expand lenticular structures, improve cellular organization, and induce gas expansion in collapsed cells, followed by drying to ~20% moisture content (Silva et al., 2005). Three cork types are produced throughout tree lifespan (Fig. 2.9) virgin cork (first harvest, 20-30 years) characterized

by structural irregularity and used for insulation boards and decorative products; second cork (first regeneration, 9+ years post-virgin) with improved uniformity but intermediate quality; and Amadia cork (second regeneration, 9-year cycles) exhibiting homogeneous structure ideal for premium wine stoppers with typical thickness of 20-50 mm (Machado et al., 2016).

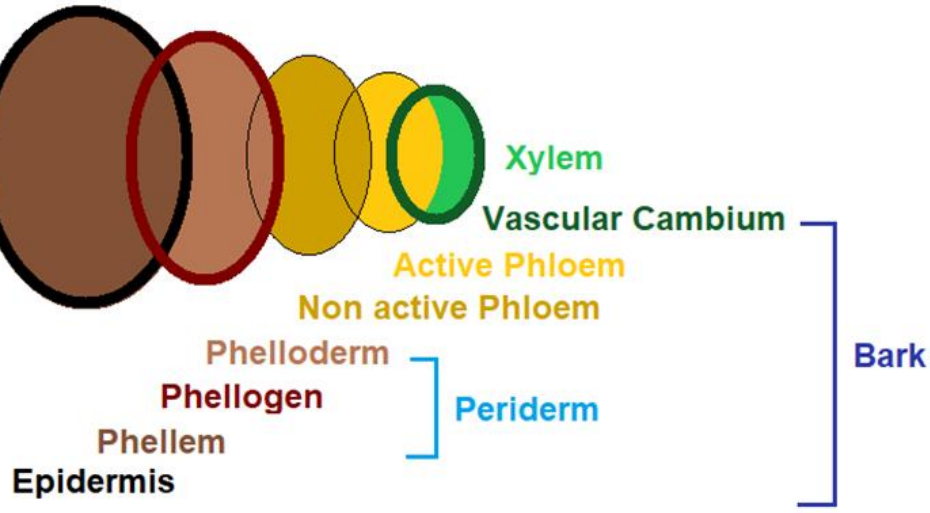


Fig. 2.8. Anatomical cross-section of a young cork oak stem depicting tissues before cork is harvesting (Pereira, 2007).

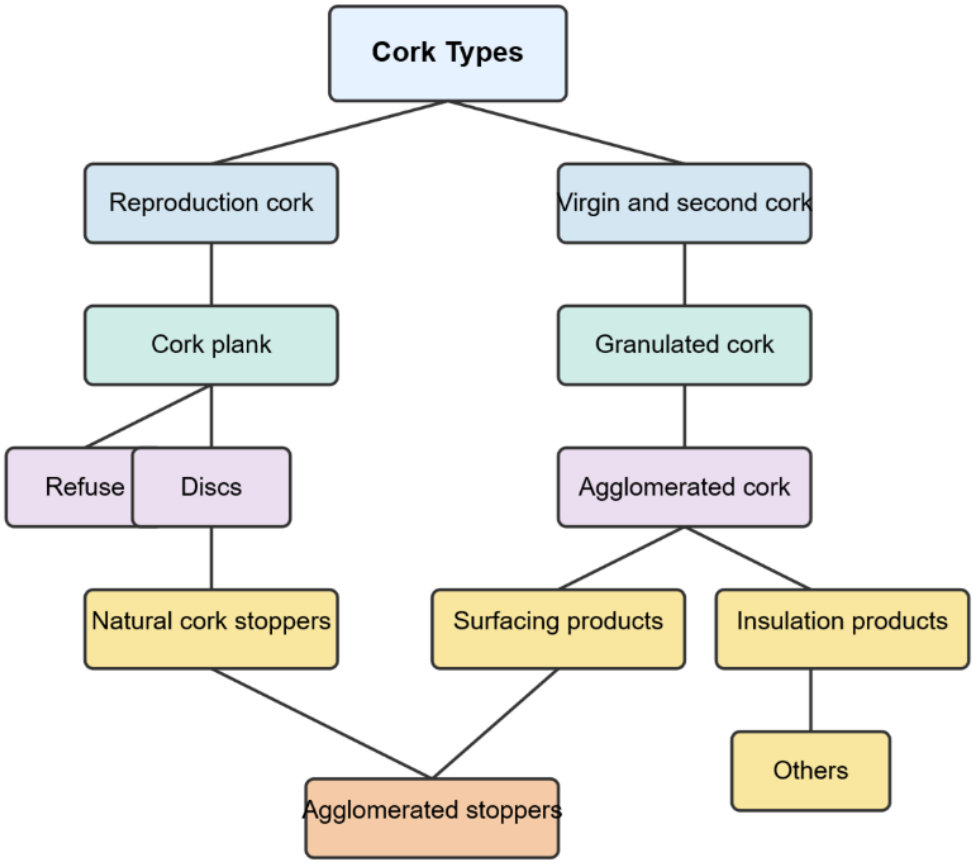


Fig. 2.9. Flowchart for the Production of Industrial Cork Products

(Dhandapani et al., 2021).

2.2.6. Morphological Characterization

Fig. 2.10 shows that cork exhibits highly organized cellular architecture comprising hexagonal prismatic cells arranged in radial rows perpendicular to the trunk axis, tightly packed base-to-base creating efficient space-filling honeycomb structure; sectional analysis reveals orientation-dependent morphologies with hexagonal profiles in longitudinal sections and stacked brick-like laminar arrangements in radial/transverse sections, fundamental to Robert Hooke's 1664 discovery of cellular structure (Xiaozhou et al., 2017). Cork demonstrates exceptional cellular density of 4×10^7 to 7×10^7 cells/cm³ despite solid material comprising <20% of total volume, with average cellular dimensions of ~40 µm prism height, ~20 µm base edge, and ~1 µm wall thickness; cells contain isolated internal cavities with no intercellular communication, exhibiting dimensional variability both intra- and inter-sample reflecting natural growth heterogeneity (Silva et al., 2005). Cork cells exhibit

characteristic wall undulation particularly on lateral prismatic surfaces at 2-3 undulations per cell face, intensifying under mechanical stress during growth to form pronounced wrinkles most evident in transitional zones between growth seasons where newly formed cells collapse under pressure from late-season cells; late-season cells with thicker walls and shorter prisms show reduced undulation and enhanced mechanical resistance, with high suberin and wax content enabling wall flexibility and layer sliding during undulation without fracturing (Pereira et al., 1987; Pereira, 2015). Cork tissue comprises dead cells lacking cytoplasmic content with gas-filled cavities bounded by thin cell walls exhibiting complex multi-layered organization: a thin inner primary wall rich in lignin and cellulose, a thicker secondary wall with alternating suberin and wax lamellae (potentially partially lignified), and a thin polysaccharide-rich tertiary layer surrounding the lumen (Xiaozhou et al., 2017). Seasonal growth rhythms produce two distinct cell types: early cork cells (spring-summer) with larger dimensions and thinner walls comprising 90-95% of cork volume in 50-150 cellular layers per annual ring, and late cork cells (late summer-autumn) with reduced height, thicker walls, darker microscopic appearance in 4-8 cellular layers representing ~20% of volume but significantly influencing mechanical properties including rigidity and compressive resistance (Pereira, 2015). Standard light microscopy reveals no apparent cell wall openings, however transmission electron microscopy detects submicroscopic plasmodesmata (~100 nm diameter)—vestigial channels from cell division facilitating pre-mortem cytoplasmic exchange; macroscopic lenticular channels represent cork porosity visible as circular points or parallel lines, with porosity coefficients ranging from <2% (premium quality) to >15% (low quality) directly influencing material properties and commercial value (Pereira et al., 1987; Costa et al., 2019).

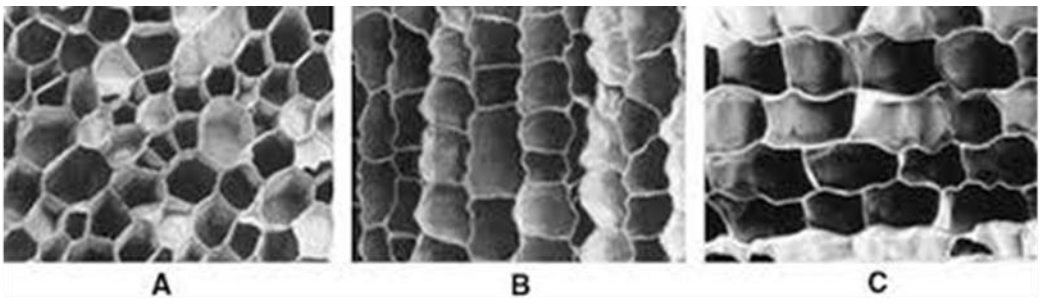


Fig. 2.10. SEM images depicting the three principal anatomical planes of cork tangential (a), transverse (b), and radial (c) sections (Pereira, 2015).

2.2.7. Chemical Properties

Chemical investigations of cork date to the 18th century by Brugnatelli (1787) and Chevreul (1815), with Klauber's (1920) report representing the first comprehensive compositional analysis, followed by identification of cellulose Zetsche & Rosenthal (1927) and extensive studies by Pereira (1988), Conde (1998), and Dehane (2014) (Pereira, 2015; Gomes, 2016). Chemical constituents form a three-dimensional solid matrix encasing air-filled cells, with composition varying based on geographical origin, climatic and edaphic conditions, genetic background, tree dimensions and age, cork type (virgin vs. regenerated), and environmental growth conditions (Silva et al., 2005). Fig. 2.11 illustrates an analytical investigation of three anatomical bark layers (rhytidome, phellem, phelloderm) reveals compositional gradients with suberin predominating across all layers, lignin as second major component, significantly higher suberin concentrations in phelloderm and phellem than rhytidome, holocellulose and lignin concentrating in outer bark, greatest compositional variance in suberin and holocellulose levels, and no significant geographical variation (Jové et al., 2011). Suberin (43% dry mass), the predominant cork component, is a glyceridic polyester conferring exceptional elasticity with monomeric composition of glycerol (40.8%), α,ω-dicarboxylic acids (36.4%), ω-hydroxy acids (21.0%), and ferulic acid (2.7%); compositional variation exists between virgin cork (ω-hydroxy acids 47.0%, α,ω-dicarboxylic acids 11.7%) and reconstituted cork (α,ω-dicarboxylic acids 53.0%, ω-hydroxy acids 30.6%), with suberin forming lamellar structures enabling cell wall deformation and recovery under mechanical stress. Lignin (22% dry mass) is a complex cross-linked aromatic polymer providing structural rigidity and compressive strength, derived from p-coumaryl, coniferyl, and sinapyl alcohols, with cork lignin profile comprising 95% guaiacyl units, 3% syringyl units, 2% p-hydroxyphenyl units, and ~14% methoxyl content. Polysaccharides (20% dry mass) represent the least structurally significant cell wall component, with cork containing substantially less cellulose/hemicellulose than wood (20% vs. 70-80%), distributed as cellulose (~10%), hemicellulose (~12%), neutral sugars (glucose 46%, xylose 25%, arabinose 18%, minor galactose/mannose/rhamnose), and uronic acids (~12% of total polysaccharides) (Pereira, 2015). Extractives (16.2% average) comprise non-polar compounds (5.8%) and polar compounds (10.4%), with total content ranging 8-24% including lipophilic compounds (triterpenes, fatty acids, alkanes, alkanols) and phenolic compounds (phenols, flavonoids) (Costa et al., 2019). Cork stopper

functionality derives from specific chemical properties: suberin imparts flexibility and compressibility, lignin provides structural rigidity, and extractives (particularly waxes) enhance impermeability to liquids/gases preventing wine oxidation, with free (non-bonded) components influencing wine organoleptic properties (Silva et al., 2005).

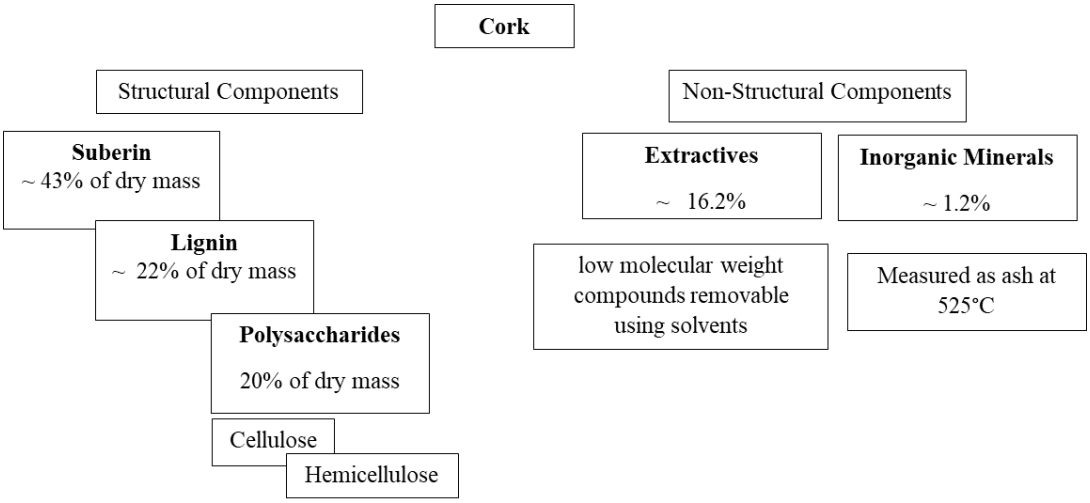


Fig. 2.11. Chemical Composition of Cork (Pereira, 2007).

2.2.8. Physical Properties

Cork exhibits remarkably low density (120-200 kg/m³) resulting from cellular structure of hollow closed cells with minimal solid material, conferring slow water absorption rate, high surface buoyancy, and exceptional lightweight characteristics (Machado et al., 2016). Cork provides outstanding thermal insulation due to high air content, small closed-cell dimensions preventing gas convection, multiple cell walls causing repeated thermal radiation absorption/reflection, low thermal conductivity of trapped air, and minimal solid material proportion, with heat transfer mechanisms (conduction, convection, radiation) significantly reduced by cellular architecture (Silva et al., 2005). Cork demonstrates exceptionally slow water diffusion with diffusion coefficients of 1×10^{-11} m²/s (non-radial) and 4×10^{-10} m²/s (radial), permeability of 280.5×10^{-13} mol/(m.s.Pa) for liquid water and 110.1×10^{-13} mol/(m.s.Pa) for water vapor, attributed to absence of open intercellular channels, hydrophobic suberin in cell walls, and lipophilic extractives; gas permeability to non-condensable gases (He, O_2, N_2, CO_2) is significantly low with transport occurring primarily via molecular flow through plasmodesmata channels following Knudsen diffusion mechanism (Pereira, 2015). Cork exhibits hydrophobicity with low

wettability toward polar liquids (water), lipophilicity with high affinity for non-polar liquids (resins) influencing adhesive/coating interactions, and high friction coefficient enhancing grip applications. Cork demonstrates low sound transmission rate with high acoustic resistance (~1051.2 $kg \cdot m^{-2} \cdot s^{-1}$), sound absorption coefficients >0.6 at 1-5 kHz (natural cork, outer surface orientation), 100% sound absorption at 2100 Hz in 85% cork composites, and particular effectiveness at 500-2000 Hz frequency range (Novais et al., 2020; Miguel et al., 2021).

2.2.9. Mechanical Properties

Cork is a unique viscoelastic material capable of substantial deformation under pressure without fracturing, complete dimensional recovery upon pressure release, and no cellular or cell wall breakage even at > 60% strain. Cork exhibits minimal perpendicular dimensional change during compression resulting in very small Poisson's ratios, with compressive properties strongly influenced by density and Young's modulus of ~10.4 MPa (radial direction) and ~9.2 MPa (non-radial direction); the cellular structure facilitates substantial energy absorption and post-deformation shape recovery suitable for shock-resistant and load-bearing applications. Tensile behavior is strongly dependent on density and porosity with fracture initiation near pores, while bending causes fracture on tensile side when critical strength is exceeded; Young's modulus is significantly lower in compression than tension due to cell wall corrugation influencing tension-compression asymmetry. Advanced nanoindentation techniques reveal hardness of ~0.54 GPa (untreated) decreasing to ~0.51 GPa (boiled) and Young's modulus of ~11.47 GPa (untreated) increasing to ~11.81 GPa (boiled), indicating that boiling enhances cell wall flexibility, reduces hardness, and improves deformation/compression capacity without fracture (Silva et al., 2005).

2.2.10. Thermal Insulation and Fire Resistance

Cork's low thermal conductivity stems from minimal solid material proportion, gas trapped within closed cells, prevention of thermal convection by small closed cells, and repeated absorption/reflection of thermal radiation on multiple cell walls; cork plays significant roles in building thermal insulation and energy conservation, with cork-based composites with alkaline-activated materials achieving thermal conductivity as low as 68 mW/m·K among the lowest recorded values (Novais et al.,

2020). Cork's specialized cell wall structure confers superior thermal stability compared to synthetic polymers (polystyrene, polyurethane), retaining fundamental cellular structure at 350°C (with some cell expansion and wall thinning) and maintaining basic structure above 2000°C; minimal polysaccharide content and suberin thermal stability contribute to high-temperature performance, positioning cork as ideal fire-resistant insulation material with promising cladding system performance versus conventional plastic foams in ignition time, heat release rate, and fume emission (Pereira, 2015; Benhalima et al., 2020).

2.2.11. Hygroscopic Properties and Porosity

Cork exhibits complex water interaction mechanisms influenced by its cellular structure and porosity characteristics. Water diffusion occurs through cellular cavities, particularly under low relative humidity, affecting physical properties and compressibility, with advanced imaging techniques (NMR, THz spectroscopy / imaging, electrical resistance measurement) enabling liquid movement tracking through the cellular structure (Teti et al., 2011). Structural modifications significantly impact water absorption: reducing cork particle size below 0.1 mm destroys ~98% of intact cells through extensive cell wall rupture, dramatically increasing exposed open cells and surface area-to-volume ratio while maintaining chemical composition but losing original physical structure and functional properties (Pereira, 2015). Water absorption proceeds through two distinct phases (Phase 1 involving cell wall swelling with dimensional and mass changes, and phase 2 with mass increase only as water enters saturated cells) with diffusion coefficients at 90°C approximately twice room temperature values, activation energy of ~62 kJ/mol comparable to polymeric materials, and a unique evaporation-condensation mechanism enabling water penetration into closed cells. Cork quality significantly influences absorption capacity, with lower-grade specimens absorbing substantially more water and showing greater thermal expansion at 100°C; dimensional stability corresponds to cell wall moisture saturation, while a 1 mm-thick cork sheet requires >1 year for full saturation, highlighting complex slow water diffusion processes (Miguel et al., 2021).

Cork porosity originates from lenticular channels—cylindrical radial passages with lignified non-suberized cell walls, loose cellular arrangement, and large intercellular spaces that facilitate gas exchange (O_2, CO_2) and moisture transfer between internal tissues and external environment. Porosity coefficients range from <2% (high-quality cork) to >15% (low-quality cork), with substantial inter-tree and intra-tree variations

representing genetic adaptation to environmental fluctuations; progressive porosity decrease from trunk base to apex results from lenticular channel size reduction, demonstrating strong genetic control and functional adaptation (Silva et al., 2005). Lenticular channel density and size critically determine permeability, mechanical properties, thermal insulation characteristics, and commercial quality for applications including stoppers and industrial uses (Costa et al., 2021).

2.3. Cork Concrete: Composite Material Properties

The incorporation of natural cork aggregate into concrete production represents a modern approach within the field of sustainable materials engineering. This strategy offers an innovative scientific contribution to the development of environmentally friendly construction materials with enhanced thermal and mechanical properties.

Virgin cork is known for its unique closed-cell microstructure, in which approximately 90% of its total volume is made up of air voids. This structure consists of a cellular microstructure comprising closed air cells enclosed by thin walls predominantly composed of suberin, a natural hydrophobic biopolymer. The organic cell walls provide relative resistance to water penetration, while fine intercellular pores enable connectivity between adjacent cells. This structure yields a highly porous material (85-95% porosity) and considerable absorption capacity under prolonged fluid exposure with low density (300-1600 kg/m³) than conventional concrete (2400 kg/m³) with density reduction up to 50% depending on cork proportion, providing benefits of lighter structural systems, cost savings in foundation design, and reduced support infrastructure requirements (Branco et al., 2013). Thermal conductivity ranges from 0.04-0.25 W/m·K compared to conventional concrete's 1.0-2.0 W/m·K representing up to 50% reduction, with energy efficiency including heating/cooling cost reduction up to 30%, high specific heat capacity providing thermal mass properties for heat absorption/storage/gradual release, excellent resistance to temperature fluctuations, minimized thermal cracking risk, and stable indoor temperatures (Barnat-Hunek et al., 2018). Cork's cellular and porous structure enhances acoustic insulation with impact noise transmission reduction up to 58 dB, sound absorption coefficient improvement up to 40% versus conventional concrete, and effectiveness at 500-2000 Hz frequency range for residential and commercial applications (Branco et al., 2013). Compressive strength ranges 2.5-10 MPa (cork content 10-50%) adequate for non-structural and certain structural applications with good flexibility and shock absorption enhancing cracking and dynamic load

resistance; tensile strength ranges 1-2 MPa (relatively low) with potential improvement through reinforcing fibers/meshes, while flexural strength ranges 0.5-2.5 MPa (inversely proportional to cork content) limiting load-bearing structural applicability but suitable for non-structural applications (Soares et al., 2014). Durability reaches up to 3× conventional material durability with hydrophobic nature ensuring long-term stability, natural resistance to fungal growth and mold ideal for humid environments, good resistance to weak acids/salts/alkalis retaining structural integrity in aggressive conditions, moderate fire resistance when treated with flame retardants, and good freeze-thaw resistance with minimal mechanical property deterioration. Sustainability profile includes reduced carbon footprint, resource efficiency utilizing cork waste, energy efficiency through superior insulation, recyclability and reuse potential, and improved indoor environmental quality, with applications in residential projects (exterior/interior walls, roofing, flooring, precast units) and specialized applications (3D printing, geopolymer composites, historic building conservation, electromagnetic/marine insulation) (Barnat-Hunek et al., 2018). Performance summary from previous studies in Table 2.1 shows physical properties with cork content 0-80% exhibiting density from 2456 kg/m³ (0%) to 614 kg/m³ (high cork replacement) and thermal conductivity from 1.52 W/m·K (0%) to 0.10 W/m·K (high cork replacement) (Ghernouti, 2023; Marcos et al., 2023 & Pacheco Menor et al., 2024) mechanical properties show compressive strength from 67.5 MPa (0%) to 0.56 MPa (≥70%) and flexural strength from 9.9 MPa (0%) to 0.8 MPa (high replacement); durability shows total porosity 4.57-49.55%, water absorption 8.5-94.36%, improved freeze-thaw resistance with mineral additives, and enhanced chloride diffusion resistance with additives, requiring critical balance between enhanced thermal properties and reduced mechanical strength (Merabti et al., 2021; Ortega et al., 2022; Ziregue et al., 2022).

Table 2.1. Comprehensive Comparison Table of Previous Studies on Cork in Construction Materials.

Study	Material Type	Mechanical Properties	Durability	Key Findings
(Pacheco Menor et al., 2024)	Granulated Cork with Bark (GCB) replacements 0–40%	Density: 1900 - 2225 kg/m³ (dry densities) Compressive: 7.2 - 7.3 (28d for 20–30% replacement) Flexural: 3.0 - 3.3 MPa (28d)	Very low strength (non-structural); water penetration depths high (avg 51.7–81.3 mm) Thermal conductivity ~0.85 - 1.05 W/m·K (28d) Total porosity 19.3 - 21.1%; gel & capillary pore distribution provided Water Abs: 8.5 - 11.2% (28d)	Suitable for non-structural lightweight blocks with good thermal insulation
(Ghernouti et al., 2023)	SCC with 0–75% EBCA (cork residue replacement)	Density: 1750 - 2370 kg/m³ Compressive: 36 → 8 MPa (control 36 MPa; drops with higher replacement of cork) Flexural: 7 → 4 MPa (decreases with replacement)	Bulk density reduction up to 21%; classified as structural lightweight at some replacements (≥17 MPa) Workability maintained at low replacements; strength and density trade-offs observed	EBCA (cork ash/residue) reduces density but also reduces mechanical strength as replacement increases
(Ortega et al., 2023)	Mortars with sand, expanded cork, natural cork, expanded clay combinations (50/50 mixes)	Density: 1050 -1400 kg/m³ (bulk density after 1 yr)	Expanded cork shows higher long-term water uptake; natural cork slightly better performance 22 - 32% (absorption after 1 yr for 50% expanded cork mixes) Permeable pore space up to 32%; 48h immersion absorption up to 28%	Important for durability; cork increases long-term water ingress especially for expanded cork
(Ortega et al., 2022)	Natural cork 50% or expanded clay 50%	Compressive < 6 MPa (natural cork mortars) Flexural < 2 MPa	Adequate long-term chloride resistance (1 yr) despite low strength; pore structure improves over time Porosity increased; cork yields less refined pores	Recommended for non-structural marine applications due to chloride resistance and insulation
(Ziregue et al., 2022)	CLCC mixes 0–70% cork content	Compressive: 24.4 (control) → 12.22 (20%) → 0.56 (70%) MPa	High replacement (≥60–70%) results in very low strength; modulus drops from 28,000 to 8,540 MPa at 20% and lower after	Compatibility issues at very high cork contents; significant loss of stiffness and strength
(Merabti et al., 2021)	Cork/ligand ratios C/L 1/1, 1/2, 1/3	Density: 614 - 1572 kg/m³ (bulk densities) Compressive 1.6 - 7.0 MPa (1–365d) Flexural : 2.5 - 8.5 MPa	Low strengths but very low thermal conductivity; suitable for insulation and non-load-bearing panels Thermal conductivity 0.10 - 0.46 W/m·K	Cork composite shows wide density & strength range depending on formulation and curing

Along the same lines, in recent years, research within the field of cork concrete has increasingly focused on integrating virgin cork, derived from the first harvest of cork oak bark, leading to the development of what is now referred to as "virgin cork concrete". (Tedjditi et al., 2020) examined the feasibility of using raw natural cork granules in lightweight concrete production through an experimental methodology involving five concrete mixtures with varying cork proportions (0%, 25%, 50%, 75%, and 100%). Comprehensive laboratory testing assessed physical and mechanical characteristics including workability via slump test, density, ultrasonic pulse velocity, compressive and tensile strength, plastic viscosity, and microstructural analysis through Scanning Electron Microscopy (SEM) to examine interfacial bonding, porosity, water absorption, and thermal properties. Results in Fig.2.12 revealed that workability exhibited notable decline with increasing cork content, shifting from high values in the reference mix to significantly lower levels in cork-rich mixtures, while density decreased progressively in direct correlation with cork proportion; conversely, both porosity and water absorption Fig.2.13, increased with rising cork percentage, reflecting substantial alterations in internal structure and permeability. A significant reduction in compressive strength was observed, decreasing from 31.4 MPa in the reference mixture to 0.5 MPa at 100% cork content Fig.2.14.

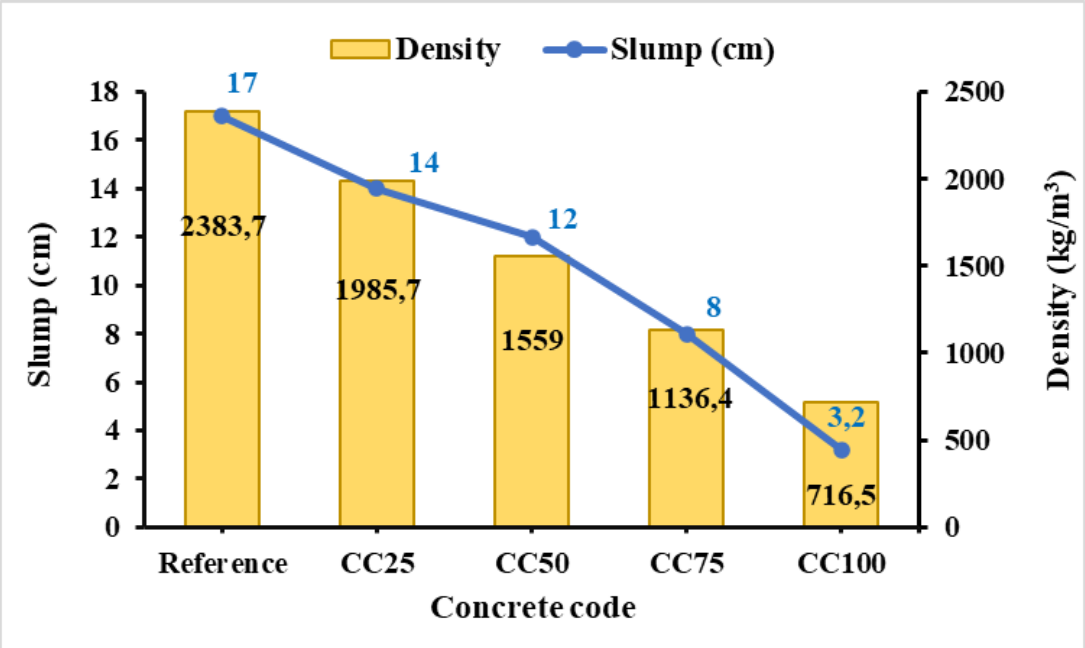


Fig. 2.12. Workability and density of the different mixtures (Tedjditi et al., 2020).

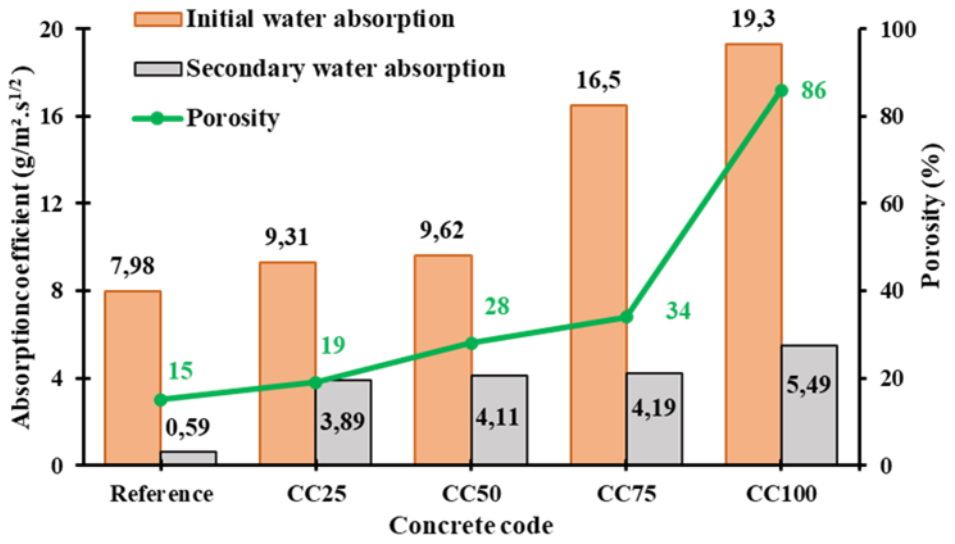


Fig. 2.13. Initial, secondary & water absorption coefficient of concretes (Tedjditi et al., 2020).

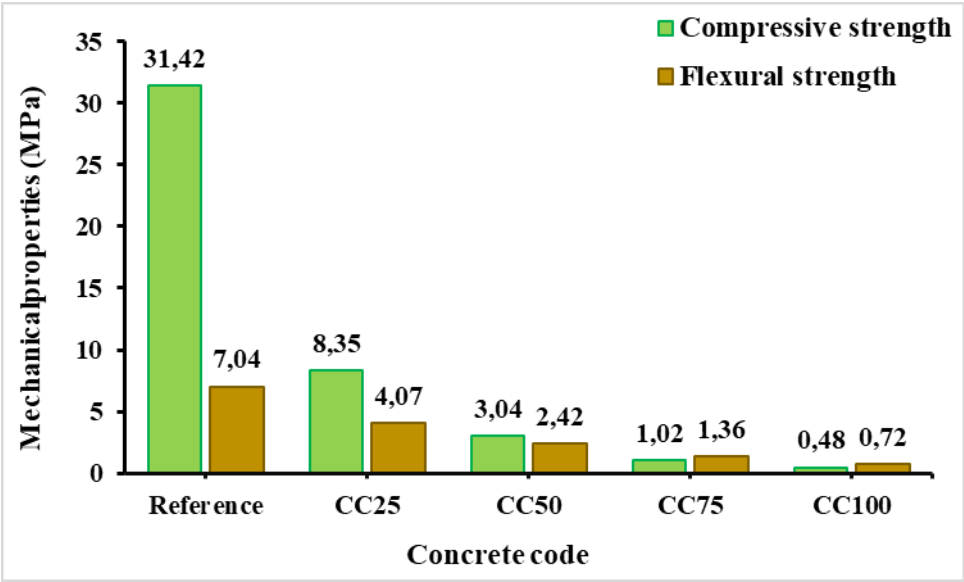


Fig. 2.14. Mechanical properties of concretes (Tedjditi et al., 2020).

Building upon this foundation, Tedjditi et al. (Tedjditi et al., 2020) further investigated the influence of different cork water absorption levels during cork concrete preparation, examining nine mixture types with varying cork ratios (25%, 50%, 75%) and three water absorption conditions: no water (W0), 2-hour water absorption (W2H), and saturation water (WSAT). Fig.2.15 demonstrated that cork water absorption capacity significantly influences concrete properties, notably enhancing consistency while reducing workability and causing linear density decrease, though all specimens remained within lightweight concrete classification. The impact on

porosity was closely related to cork proportion, with the highest mercury intrusion volume recorded in WSAT samples; specifically, the CC75WSAT specimen reached 51.4% open porosity, representing a 95% increase. Thermal conductivity values ranged between 140 and 1230 mW/(m·K), with optimal performance observed in the W2H mix, while specific heat capacity at 23°C varied from 889 to 1159 J/(kg·K), reaching maximum values in WSAT samples. Results indicated noticeable improvement in hygroscopic performance with increased cork water absorption; however, compressive strength decreased with increasing cork absorption, showing clear inverse relationship with cork content. These comprehensive investigations collectively demonstrate that raw cork represents a sustainable and environmentally friendly alternative material for lightweight concrete production, distinguished by reduced density, favorable thermal insulation properties, and adequate mechanical performance for non-structural applications, while cork incorporation contributes to reducing the environmental footprint of construction materials through utilization of renewable natural resources.

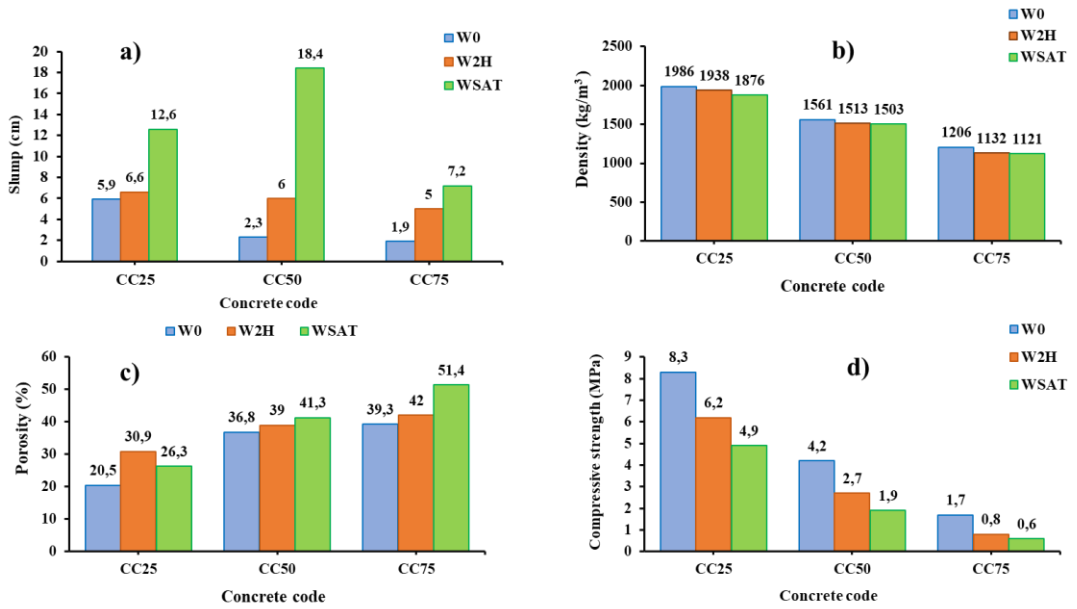


Fig. 2.15. Physical and mechanical properties of cork concrete (Tedjditi et al., 2020): a) Workability, b) Density, c) Mercury porosity, d) Compressive strength.

In summary, cork concrete serves as a compelling example of innovation within sustainable building materials, effectively combining exceptional thermal and acoustic insulation properties, low environmental footprint, and structural performance suitable for diverse applications, positioning virgin cork concrete as a

promising material warranting further research and development amid increasing global emphasis on green construction and energy efficiency.

2.4. Lime concrete: a versatile building material

Lime concrete is a specialized type of concrete that incorporates limestone, a sedimentary rock predominantly composed of calcium carbonate ($CaCO_3$) originating from the fossilized remains of ancient marine organisms. Owing to its wide availability, durability, and versatility, limestone has been extensively used as a construction material for centuries. In recent years, the incorporation of limestone into concrete mixtures has attracted increasing attention in the construction sector, as it offers distinctive properties that make it suitable for a broad range of applications.

One of the key reasons for selecting limestone ($CaCO_3$) as a mineral addition in this study is its wide availability, low cost, and its role as a mineral filler in cementitious systems.

Furthermore, the studies summarized in Table 2.2 indicate that the incorporation of limestone into concrete mixtures results in multiple improvements in material properties, positively influencing overall performance and durability. Limestone contributes to enhanced compressive strength, with reported increases of up to approximately 20% compared to conventional concrete, making it suitable for load-bearing applications. Beyond mechanical enhancement, the smooth and rounded morphology of limestone particles improves concrete workability, facilitating placement and finishing operations. Its inherent resistance to weathering and chemical attack further enhances durability, enabling improved long-term resistance to environmental degradation. Additionally, the high thermal mass of limestone contributes to improved thermal performance by moderating temperature fluctuations, thereby supporting building energy efficiency. Finally, limestone incorporation helps reduce shrinkage commonly associated with conventional concrete mixtures, leading to improved dimensional stability and long-term performance (Zareei et al., 2017; Turk et al., 2022 & Chang et al., 2024).

Table 2.2. Summary of Research Findings on Limestone-Based Concrete.

Study	Limestone Content	Results
(Kim et al., 2018)	Concrete with varying % limestone powder replacing cement (10%, 20%, 30%) different mixes tested and compared.	10% LP replacement: 28-day compressive strength close to control, splitting tensile & flexural strength only slightly lower; 20%–30% replacement: strength reduction more significant; durability (porosity, permeability) slightly improved at low LP.
(Ahmed et al., 2020)	In some mixes, limestone powder up to 15% by weight of cement replaced cement in self-compacting concrete (SCC) mixes.	Fresh-state self-compactibility achieved; but compressive strength decreased with increasing LP replacement (because of dilution effect), compared to pure-cement SCC.
(Zhang et al., 2025)	Limestone powder (LP) used as part of cementitious materials (LP content ranged 0–35% by mass of cementitious materials). Optimal results when LP ≤ 15%.	For LP content ≤ 15% and LP-specific surface area ≤ 600 m^2/kg, concrete showed improved physical (workability) and mechanical properties. If LP content increases, strength and freeze–thaw resistance decrease (for higher LP).
(Chang et al., 2024)	Concrete with manufactured sand & limestone powder (LP used as fine material) from 5 to 20%	Mechanical strength and durability improved when mixing method optimized: better workability, acceptable compressive strength, improved permeability/durability metrics.
(Turk et al., 2022)	In this ECC (Engineered cementitious composites) study, limestone powder (LSP) replaced silica sand (SS) by 50% or 100% by mass of the sand fraction.	Replacement of sand by LSP improved both compressive and flexural strength, and enhanced durability (lower permeability, better freeze–thaw and chloride resistance) due to pore refinement.
(Zareei et al., 2017)	Lightweight aggregate concrete mixes with limestone powder replacing cement at (0–20%) plus micro-silica and lightweight aggregates	7- and 28-day tests: shows optimum replacement levels (often lower % LP), concrete remains structurally viable; higher LP tends to reduce compressive strength but can still be acceptable depending on mix and use-case. Water absorption is low and chloride penetration decreases with increasing LP.

2.5. Conclusion

This chapter examines plant-based materials with potential for integration into concrete mixtures, with particular emphasis on cork as a promising prospect in the construction sector due to its distinctive physical properties and its abundance within Algeria's forest resources. The chapter also provides a systematic review of previous studies addressing the use of cork in concrete and mortar. The literature survey reveals that most existing research has focused on cork derived from waste generated during bottle-stopper manufacturing or from industrially processed expanded insulation boards, while the use of raw, natural cork as aggregate in cementitious mixtures has received comparatively little attention.

Based on preliminary results obtained in our laboratory regarding the incorporation of raw cork into concrete mixtures, it has been demonstrated that this natural material constitutes a suitable alternative for the development of lightweight concrete. The resulting composite is characterized by low density and effective thermal insulation performance. Moreover, the water absorption capacity of cork during the mixing stage emerges as a key parameter influencing the overall properties of cork concrete, with absorption effects increasing proportionally to the amount of cork introduced into the mixture. Notably, concrete produced with water-saturated cork exhibited the highest specific heat capacity. Although increased cork absorption leads to a reduction in compressive strength, cork concrete maintains adequate performance for non-structural and insulating applications.

The following chapter will present a detailed description of the raw materials used in preparing the concrete mixtures, along with an explanation of the laboratory procedures and methods employed to determine and evaluate their various properties.

Chapter 3

Characterization of raw materials and experimental methods

Introduction

The current chapter outlined the adopted research methodology in detail, covering all phases from the identification of key study variables to the development of an integrated experimental framework. A comprehensive characterization of the raw materials used in this study—including cement, fine and coarse aggregates, and both chemical and mineral admixtures—was carried out in accordance with international standards, highlighting their physical and chemical properties.

In addition, the procedures used to design and prepare the various concrete mixtures were thoroughly explained. This included determining the appropriate mix proportions, methods of mixing, casting, and curing, as well as the testing techniques employed to evaluate the fresh and hardened properties of the concrete. A combination of standard and advanced testing protocols was used to ensure a reliable and in-depth assessment.

3.1. Experimental study presentation

This study builds upon a series of previous investigations that established a solid knowledge base regarding the feasibility of using virgin cork as an alternative aggregate in concrete systems, leading to the development of preliminary formulations based on this renewable natural resource. In particular, the formulation proposed by (Tedjditi et al., 2020) identified a cork substitution rate of approximately 25% as an optimal threshold, providing a balance between weight reduction and acceptable mechanical performance, while highlighting the significant reduction in compressive strength observed at higher cork contents, which limits their applicability in structural concrete.

In addition, earlier findings demonstrated that pre-treating 25% of the cork by soaking it in water for two hours prior to mixing significantly enhanced mix homogeneity, reduced particle distribution irregularities, and improved the mechanical properties of the interfacial transition zone between the cork and the cement paste, while also contributing to a reduction in thermal conductivity. However, these improvements remained limited in mixtures with higher cork contents, where particle segregation and weak internal bonding were observed, ultimately leading to a pronounced decline in mechanical strength and restricting their use to non-structural applications (Tedjditi et al., 2022).

This work forms part of a comprehensive research program dedicated to developing virgin cork concrete and investigating its physical and mechanical properties under laboratory conditions. The central challenge lies in enhancing the structural performance of cork concrete while preserving its inherent environmental and thermal advantages. Within this context, the study focuses on evaluating the behavior of this concrete type under aggressive marine environments by examining chloride ion diffusion mechanisms through its porous matrix.

To achieve these objectives, the cement dosage was increased to 450 kg/m³ to enhance mechanical performance, and a 10% limestone powder addition was incorporated to refine the microstructure, while maintaining standardized mixing protocols. The water-to-cement ratio was also reduced to improve internal cohesion and minimize crack formation or undesirable increases in porosity.

Based on these considerations, and to assess the effect of cork pre-treatment, a comparative study was conducted between two concrete formulations containing 25% cork replacement, with or without limestone powder:

- **Formulation A:** Direct incorporation of the calculated absorbed water during mixing, corresponding to the amount absorbed by the cork over a two-hour period—identified as the transition from rapid to slow absorption approaching saturation ($OC+HC_{2h\,AW}$).
- **Formulation B:** Pre-soaking the cork for two hours prior to its incorporation into the concrete mixture ($OC+HC_{2h\,IW}$).

This study contributes to the advancement of sustainable concrete technologies by developing improved cork-based concrete formulations that satisfy structural requirements. Furthermore, the enhanced understanding of chloride ion transport mechanisms in this material provides a scientific foundation for assessing its durability under harsh environmental conditions, thereby supporting the design of sustainable infrastructure solutions.

3.2. Materials

This chapter provides a comprehensive overview of the primary constituents employed in the preparation of concrete mixtures, namely the hydraulic binder (cement), high-range water-reducing admixtures (superplasticizers), mineral aggregates, and bio-based cork aggregates. It also outlines the various mixture formulations adopted in the present study, accompanied by a detailed description of the specimen preparation procedures, carried out in accordance with established technical standards. The chapter concludes with an in-depth presentation of the experimental methodologies and analytical techniques applied to assess the performance of cork-based concrete systems.

This section specifically focuses on the classification and characterization of the physical and microstructural properties of the raw materials used in the production of cork concrete. The materials under investigation include the cementitious binder, mixing water, conventional mineral aggregates (e.g., sand and gravel), and bio-sourced aggregates in the form of cork.

3.2.1. Cement

Throughout the experimental campaign, a type of blended Portland cement classified as CPJ CEM II/A 42.5N was used. This cement complies with the Algerian standard (NA 442, 2013) and is produced by the Beni Saf Cement Company (SCIBS), located in (Beni Saf) Aïn Temouchent city.

The apparent density (ρ_{app}) and the absolute density (ρ_{abs}) of the cement were determined according to the (EN 196-6, 2010) standard. The specific surface area (Blaine fineness) was evaluated using a Blaine air permeability apparatus (Fig. 3.1). A summary of the physical properties of the cement is presented in Table 3.1**,** while its chemical composition is detailed in Table 3.2**.**

3.2.2. Limestone

The limestone filler used in this study belongs to the 0/125 µm particle size class and is sourced from the El Maleh quarry, located approximately 12 km from the city of Aïn Temouchent. This quarry is operated by the National Aggregates Company (NAC). The parent rock is of dolomitic limestone origin. Chemical analysis indicates that the limestone is primarily composed of approximately 53% calcium oxide (CaO). The absence of clay minerals within the limestone matrix was confirmed by methylene blue testing (Taleb, 2017). The relevant physical properties of limestone filler are summarized in Table 3.1, while the chemical composition of the limestone is detailed in Table 3.2. Scanning Electron Microscopy (SEM) observations revealed that the limestone exhibits a soft, powdery texture with particles predominantly presenting a rhomboidal morphology, as illustrated in Fig.3.2.

Table 3.1. Cement & limestone physical properties

Materials	Bulk density (kg/m^3)	Particle density (kg/m^3)	Blaine Specific surface area (cm^2/g)
Cement	1019	3037	3615
Filler	966	2700	5162

Table 3.2. Cement & limestone chemical properties (Taleb, 2017).

Component / Oxide	SiO_2	Al_2O_3	Fe_2O_3	CaO	MgO	K_2O	Na_2O	SO_3	P_2O_5	TiO_2	Loss on Ignition	Cl	Other Components
Cement (%)	22.24	7.11	4.76	56.99	1.51	0.42	0.59	2.05	0.16	0.41	2.60	/	1.16
Limestone (%)	0.06	0.29	0.22	52.63	0.84	0.01	0.08	0.02	0.02	0.02	42.77	0.005	/



Fig. 3.1. Blaine permeabilimeter.

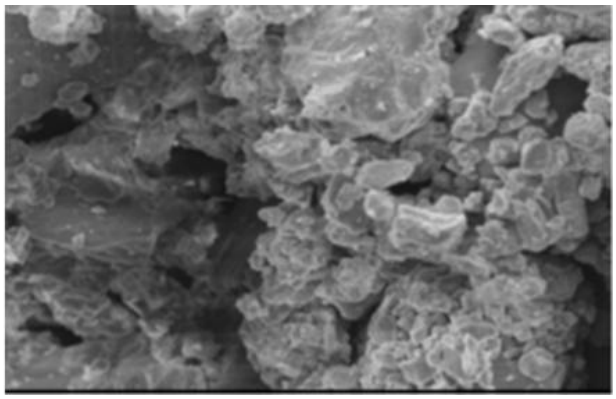


Fig. 3.2. SEM observation of limestone (x5000 enlargement) (Taleb, 2017).

3.2.3. Mineral Aggregates

In this study, crushed limestone aggregate was used as the primary material, supplied by the National Aggregates Company *(NAC)*, located in Sidi Abdelli, Tlemcen city.

The aggregate used in this study was classified into three granulometric categories in accordance with internationally recognized standards in materials engineering. These categories include: sand with a particle size range of (0-4 mm), representing the fine fraction of the mix; small gravel (4-8 mm), constituting the intermediate fraction and coarse gravel (8–16 mm), representing the coarse fraction of the aggregate structure.

The particle size distribution analysis of the aggregates was conducted following the British-European Standard (BS EN 932-1, 2012), which outlines standardized procedures for determining aggregate gradation using the sieve analysis method. Laboratory results, presented in Fig. 3.7, show that all aggregate fractions exhibit a continuous and uniform gradation, indicating compliance with the technical specifications prescribed by international standards.

In this study, the sand exhibited a fineness modulus of 2.92 and contained 12.94% fine particles. These results indicate that the sand falls within the medium grading range, which is generally suitable for concrete applications. However, the fines

content suggests a moderate level of fine materials that may include silt and clay fractions, which should be carefully considered in relation to concrete workability and durability requirements.

These aggregates were used according to the standard EN. The particle size distribution of the aggregates as shown in Fig. 3.6. All laboratory results related to bulk and absolute densities (BS EN 1097-3, 1998). (BS EN 1097-6, 2013), along with the 24-hour water absorption rate (Abs_{24h}), were compiled and presented in an organized manner in Table 3.3. Before mixing, aggregates were dried at 105 °C for 24 hours.

Table 3.3. Physical properties of mineral aggregates.

Mineral aggregates	Bulk density (kg/m^3)	Particle density (kg/m^3)	Water abs_{24H} (%)	Inter particle porosity (%)
Sand 0-4 mm	1636.4	2701.1	1.71	39.4
Gravel 4–8 mm	1310.9	2592.2	1.59	49.4
Gravel 8–16 mm	1179.6	2580.0	1.22	54.3

3.2.4. Virgin Cork Aggregate

In this study, virgin male cork was utilized as a partial replacement for conventional mineral aggregate, while maintaining the same particle size distribution adopted for the reference mineral aggregate.

The cork used in this investigation was sourced from the Ahfir Forest, located approximately 10 kilometers south of the city of Tlemcen. This location was strategically selected due to the availability of high-quality cork oak trees and its proximity to the experimental site, which minimizes environmental impact from transportation and helps preserve the natural characteristics of the material.

To ensure consistency and reliability in comparative analyses, the same granulometric classification applied to the mineral aggregate was also used for the cork aggregate. This classification includes three primary size fractions: fine (0–4 mm), which improves workability; medium (4–8 mm), which supports structural cohesion; and coarse (8–16 mm), which enhances the mechanical strength of the final concrete mix.

3.2.5. Water

Potable water was used for mixing the prepared concrete batches. The chemical composition of this water complies with the requirements specified in BS EN 1008 (BS EN 1008, 2002). A chemical analysis of the water was conducted at a constant temperature of 20 °C, and the pH value was also determined. The detailed results of these characteristics are presented in Table 3.4.

Table 3.4. Chemical Composition and pH of the Mixing Water (mg/L)

(Tedjditi, 2021).

Ca^{2+}	Mg^{2+}	Na^{+}	K^{+}	Cl^{-}	SO_4^{2-}	HCO_3^{-}	pH (-)
110.621	42.282	-	-	99.400	312.740	473.515	8.0

3.2.6. Superplasticizer

The superplasticizer employed in this study was Master Glenium SKY 841, it is a high-performance water-reducing admixture based on polycarboxylate ether (PCE) technology. It possesses a density of 1060 kg/m³, a chloride content of less than 0.1%, and a pH value of 5.5. This admixture is specifically designed for concrete applications requiring extended workability and enhanced mechanical properties. Its formulation complies with the performance criteria outlined in the European standard (EN 206, 2013). The product was sourced from BASF Construction Chemicals company, located in Algiers city, Algeria.

The optimal saturation dosage of the superplasticizer was determined by conducting a flow spread test using the mini-cone apparatus (Fig. 3.3). Due to variations in cement quality resulting from the incorporation of limestone, it was found that the optimal dosage of the superplasticizer ranged between 0.6% and 0.7% of the binder mass, corresponding respectively to the concrete mixtures with and without limestone addition.



Fig. 3.3. Adjuvant used & mini-cone spread test.

3.3. Mechanical Processing and Preparation

The preparation of cork aggregate began with an initial phase of manual collection and sorting within the Ahfir Forest, where high-quality male cork pieces free from impurities were carefully selected. This was followed by mechanical grinding, carried out using a milling machine specifically designed and developed by the research team at laboratory EOLE. The machine was tailored to accommodate the unique physical properties of cork and to ensure the production of a uniform final material.

Upon completion of the grinding process, mechanical sieving was employed to separate and classify the resulting aggregate into three well-graded particle size fractions (Fig. 3.4). These fractions were categorized based on their granulometric size as follows: Fine cork aggregate (0–4 mm), Medium cork aggregate (4–8 mm), Coarse cork aggregate (8–16 mm) (Fig. 3.5).



Fig. 3.4. Virgin Cork Preparation.

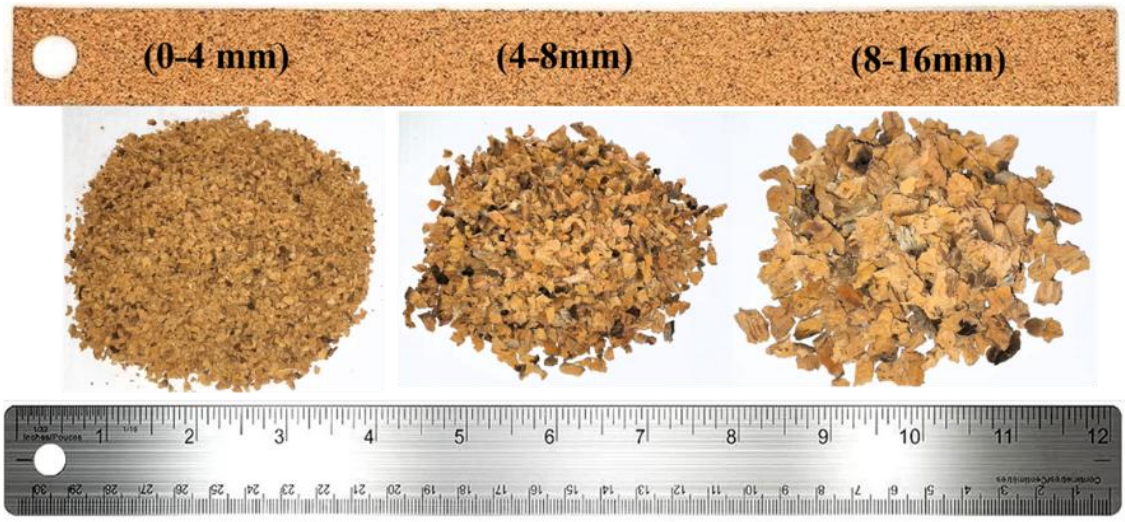


Fig. 3.5. Virgin Cork Classes.

3.3.1. The particle size classification of virgin cork

As for the cork aggregate, its particle size distribution was also assessed in accordance with BS EN 933-1 (BS EN 933-1, 2012). However, due to the unique physical characteristics of cork-particularly its low bulk density compared to conventional mineral aggregates-modifications to the standard testing protocol were necessary to ensure accuracy and applicability. In light of these physical limitations, an adapted methodology was employed, involving the use of sample quantities corresponding to the volume of a single sieve tray. These quantities varied depending on the particle size class being analyzed, with sample weights ranging from 160 to 180 g per fraction. This approach ensured statistically representative sampling while maintaining test feasibility.

The granulometric curves presented in Fig. 3.6 highlight the distinctive distribution characteristics of the various cork aggregate types used in this experimental work. A comparative analysis reveals a relatively uniform particle size distribution in the medium and coarse cork fractions (4-8 mm & 8-16 mm), closely aligning with those of their mineral aggregate counterparts, with only minor variations that do not significantly impact the mix's engineering properties. Conversely, the fine cork aggregate (0-4 mm) exhibits a more pronounced divergence in gradation compared to conventional sand, despite containing a substantial proportion of fine particles. This variation may influence the workability and cohesiveness of the resulting concrete mixes.

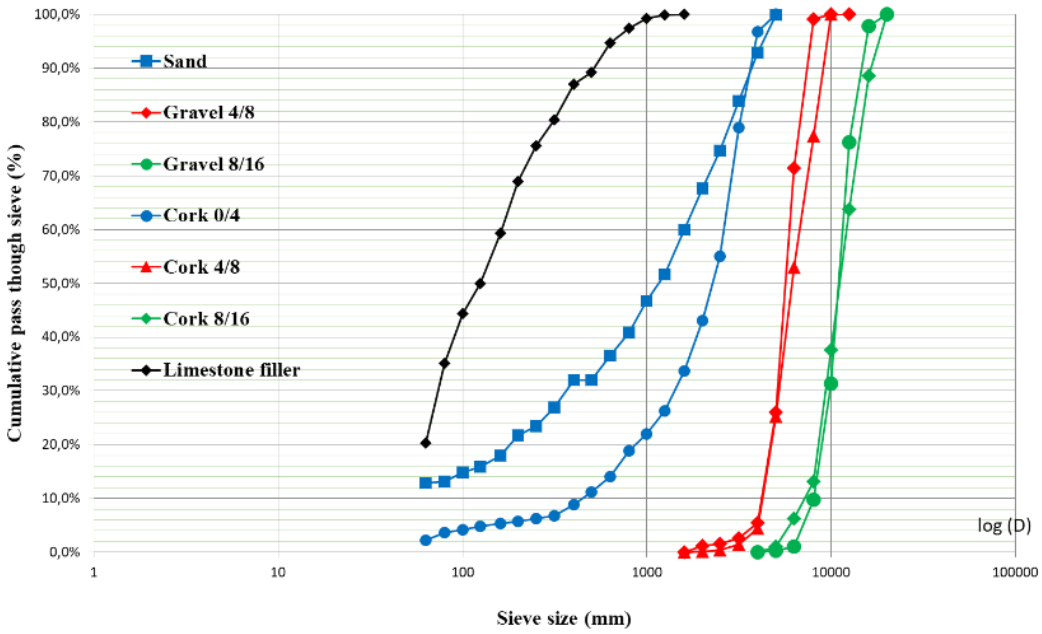


Fig. 3.6. Granulometric curves of mineral and virgin cork granules.

3.3.2. Characterization of virgin cork: Density and absorption

The same standard methodologies used to characterize mineral aggregates were adopted to determine both the bulk and absolute densities of cork aggregate. This ensured methodological consistency, allowing for accurate scientific comparisons and statistically reliable analyses.

Bulk density was measured in accordance with the procedures outlined in BS EN 1097-3 (BS EN 1097-3, 1998), Absolute density was determined using the balloon method, following the specifications of BS EN 1097-6 (BS EN 1097-6, 2013), as shown in Fig. 3.7a. In this latter test, samples of a constant mass of 30 grams were used to ensure uniform testing conditions. Prior to testing, the virgin cork aggregates were dried at a temperature of 60 °C until mass stabilization was achieved. They were then immersed in water for a period of 24 hours to determine their water absorption rate over this duration (Fig. 3.7b). Additionally, the inter-particle porosity was calculated for the various particle size fractions.



(a) (b)

Fig. 3.7. Absolute density test (a), 24 h virgin cork absorption (b).

The average values of bulk and absolute densities for the different cork aggregate types were calculated based on at least three samples per category to ensure statistical reliability. The obtained results are summarized in Table 3.5.

Table 3.5. Virgin Cork Physical Characteristics

Cork aggregate	Apparent density (kg/m^3)	Particle density (kg/m^3)	Water abs $_{24H}$ (%)	Inter particle porosity (%)
Cork 0–4 mm	98.5	200.8	154.6	51
Cork 4–8 mm	91.7	170	91.4	46
Cork 8–16 mm	95.4	207.5	54.2	54

The experimental results indicate that the cork aggregate used in this study, similar to most bio-based materials reported in the literature, exhibits a high-water absorption capacity that can reach nearly twice its dry weight. This value is significantly higher than that observed for conventional mineral aggregates, which generally display very low absorption rates. The absorption behavior is closely related to the particle size distribution of the cork aggregate as well as to the specific surface area available for water interaction. Finer fractions, particularly within the 0–4 mm size range, provide a larger specific surface area and greater water–solid contact, thereby enhancing capillary absorption within the porous cork structure. In addition, the mechanical cutting process leads to more intensive fragmentation of the finer cork particles compared to coarser fractions such as 4–8 mm and 8–16 mm, resulting in a higher proportion of voids and open porosity. Consequently, these microstructural characteristics contribute to the markedly higher water absorption capacity observed in the finer cork aggregate fractions.

3.3.3. Assessment of Virgin Cork Absorption Properties

A series of rigorous laboratory experiments were conducted to elucidate the behavior of cork samples when exposed to different aqueous media, following a two-stage experimental protocol:

- **Cork Water Absorption Tests**

Virgin cork samples were immersed in deionized water under controlled laboratory conditions (20 ± 2 °C). Volumetric changes were monitored daily for 30 days using high precision measurement techniques, whereas mass variations were tracked for 24 days (see Fig. 3.8).

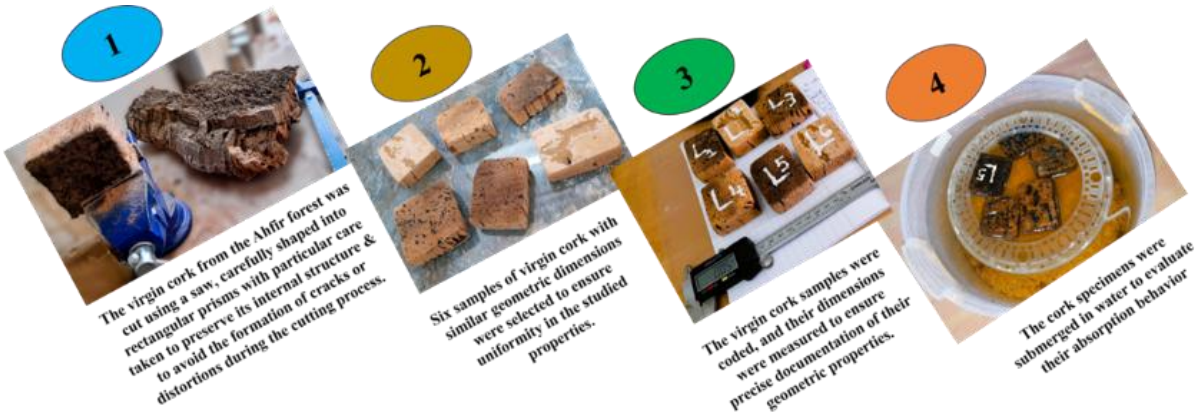


Fig. 3.8. Virgin Cork Water-Absorption Tests.

Experimental investigations conducted on natural virgin cork demonstrated its pronounced capacity for water absorption. However, the three categories of cork samples prepared in the form of fine granules exhibited significantly higher water uptake compared to those manufactured as parallelepiped specimens.

It was further observed that although cork rapidly absorbs water, it also releases it quickly once removed from the water medium. The drying process initiates immediately, and within less than one hour, the material returns to its original dry mass. This behavior plays a particularly important role during the early stages of concrete curing, where the gradual release of stored water promotes internal curing. Consequently, this mechanism contributes to pore structure refinement at the microscopic scale, which positively influences the long-term mechanical performance of cork-based concrete.

The study adopted a systematic experimental approach involving three parallelepipeds virgin cork specimens immersed in water for a total duration of 24 days. The samples reached a saturated state after approximately 18 days of immersion. The recorded parameters included the initial dry mass, post-immersion mass, and the corresponding mass variations, as presented in Fig. 3.9 and summarized in Table 3.6.

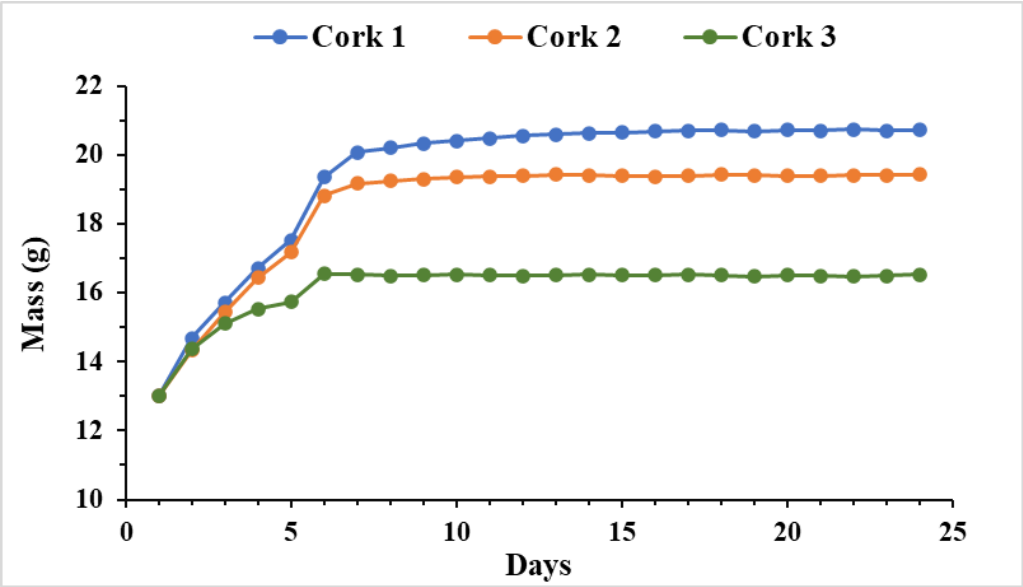


Fig. 3.9. Mass variation after 24 days of immersion.

Table 3.6. Mass evolution after 24 days of continuous immersion.

Virgin Cork Codes	Cork 1	Cork 2	Cork 3
Dry Mass at Initial State (g)	13	13	13
Mass After 24 Days of Immersion (g)	19.52	18.52	16.15
Mass increase (%)	50.2	48.4	25.8

The water absorption kinetics of the three virgin cork specimens shaped as parallelepipeds revealed a clear two-stage behavior over the 24 days immersion period. All samples started from the same initial dry mass (13 g). The first stage corresponds to rapid absorption during the initial seven days, characterized by a steep increase in mass due to fast capillary filling of large and open pores. This phase is followed by a second stage (7–24 days), during which the absorption rate gradually decreases until equilibrium is reached.

Quantitative results indicate significant variability among the samples. Cork 1 exhibited the highest mass increase, reaching 50.2% (19.52 g), followed by Cork 2

with 48.4% (18.52 g). In contrast, Cork 3 showed a substantially lower increase of only 25.8% (16.15 g), representing nearly a 95% difference compared to Cork 1. This pronounced variation reflects fundamental differences in pore structure, pore size distribution, and apparent density. Higher absorption levels are associated with a more open cellular structure and greater overall porosity.

Furthermore, Fig. 3.10 and Table 3.7 illustrate the mass evolution of cork granules of different particle sizes during a 12-day immersion period. Small-sized particles (0–4 mm) exhibited continuous and rapid mass growth, reaching saturation by the 9 days at 139 g and recording the highest relative increase (178%). In contrast, larger particles (6–8 mm) showed the lowest growth rate (118%) and the smallest overall mass change (96%). For all three particle size categories, mass stabilization was observed from the ninth day onward.

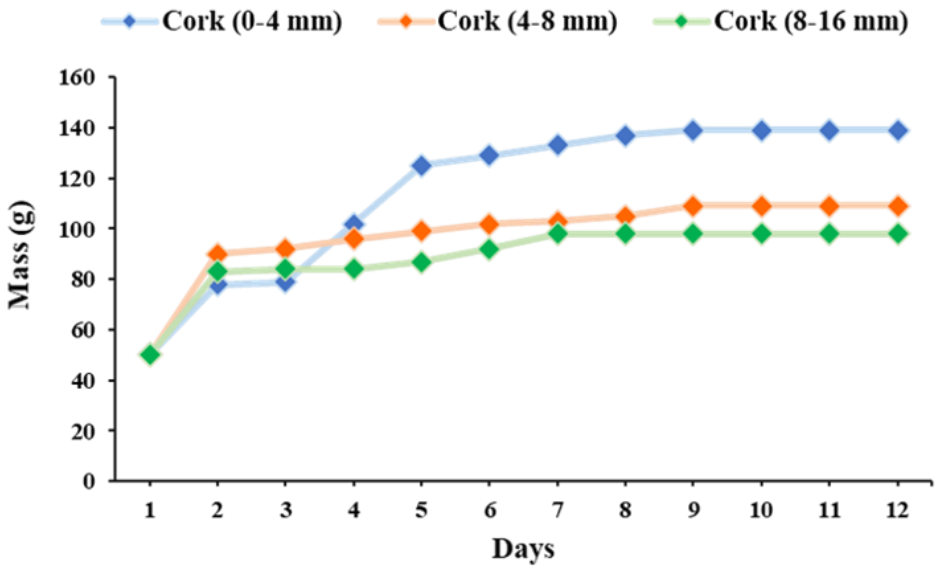


Fig. 3.10. Mass variation of the three categories of cork after immersion to saturation.

Table 3.7. Mass differences in the three cork types after immersion until saturation.

Cork Classes	1	2	3	4	5	6	7	8	9-12	Mass increase (%)
0 - 4 mm	50	78	79	102	125	129	133	137	139	178
4 - 8 mm	50	90	92	96	99	102	103	105	109	118
8 -16 mm	50	83	84	84	87	92	98	98	98	96

These findings demonstrate a clear inverse relationship between particle size and mass growth rate. Smaller cork particles, due to their higher surface area-to-volume ratio, displayed greater water absorption capacity. This enhanced absorption can be attributed not only to the intrinsic porosity of cork but also to the higher number of surface perforations generated during the cutting process, which are more pronounced in smaller particles.

Fig. 3.11 & Fig. 3.12 present a comparative analysis of two distinct methodologies employed for measuring the volume of virgin cork specimens, an aspect of considerable significance in the field of material characterization and physical measurements. The first approach, known as the dimensional method, relies on the direct measurement of linear dimensions (length, width, and height), followed by mathematical calculation of volume. This conventional technique assumes that the specimen possesses a regular geometric configuration. The second approach, the displacement method, is based on Archimedes' principle, whereby the actual volume is determined through measurement of the quantity of displaced liquid. This method is generally characterized by higher accuracy, particularly when dealing with irregularly shaped objects.

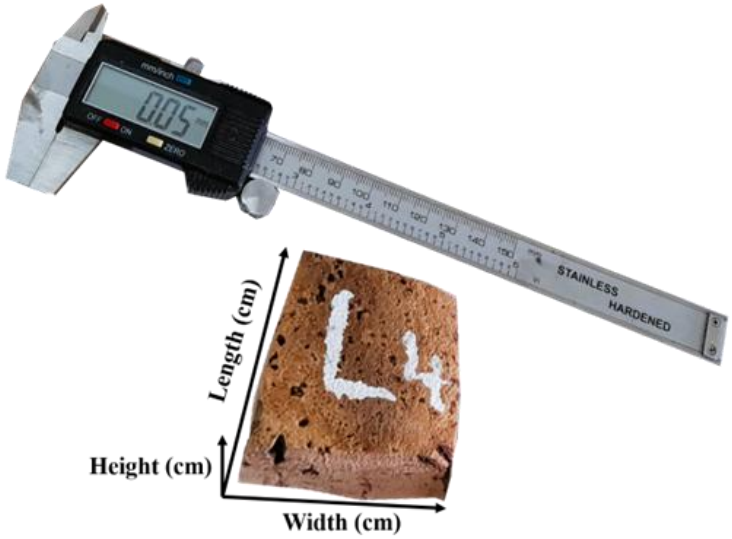


Fig. 3.11. Average volume calculated from dimensional measurements.

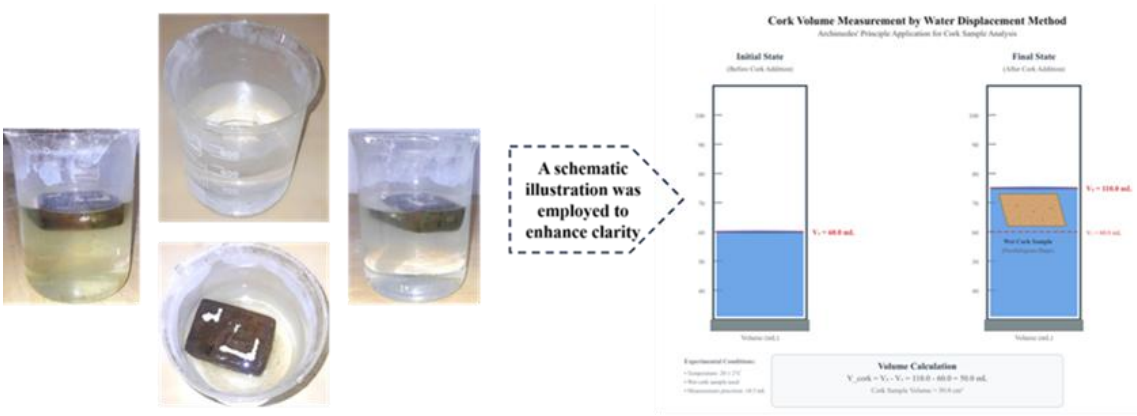


Fig. 3.12. Schematic representation of volume measurement by water displacement.

Table 3.8 demonstrates clear volumetric stability for all three types of cork after 30 days of immersion. The dimensional method recorded nearly identical values (60.04–60.07 cm^3), while the displacement method yielded a consistent value of 60 cm^3, with a deviation between the two methods not exceeding 0.12%. These findings indicate that cork is capable of absorbing significant amounts of water (corresponding to a mass increase ranging from 25.8% to 50.2%) without exhibiting measurable volumetric expansion. This behavior can be attributed to its closed cellular structure and the elasticity of its cell walls.

From an applied perspective, such dimensional stability represents a favorable characteristic, as it prevents the development of expansive stresses and cracking in concrete under moisture exposure. Nevertheless, this stability does not eliminate the challenge associated with the material's high water absorption capacity.

Table 3.8. Average volume of cork samples after 30 days of immersion

	Dimensional Method (cm^3)	Displacement Method (cm^3)
Cork 1	60,04	60
Cork 2	60,03	60
Cork 3	60,07	60

As previously mentioned, the volume of the cork samples remained nearly constant throughout the immersion period, while an increase in mass was observed. This suggests that water absorption occurred only at the surface level. This observation was confirmed by cutting the cork samples after 60 days of immersion, where it was found

that the inner core of the samples remained dry, indicating that water had not penetrated the interior of the material. This finding is illustrated in Fig. 3.13.



Fig. 3.13. Longitudinal section of immersed virgin cork for internal examination.

3.4. Methodology for the composition of virgin cork-based concretes

The methodology adopted in this experimental campaign for formulating cork-based concretes was based on the principle of volumetric replacement of the mineral aggregates used in conventional concrete with natural cork aggregates. The mix design of the two reference concretes was determined using the established Dreux-Gorisse method, and these references served as the comparative baseline throughout the experimental study.

Building upon this reference mix, various cork-based concrete formulations were developed by substituting 25% of the total volume of mineral aggregates with an equivalent volume of natural cork aggregates. In order to maintain the initial density of the mix and avoid major variations, a homogeneous replacement strategy was applied. This approach involves replacing each granulometric fraction of mineral aggregate with cork aggregate of the corresponding particle size. Specifically, sand is replaced by cork particles sized (0-4 mm), gravel in the (4-8 mm) range is replaced by cork of the same range, and the (8-16 mm) gravel fraction is replaced by (8-16 mm) cork particles. Meanwhile, these investigations consistently show that integrating cork into concrete results in a lightweight material with excellent thermal

and acoustic insulation properties, but reduced mechanical properties, marked by relatively poor microstructural properties (Tedjditi et al., 2020).

In order to extend the use of this material to structural elements in a building, the experimental aspect of this study focuses on enhancing the mechanical performance of virgin cork-based concrete. To achieve this objective, a cementitious paste containing 450 kg/m³ of cement was reinforced by incorporating 10% fine limestone, used as a supplementary cementitious material. Additionally, the water-to-binder ratio was reduced to 0.38 to improve the internal structure and mechanical performance of the concrete. Building upon previous studies that reported favorable results in terms of workability, mechanical strength, and thermal insulation when 25% of pre-soaked raw cork (immersed in water for 2 hours) was incorporated, two experimental procedures were adopted to examine the influence of the cork mixing method on concrete properties. In the first procedure, dry raw cork was used and mixed with an equivalent amount of water-empirically determined-representing the quantity it absorbs during a 2 hours immersion. The remaining components were then added. In the second procedure, raw cork was immersed in water for 2 hours prior to being integrated with the other concrete components (Fig. 3.14).



Fig. 3.14. Immersion of virgin cork in water.

This dual approach was designed to assess the discrepancy between theoretical and actual water absorption values of male cork and to investigate how this disparity influences the physical and mechanical properties of the resulting concrete. Accordingly, the results of both procedures were systematically compared.

The experimental program included testing six concrete formulations:

- Ordinary concrete (OC)
- Wet cork concrete using absorbed water (OC+HC $_{2h\ AW}$)
- Wet cork concrete immersed in water (OC+HC $_{2h\ IW}$)
- Concrete with limestone filler only (OC+F)
- Wet cork concrete using absorbed water with limestone filler (OC+F+HC $_{2h\ AW}$)
- Wet cork concrete immersed in water with limestone filler (OC+F+HC $_{2h\ IW}$)

3.4.1. Mixing Procedure and Sample Preparation

Based on the results of the mini-cone spread test, a dosage of 0.7% of superplasticizer was adopted for concretes without limestone filler, while a reduced dosage of 0.6% was used for those containing limestone filler. Table 3.9 summarizes the complete details of the mix designs used in the experimental program, with all component quantities expressed in kg/m^3.

Table 3.9. The composition of the concretes prepared in the experimental campaign (kg/m^3).

Composition	OC	OC+HC$_{2hAW}$	OC+HC$_{2hIW}$	OC+F	OC+F +HC$_{2h\ AW}$	OC+F +HC$_{2h\ IW}$
Cement	450	450	450	450	450	450
Limestone filler	0	0	0	45	45	45
Effective water (Weff)	171.0	171	171.0	188.1	188.1	188.1
Water absorbed cork	0	20.4	26.5	0	19.3	25.1
Total water	171.0	191.4	197.5	188.1	207.4	213.2
Super-plasticizer	3.2	3.2	3.2	3.0	3.0	3.0
Sand 0-4 mm	731.5	515.1	548.8	712.4	497.6	526.3
Gravel 4-8 mm	170.5	143.6	128.4	166.1	139.9	123.6
Gravel 8-16 mm	819.8	644, 5	615.0	798.3	622.4	598.7
Cork 0-4 mm	0	13.3	13.3	0	12.6	13.0
Cork 4-8 mm	0	2.8	2.8	0	2.6	2.7
Cork 8-16 mm	0	16.5	16.5	0	15.6	15.5
Weff/B	0.38	0.38	0.38	0.38	0.38	0.38

Based on previous studies conducted in our laboratory, a soaking duration of exactly two hours was selected, as this time corresponds to the onset of a phase characterized by relatively slow absorption kinetics. Additionally, concrete containing 25% virgin cork, immersed in water for two hours, exhibited good fresh homogeneity, resulting in a significant improvement in the consistency of cork concrete. Accordingly, this

research adopted the same two hours soaking duration, as well as the same mixing method and equipment.

A vertical-axis mixer (see Fig. 3.15) was used in the mixing process. For OC+HC_{2hAW} Concrete, dry virgin cork granules were introduced along with the amount of water absorbed over two hours. For OC+$HC_{2h\ IW}$ Concrete, the virgin cork was immersed in water for two hours, and after soaking, it was introduced into the mixer. In both OC+$HC_{2h\ AW}$ and OC+$HC_{2h\ IW}$ Concrete, the cork was mixed for 90 s. Subsequently, cement, limestone powder (for mixtures containing limestone), sand, and 50% of the superplasticizer mixed with water were added, then the mixture was blended for 4 min. During this step, water was added gradually over a 90 s period. Following this, gravel and the remaining superplasticizer solution were introduced and mixed for an additional 1 min. Finally, the entire mixture was stirred for 90 s (Tedjditi et al., 2022) (Hariz et al., 2022).

This mixing sequence, in which cork was initially mixed with cement and limestone, aimed to coat the wetted cork granules with cement particles. Moreover, ultra-fine limestone powder was incorporated early in the process to fill micro-voids and enhance the internal structure of the concrete. Mineral additives were added later. This sequence was adopted to strengthen the bond and cohesion between all components, ensuring a homogeneous mixture and minimizing the risk of segregation.

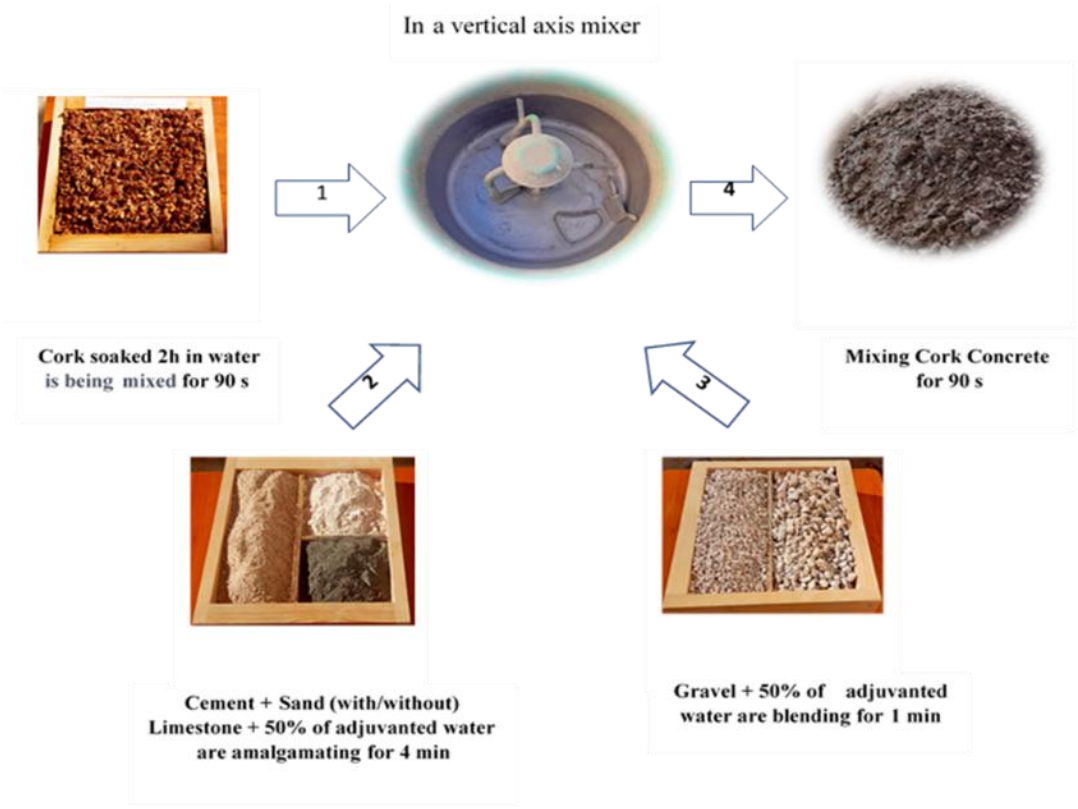


Fig. 3.15. Cork concrete mixing process.

After mixing, the fresh concrete was cast into cylindrical molds (110 mm in diameter and 220 mm in height) and prismatic molds (100 × 100 × 400 mm³) (Fig. 3.16). Depending on the consistency of the mix, the molds were filled either by vibration using a vibrating table or by tamping with a metal rod. Following demolding, all samples underwent full wet curing for 28 days in a water tank, following standard curing procedures for conventional concrete according to EN 12390-2 (EN 12390-2, 2021) (Fig. 3.17). Finally, the specimens were removed from the curing tank for hardened-state characterization tests It is also worth noting that, for some samples, surface smoothing was required prior to testing. This was achieved by trimming the surface using a concrete saw (Fig. 3.18).



Fig. 3.16. Casting fresh concrete into molds.



Fig. 3.17. Moist curing of concrete.



Fig. 3.18. Concrete saw.

3.5. Concrete Characterization Methods

3.5.1. Workability and Visual Inspection

The workability of the prepared concrete mixtures was assessed throughout the experimental campaign using the slump test with the Abrams cone, in accordance with BS EN 12350-2 (BS EN 12350-2, 2009). Additionally, a visual inspection was conducted to evaluate the homogeneity of the fresh cork concrete and to detect any signs of instability phenomena.

3.5.2. Plastic Viscosity Analysis

The plastic viscosity of fresh concrete was measured using a rheometer equipped with a coaxial vane geometry, assisted by a Heidolph mechanical agitator (Fig. 3.19). Viscosity tests were conducted 10 minutes after the completion of mixing. The initial experimental data showed the relationship between torque and rotational speed, which was subsequently converted into shear stress and shear rate to characterize the flow behavior of the material.

In general, the rheological behavior of fresh concrete in rotational rheometry is better described by the Reiner–Riwlin model, as shown in Fig. 3.20. In this approach, the relationship between shear stress and rotational parameters is used to characterize the flow behavior of heterogeneous materials such as concrete containing aggregates.

The Reiner–Riwlin framework relates the measured torque and rotational speed to the rheological parameters of the material, allowing the determination of apparent yield stress and plastic viscosity under non-ideal flow conditions. This approach more realistically represents the complex flow behavior of fresh concrete in rheometer systems.

The plastic viscosity was determined from the slope of the linear region of the torque–rotational speed relationship following the method proposed by Estellé et al. (2008). The yield stress was obtained by extrapolating the fitted flow curve to the stress axis, representing the threshold required to initiate flow.



Fig. 3.19. Plastic viscosity test.

3.5.3. Density

The density of the concrete was determined in accordance with BS EN 12390-7 (BS EN 12390-7, 2009) using cylindrical specimens with a diameter of 110 mm and a height of 220 mm. The density was calculated as the average of three different specimens by measuring the mass and dimensions of each sample, applying the following formula:

$$\rho = \frac{M}{V} \quad (2)$$

Where: ρ is the density (kg/m³), M is the mass of the specimen (kg), V is the volume of the specimen (m³).

3.5.4. Mechanical Properties

a. Compressive Strength

Compressive strength tests were performed on cylindrical specimens with a diameter of 110 mm and a height of 220 mm at the ages of 28 and 90 days, in accordance with the BS EN 12390-3 (BS EN 12390-3, 2009) standard. The final compressive strength value for each mixture was calculated as the average of three individual specimens.

b. Flexural Strength

Flexural strength was evaluated using a three-point bending test at 28 days, following the BS EN 12390-5 (BS EN 12390-5, 2009) standard. The test was conducted with a universal testing machine on prismatic specimens measuring 100 × 100 × 400 mm³.

For each concrete formulation, the final flexural strength value was determined as the average of three distinct samples.

3.5.5. Water Porosity Measurement

Porosity constitutes a fundamental parameter governing both the mechanical performance and long-term durability of concrete, as it directly controls permeability and resistance to aggressive environmental agents. Accurate characterization of porosity requires a comprehensive, multi-technique approach capable of evaluating total pore volume, pore size distribution, and the connectivity of the pore network.

The reduction of porosity in concrete composites relies primarily on optimizing mixture design parameters, particularly through lowering the water-to-cement ratio and incorporating low-porosity mineral admixtures such as finely ground limestone powder. This strategy is based on the principle of optimal particle packing, whereby voids between coarse aggregates are progressively filled by sand particles, interstitial spaces between sand grains are occupied by cement particles, and ultrafine voids between cement grains are filled by even finer particles. Such hierarchical densification enhances matrix compactness, reduces pore connectivity, and ultimately improves both mechanical strength and durability performance.

The water porosity of concrete was evaluated in accordance with the French standard AFPC-AFREM (AFPC-AFREM, 1997), This methodology is based on the principle of hydrostatic weighing and Archimedes' law to determine the apparent volume of the specimen and the volume occupied by open pores. Using cylindrical specimens (110 x 50mm) extracted from the cores of concrete blocks (Fig. 3.20). This sampling method was chosen to enhance measurement reliability and to minimize potential errors arising from particle segregation, a phenomenon commonly observed during casting and curing.



Fig. 3.20. Cylindrical concrete specimen for testing.

Particle segregation refers to the tendency of heavy aggregates to settle at the bottom of a concrete element, while lighter components such as cement paste and admixtures rise toward the top. This non-uniform distribution leads to vertical variations in physical and porosity characteristics, potentially compromising measurement accuracy. The issue becomes particularly significant when incorporating materials with markedly different densities—such as lightweight cork—with conventional high-density aggregates, which increases the likelihood of segregation and necessitates special measures to ensure uniform distribution.

The experimental procedure began with drying the samples in a laboratory oven at 60°C, a relatively low temperature selected to prevent damage to the concrete's microstructure. Drying continued until mass stabilization, determined by successive weight measurements taken at regular intervals until the variation between two consecutive readings was less than 0.05%, ensuring an accurate determination of the dry mass (M_d).

The dried specimens were then subjected to degassing and water saturation using a specialized vacuum system comprising a high-efficiency vacuum pump and a custom-designed desiccator (Fig. 3.21). This process aimed to remove trapped air from within the pores and achieve full saturation of all open pores with distilled water. Degassing was conducted gradually to prevent structural damage, maintaining low pressure for a sufficient period to expel all entrapped gases. Distilled water was then introduced slowly under continued vacuum to ensure thorough infiltration into the open pores.

The mass of the sample was measured in two states:

1. Saturated mass in air (M_{air}): Measured after gently removing excess surface water with a damp cloth, ensuring no water was removed from within the pores.
2. Saturated mass underwater (M_w): Measured using a hydrostatic balance equipped with a submerged weighing basket, taking care to eliminate any air bubbles from the specimen surface.

Water porosity (P) was calculated using the following equation:

$$P = \frac{M_{air} - M_d}{M_{air} - M_w} \times 100 \qquad (3)$$

Where: P is the water porosity (%), M_{air} is the mass of the saturated sample in air (g), M_d is the dry mass of the sample (g), M_w is the mass of the saturated sample under water (g).



Fig. 3.21. Vacuum saturation device.

3.5.6. Pore size distribution

The determination of pore size distribution and the critical pore diameter represent a fundamental parameter in the microstructural characterization of concrete. The critical pore diameter is defined as the dominant pore size corresponding to the highest peak in the pore size distribution curve, playing a pivotal role in governing the material's physical and mechanical properties. To achieve this, Mercury Intrusion Porosimetry (MIP) (Fig. 3.22) was employed as an advanced and scientifically recognized analytical technique for assessing pore size distribution in porous materials. Measurements were carried out using an Autopore V9620 porosimeter (Micrometrics®), which offers a wide operational pressure range exceeding 400 MPa, enabling the detection of pore diameters from 0.003 μm to 1100 μm. This range encompasses a broad spectrum of pores present in concrete, from nanopores to macropores.

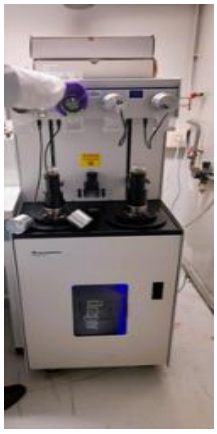


Fig. 3.22. Mercury porosity measurement device.

(LaSIE Laboratory, La Rochelle University).

For sample preparation, the specimens were manually cut with utmost care to preserve their original microstructural integrity and avoid any damage or alteration to the native pore network. Subsequently, the prepared samples were dried at 45°C under vacuum conditions to ensure complete removal of moisture prior to testing, a necessary step to guarantee measurement accuracy and eliminate water interference during mercury intrusion. Despite existing criticisms in the specialized literature regarding the suitability and precision of MIP-particularly concerning the potential effects of intrusion pressure on pore structure and the possibility of pore deformation during measurement-this technique remains one of the most widely used and accepted methods in contemporary scientific research for the characterization of porous materials in general, and concrete in particular (Cherif et al., 2020 & Aït-Mokhtar et al., 2002).

3.5.7. Capillary Absorption

Capillary absorption is a physical phenomenon that occurs in porous materials such as concrete, where water migrates through fine capillaries and interconnected pores due to surface tension and molecular cohesion forces. It is considered one of the primary mechanisms of moisture transport in building materials and the capillary absorption coefficient plays a critical role in determining the durability of concrete and its resistance to various environmental factors such as chloride ion ingress, carbonation and chemical attack.

To determine the capillary water absorption coefficient, the ASTM C1585-04 standard (ASTM C1585-04, 2004) was followed. Cylindrical concrete specimens with precisely defined dimensions (110 mm in diameter and 50 mm in height) were

prepared and cured under controlled conditions. The curing process involved maintaining constant temperature and relative humidity for at least 28 days to ensure that the concrete reached the desired maturity level. To guarantee unidirectional water flow during testing, the upper and lateral surfaces of the specimens were coated with epoxy resin providing a waterproof and vapor-resistant seal. This step is crucial, as it simulates real-world conditions where capillary absorption occurs primarily in one direction, thus enhancing the accuracy and practical relevance of the results. The test begins by determining the dry mass of each specimen (M_d) after drying in an oven at 60 ± 2 °C until a constant mass is achieved. This step is essential to eliminate residual moisture that could compromise measurement accuracy. Specimens are then partially immersed in water to a depth of 5 ± 2 mm (Fig. 3.23), and their masses are recorded at precisely defined time intervals. Water absorption is calculated as the average of three specimens for each concrete mix.

The water absorption is calculated using the following equation:

$$I = (M_t - M_d)/(A) \quad (4)$$

Where: I: the water absorbed per unit surface area [kg/m²]. M_d: the dry mass of the specimen [kg]. M_t is the wet mass of the specimen at time t [kg]. A: the surface area exposed to water [m²].

The absorption coefficient was carried out in two distinct phases:

- **Phase 1: Primary Absorption Coefficient**

The primary absorption coefficient represents the slope of the linear portion of the curve $I = f(\sqrt{t})$ within the time ranges from 5 minutes to 24 hours. It reflects the initial absorption rate (Rapid), which is largely governed by pore size distribution, degree of pore connectivity, rheological properties of the absorbing fluid and condition of the surface in contact with water

- **Phase 2: Secondary Absorption Coefficient**

Once near-equilibrium is reached (typically around Day 6), the slope of the secondary linear segment of the absorption curve is calculated. Although this coefficient is of

lesser practical importance, it is valuable for understanding the material's long-term behavior.

Furthermore, it should be noted that several parameters significantly influence capillary absorption in concrete such as: The (w/c) ratio is a dominant factor; higher ratios increase porosity and absorption rate. As well, the optimized aggregate grading lowers porosity and enhances capillary resistance and the temperature affects the viscosity of water inversely, thereby influencing the rate of absorption.

Despite its comprehensiveness, ASTM C1585-04 (ASTM C1585-04, 2004) presents several limitations, as it assumes material homogeneity, ignores gravitational effects in taller specimens, requires highly accurate mass measurements (±0.01 g), necessitating the use of analytical balances and demands stable environmental conditions throughout the extended testing period (up to one week).



Fig. 3.23. Experimental measurement of capillarity.

3.5.8. Effective diffusion coefficient of chloride ions in concrete

Chloride ion migration is governed by two distinct regimes: the transient (or non-steady-state) regime and the steady-state regime. The transient regime is characterized by nonlinear variations in ion concentration, with its duration depending on the specific properties of the concrete. In contrast, the steady-state regime exhibits a constant chloride ion flux.

The transient regime comprises two successive sub-stages: an initial phase, marked by a very slow increase in chloride concentration, followed by a transition phase where the rate of increase accelerates while retaining its nonlinear nature. Upon

reaching the steady-state condition, the concentration evolves linearly over time. This linear portion of the curve is used to calculate the chloride diffusion coefficient, where the ion flux is determined by calibrating experimental data points based on the slope of the linear regression line of the steady-state curves (Touil et al., 2017). Furthermore, the intersection point of the linear curve with the time axis in the steady-state phase is used to determine the lag time, i.e., the period required for chloride ions to first appear in the downstream compartment (Touil, 2017).

Based on steady-state electrochemical migration, offers an advanced alternative to traditional long-term diffusion tests by enabling reliable results within 2-4 weeks in contrast to natural diffusion tests that may require months or years (Truc et al., 2000). The experimental setup comprises specimens with a diameter of 110 ± 1 mm, thickness of 50 ± 2 mm, and chamber volumes of approximately 1.82 L each, utilizing a cell body constructed from polycarbonate or chemically resistant glass, electrodes made of nobium copper (see Fig. 3.24).

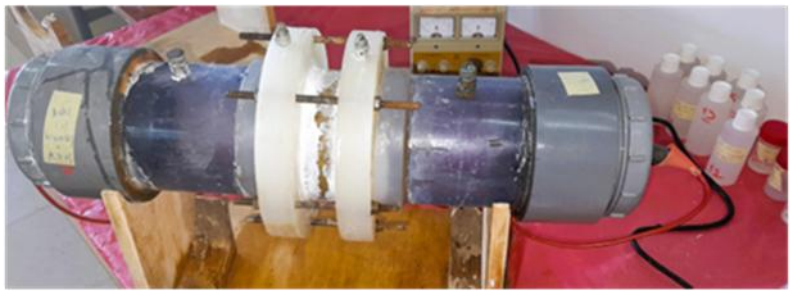


Fig. 3.24. Chloride migration test.

The sample preparation involves a rigorous curing process including 28 days wet curing at 20 ± 2°C, full saturation in a basic solution (NaOH, KOH) for 72 hours under vacuum, and air removal via vacuum pump, followed by surface preparation consisting of cleaning to remove contaminants, inspection for cracks or surface defects, dimensional measurement with ±0.1 mm precision, and sample weighing to determine bulk density. The anodic chamber (upstream) contains sodium hydroxide (NaOH) at 0.025 ± 0.001 mol/L, potassium hydroxide (KOH) at 0.083 ± 0.002 mol/L, and sodium chloride (NaCl) at 0.513 ± 0.005 mol/L. This solution has a pH of approximately 13.5 and simulates the alkaline pore environment of concrete. The Na/K ratio reflects the typical composition of concrete pore solutions. The chloride concentration replicates seawater conditions and ensures a steady ionic flux. The

cathodic chamber (downstream) contains NaOH at 0.025 ± 0.001 mol/L and KOH at 0.083 ± 0.002 mol/L. This solution maintains ionic equilibrium, prevents undesirable pH gradients, and ensures stable electrical conductivity.

The experimental procedure begins with assembly and calibration involving mounting the specimen between chambers with tight sealing, filling chambers with prepared solutions, connecting electrodes, checking for leakage, measuring initial system resistance, applying voltage to maintain 12 ± 0.5 V across the specimen (Andrade, 1993 & Arsenault, 1999), and monitoring current stability over 24 hours. The following operation step consisting of a pre-steady-state (non-steady sate) (Fig. 3.25) phase lasting 7-14 days, steady-state measurement period of 14-21 days, and data recording every 24 hours while monitoring parameters including constant voltage,

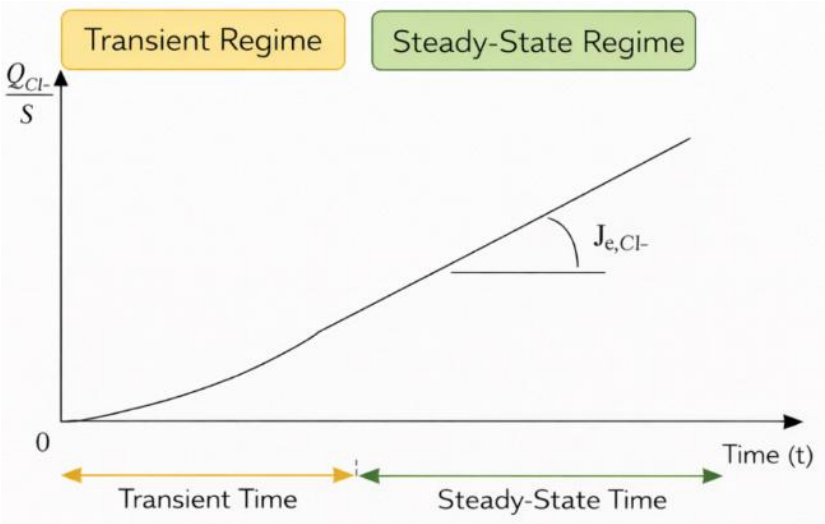


Fig. 3.25. Evolution of chloride penetration: Transient to steady state.

hourly current readings, temperature stability within ±0.5°C, and daily solution level checks. Chemical analysis (Fig. 3.26) involves daily sampling from the anodic chamber (1-2 mL) using Mohr titration with $AgNO_3$ with chloride concentration (Touil, 2017) calculated as:

$$[CL^-] = \frac{V_{\{AgNO_3\}} \times N_{\{AgNO_3\}}}{V_{\{sample\}}} \quad (5)$$

Where: $V_{\{AgNO3\}}$ denotes the volume of silver nitrate solution consumed during titration, $N_{\{AgNO3\}}$ represents its normality, and V{sample} corresponds to the volume of the extracted sample solution.

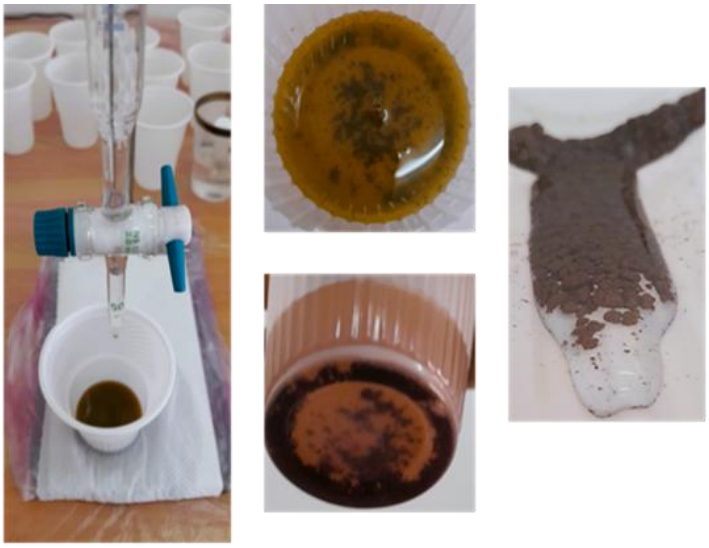


Fig. 3.26. Chemical analysis of solution samples.

Steady-state evaluation requires stability criteria including chloride concentration variation less than 2% over 7 consecutive days, current stability within ±5%, and a linear concentration-time relationship, with statistical analysis using linear regression expressed as:

$$C(t) = C_0 - \left(\frac{J \times S \times t}{V \times 1000}\right) \quad (6)$$

Where: C(t) represents concentration at time t, C_0 is the initial concentration, S is the specimen area, V is the volume. The acceptable linearity is defined as $R^2 \geq 0.95$.

In migration test, the D_e coefficient is determined from the simplified Nernst-Planck relation (Andrade, 1993):

$$D_e = \frac{J \times R \times T \times L}{Z \times F \times U \times C_0} \quad (7)$$

Where: R is the universal gas constant equal to 8.3144 J/mol·K, T is absolute temperature (K) maintained within ±0.5°C, L is specimen thickness equal to 0.050 m, z is chloride ion valency equal to 1, F is Faraday constant equal to 96,485 C/mol, U is applied voltage across the sample at 12.0 ± 0.5v, C_0 is initial chloride concentration at 513 mol/m³, and J is the molar flux [mol/m²·s] computed as:

$$J = \frac{(\Delta Q_{Cl-})}{(S \times \Delta t)} \quad (8)$$

Where: ΔQ_{Cl-} is the variation in the cumulative quantity of chlorides in the downstream compartment (mol/m^3), S the surface area of the sample (m^2), and Δt the time interval considered (s).

3.5.9. Scanning Electron Microscopy (SEM) Morphological Analysis

A comprehensive morphological investigation was conducted to analyze the microstructure of conventional concrete, cork concrete, and cork–limestone concrete using a Hitachi TM1000 tabletop scanning electron microscope (SEM) (Electron Microscopy Laboratory Faculty of Sciences, Abou-Bekr Belkaid University), (Fig. 3.27), which offers high-resolution imaging capabilities under low-vacuum conditions. This morphological examination was complemented by elemental and chemical characterization through Energy Dispersive Spectroscopy (EDS) performed on the same device, enabling the acquisition of detailed information on the chemical composition and elemental distribution of the studied specimens.

Sample preparation involved producing irregularly shaped fragments of cork concrete with approximate dimensions of 5 × 5 × 5 mm^3, ensuring optimal compatibility with the sample holder and the dimensional constraints of the SEM chamber. Following crushing, the specimens underwent oven-drying at a controlled temperature of 60 °C for 24 hours to eliminate any residual moisture that could compromise image quality or introduce artifacts in the micrographs. Since the Hitachi TM1000 is designed to operate in low-vacuum mode, conventional conductive coating was unnecessary, thereby simplifying sample preparation and minimizing potential damage to the specimens. For both mechanical and electrical stability during imaging, the samples were mounted on aluminum stubs using high-quality conductive carbon tape, which enhanced electron conduction and reduced electrostatic charging effects that could otherwise distort or obscure images.

The microscopic investigation focused primarily on the Interfacial Transition Zone (ITZ) between virgin cork particles and the cementitious matrix—identified as a critical region governing the mechanical and physical performance of cork concrete. The analysis encompassed the assessment of chemical and physical bonding between cork and cement, the evaluation of interfacial adhesion quality, and the detection of any morphological or chemical alterations occurring on the cork surface due to interaction with the alkaline cement environment. Additionally, the pore distribution

and geometry within this region were examined, given their key role in determining the concrete's behavior under various loading conditions.



Fig.3.27. Scanning Electron Microscopy test
(Electron Microscopy Laboratory, Tlemcen University).

The EDS technique was applied to characterize the elemental and chemical distribution on the specimen surfaces, with particular attention to the quantification of key elements such as calcium (Ca), silicon (Si), oxygen (O), and carbon (C), which serve as critical indicators for understanding chemical interactions and the evolution of the microstructure. To ensure accuracy, micrographs were captured at multiple magnifications ranging from 250 x to 2000 x, while maintaining an accelerating voltage of 15 kV to achieve an optimal balance between electron penetration depth and image clarity. EDS analyses were conducted at both selected points and mapped areas to ensure representative coverage of the overall structure.

This integrated methodology provides a comprehensive insight into the morphological and compositional characteristics of the studied concrete types, contributing to a deeper understanding of their mechanical and physicochemical behavior under varying service conditions.

3.5.10. Thermogravimetric Analysis (TGA)

Thermogravimetric Analysis (TGA) is a well-established analytical technique that relies on monitoring the mass changes of a specimen when subjected to a controlled temperature program. This method has wide-ranging applications in scientific research, from polymer characterization to the study of oxidation kinetics at elevated temperatures. In the context of the present study, TGA was employed to quantify

hydration products and accurately determine the degree of hydration. It also serves as a critical tool for understanding the thermal stability and properties of cork-containing concrete, thereby assessing its long-term performance, highlighting its significance in this research. The experimental work was conducted using a SETARAM – SETSYS Evolution 16/18 apparatus (LaSIE Laboratory, La Rochelle University) (Fig. 3.28), which integrates several essential components: a sealed chamber to regulate the gaseous environment surrounding the specimen, a high-precision furnace for temperature control, an ultra-sensitive microbalance capable of detecting minute mass changes, a thermocouple for accurate temperature monitoring, and an advanced computerized unit for automated system control and data acquisition.

The system operates under an inert argon atmosphere, which surrounds the microbalance to prevent interactions with reactive gases. The choice of argon, with its relatively low density, ensures stable and reliable measurements. Additionally, the apparatus is equipped with a water-cooling system to maintain thermal stability of sensitive components. During the measurement, the temperature is gradually increased from ambient conditions to 1200 °C at a constant heating rate of 10 °C/min. At the end of the test, a thermogravimetric curve is obtained, illustrating the relationship between the specimen's mass evolution and temperature, thereby enabling a comprehensive quantitative assessment of the thermal properties of the studied materials.

TGA is an advanced analytical methodology designed to investigate the thermal stability and chemical composition of materials by monitoring mass variations as a function of temperature or time under controlled conditions, in either oxidizing or inert atmospheres, according to predefined heating programs. In the experimental procedure adopted in this study, the concrete samples were finely ground to achieve a high degree of homogeneity, ensuring measurement accuracy (Fig. 3.29). The prepared powders were placed in thermally inert crucibles, and the initial mass of each specimen was precisely recorded. The samples were then subjected to continuous monitoring of mass changes, whether by loss or gain, during the programmed heating process. The significance of this experiment lies in its ability to correlate TGA results with the chemical composition and degree of hydration of cork-containing concrete, allowing an assessment of its thermal stability and long-term performance. This

directly supports the study's objectives of improving sustainable construction materials.



Fig. 3.28. Thermogravimetric Analysis Apparatus device (LaSIE Laboratory, La Rochelle University).



Fig. 3.29. Sample Grinding for TGA.

3.5.11. Thermo-Diffusive Investigation

To investigate the interrelationship between the diffusion coefficient and temperature, a specialized experimental apparatus was developed (Fig. 3.30), consisting of a thermally insulated water bath with a volumetric capacity of 15 liters. The system's engineering design incorporates a submersible heating element installed on the left side of the bath to generate thermal energy, while a tubular coil assembly on the right side is connected to a refrigeration unit comprising a compressor and an evaporator to circulate the refrigerant and provide the required cooling capacity. Both thermal components are immersed in a heat transfer medium composed of a homogeneous mixture of water and rapeseed oil, and their operation is regulated via an electronic control panel equipped with two independent thermostatic controllers for precise management of high and low temperature ranges, respectively. Furthermore, the system is equipped with a variable thermal regulator, enabling accurate and fine-tuned control of the desired thermal gradients.

To condition the concrete specimens at the predetermined target temperature, a circular tubular coil connected to the water bath was installed around the perimeter of the concrete disc, with complete thermal insulation applied to minimize heat losses. The heat transfer fluid is circulated within a closed-loop system equipped with a

peristaltic pump, maintaining the programmed temperature constant for a minimum duration of four hours to ensure homogeneous heat distribution and full penetration to the core of the concrete specimen. The electrical migration test is initiated only after verification of complete thermal homogeneity throughout all sections of the specimen.

Within the framework of this thermo-diffusive study, migration testing was conducted on all concrete specimens at two specified temperatures: 5°C and 50°C. The experimental protocol yielded a distinct diffusion coefficient corresponding to each investigated thermal condition. This investigation is of critical importance in the thesis, as it provides a detailed understanding of how temperature gradients influence ion transport within concrete. By examining diffusion behavior at different temperatures, the study offers insights into the coupled effects of heat transfer, i.e., the movement of thermal energy within the concrete, and mass transfer, i.e., the movement of ions within the concrete pores. Such information is essential for predicting the durability and service life of concrete structures exposed to varying environmental conditions and contributes to the development of enhanced models for chloride migration and overall concrete performance.



Fig. 3.30. Thermo-Diffusive Apparatus device (EOLE laboratory, Tlemcen university).

3.5.12. Chloride–Concrete Interactions

A comprehensive experimental methodology was employed to investigate the interactions of chloride ions with different concrete matrices through isothermal equilibrium testing. The analytical program considered powdered concrete samples derived from four distinct mixtures: ordinary reference concrete, limestone concrete,

wet cork concrete as an innovative material, and a combined wet cork–limestone concrete. The experimental procedure followed the standardized protocol established and refined by (Tang and Nilsson 1993; AFREM, 1997).

This experimental methodology is based on the principle of controlled immersion, whereby a defined quantity of powdered concrete is exposed to a chloride solution of known concentration. The protocol involves periodic measurements of chloride ion concentrations in the solution until equilibrium is reached, defined by the temporal stabilization of ion concentrations. Once equilibrium is established, the solution is analyzed using potentiometric titration techniques to determine the final concentration of free chlorides. The concentration of bound chlorides is then calculated as the difference between the initial concentration and the equilibrium concentration measured within the saturated material. The theoretical framework of the test relies on two fundamental assumptions that ensure the accuracy and scientific reliability of the results:

1. **First assumption:** At chemical equilibrium, the concentration of free chlorides within the pore network of the concrete matrix is equal to their concentration in the external saline solution.
2. **Second assumption:** The observed decrease in chloride concentration within the immersion solution is attributed to the chemical and physical interactions between chloride ions and the constituents of the cementitious matrix, with external influences or secondary phenomena being excluded.

❖ **Methodology for Material Preparation and Preliminary Sample Treatment**

The materials were extracted from the central core of cylindrical concrete specimens (standard diameter of 5 cm) to ensure homogeneity and to minimize potential influences from surface layers. The extracted materials underwent a controlled, stepwise crushing process using a mortar and pestle (Fig. 3.31), with a gradual reduction in particle size to achieve an optimal balance between particle dimensions and testing efficiency. Coarse particles were avoided to reduce the equilibrium time required, while excessively fine particles were excluded to prevent the formation of colloidal suspensions that could compromise the accuracy of quantitative measurements.

Subsequently, wet sieving was performed to obtain a uniform particle size distribution ranging between 0.25 and 2.0 mm, ensuring an optimal specific surface area for interaction. The sieved materials were then subjected to controlled drying in a calibrated oven at 40 ± 2 °C until absolute mass constancy was achieved, thereby eliminating free moisture without altering the chemical structure of the material.



Fig.3.31. Preparation of Cork Concrete Samples for Chloride Interaction.

❖ **Preparation of Solution and Experimental Protocols**

The powdered materials were divided into four distinct experimental groups (ordinary concrete, limestone concrete, wet cork concrete, and wet cork–limestone concrete), each with a standardized mass of 100 ± 0.1 g, and placed in pre-weighed, calibrated glass containers labeled for precise identification. To each container, 400 ± 0.5 mL of an alkaline solution was added, prepared under controlled laboratory conditions and consisting of 1.00 g/L NaOH and 4.65 g/L KOH dissolved in deionized water, thereby simulating the alkaline chemical environment characteristic of concrete pore solutions. The experimental matrix included six graded initial chloride concentrations (C_0): 0.05, 0.25, 0.5, 1, 1.5 & 2 M, providing a comprehensive and balanced coverage of a wide range of chloride exposure scenarios in both natural and industrial environments.

After uniform mechanical stirring to ensure complete homogenization and optimal solute distribution, the containers were stored under controlled thermal conditions at three different temperatures (5 ± 2, 20 ± 2, and 50 ± 2 °C) (Fig. 3.32) for a period of two months, ensuring attainment of the final chemical equilibrium state. All containers were sealed with airtight lids to prevent evaporative water loss, and periodic mass checks were performed to confirm the constancy of the system's total mass.



Temperature = 5 °C



Temperature = 20 °C



Temperature = 50 °C

Fig. 3.32. Specimens Storage under Controlled Temperatures.

❖ **Analytical Techniques and Concentration Determination**

Upon confirmation of chemical equilibrium, the solutions were titrated to determine the final chloride concentrations, and the bound chloride content was subsequently calculated by subtracting the equilibrium concentrations from the initial values. Titration was performed using the precipitation method with a standardized 0.01 M ($AgNO_3$) solution. The bound chloride concentration per unit mass of solid material was determined using the mathematical model developed by (Tang & Nilsson, 1993):

$$C_b = \frac{35{,}453\, V\,(C_0 - C_f)}{M} \qquad (9)$$

Where: C_b is the bound chloride concentration (mol/g), C_0 is the initial chloride concentration in the immersion solution (mol/L), C_f is the equilibrium chloride concentration (mol/L), V is the solution volume (mL), M is the dry mass of the sample (g).

3.6. Conclusion

This chapter presents an experimental program aimed at evaluating the performance of cork-based concrete within the framework of this thesis. The program included the characterization of virgin cork, mixture design, and specimen preparation, followed by the investigation of fresh and hardened state properties through mechanical and physical testing.

Durability-related properties were assessed by measuring porosity, capillary absorption, and the effective chloride diffusion coefficient, in addition to examining

the microstructure of the material. Overall, these investigations provided a comprehensive evaluation of cork-based concrete and contributed to achieving the scientific objectives of this research.

Following the presentation of the experimental program, the next chapter will address the results concerning the mechanical properties and durability of male cork concrete, accompanied by an analysis of its performance under various conditions.

Chapter 4

Comprehensive Characterization of Male Cork Concrete Performance: Analysis of Mechanical Properties and Durability

Introduction

The current chapter presents the detailed findings of the first phase of the experimental program. A wide array of tests and measurements was conducted to assess the performance of the developed concrete mixtures from different angles. These include mechanical performance indicators such as compressive and tensile strength, as well as durability-related properties.

The analysis and discussion of these results, in relation to the defined research objectives and hypotheses, provide a solid foundation for understanding the behavior of the studied materials. This chapter, therefore, lays the groundwork for a comprehensive evaluation of cork concrete and serves as a critical step toward formulating the final conclusions of the study.

4.1. Performance assessment of cork-based concrete: An evaluation of its effectiveness

Experimental analyses of the constituent materials of cork concrete revealed significant findings regarding the behavior of male cork aggregate in construction applications. In terms of particle size distribution, the study demonstrated that aggregates derived from male cork, specifically those in the 4-8 mm and 8-16 mm size fractions, exhibit grain size distribution curves that align with the established standards for conventional mineral aggregates.

However, the analysis of the 0-4 mm cork aggregate fraction revealed a notable deviation, characterized by a clear deficiency in fine particles compared to natural sand, which typically contains around 13% fine material. This lack of fine particles may negatively impact the cohesion and workability of concrete mixes.

The microstructure of male cork aggregate is distinguished by its complex cellular nature, containing a widespread network of internal voids and pores. This structure is fundamentally different from the homogeneous texture of conventional mineral aggregates. Such porous microstructural characteristics directly influence the bulk density of the material, with cork aggregate exhibiting exceptionally low values compared to that of the density of equivalent mineral aggregates.

This considerable disparity in density presents a significant technical challenge during the mixing and preparation of cork concrete, as it may lead to difficulties in achieving uniformity and may cause segregation or uneven distribution of components during mixing and casting processes.

In addition to its low density, laboratory absorption tests have shown that male cork aggregate possesses an exceptionally high-water absorption capacity. Experimental results indicate that the absorption rate may exceed 100% of the material's dry weight, meaning it can absorb more water than its own mass. This property necessitates a re-evaluation of water content in mix design and may require specific treatments or adjustments to ensure optimal performance of the final concrete product.

Prior to examining the properties of these cork-based concrete mixtures, it was essential to assess their homogeneity in the hardened state. This assessment was

conducted using cylindrical specimens with a diameter of 110 mm and a height of 220 mm. Transverse homogeneity was evaluated by extracting samples from the lower, middle, and upper sections along the height of each cylinder (Fig. 4.1). Longitudinal homogeneity was verified through a vertical cross-section.

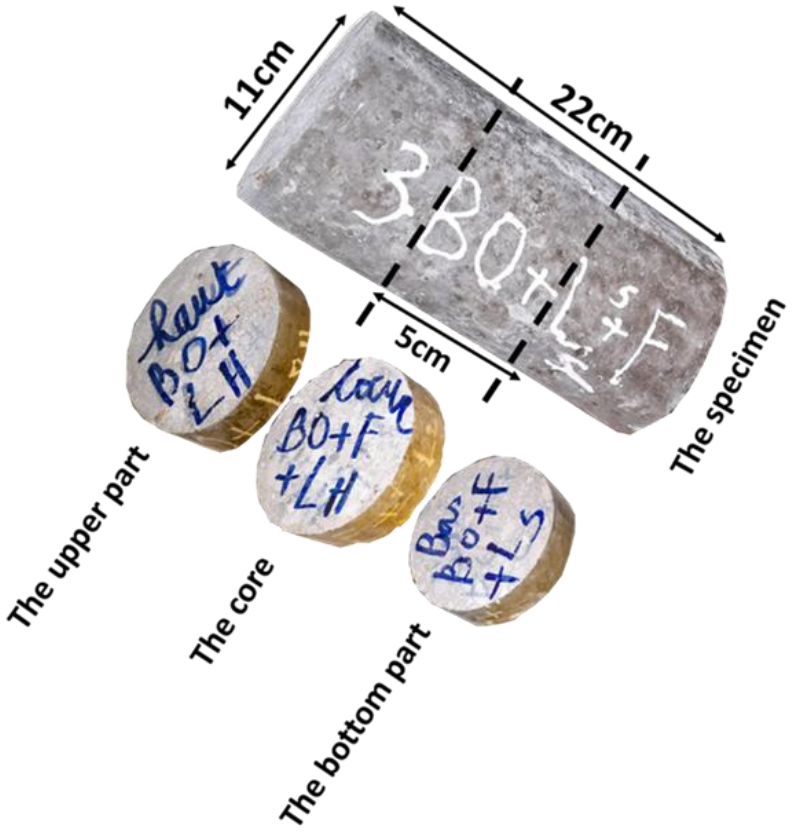


Fig. 4.1. Sectioning the cylindrical sample into various portions for testing.

The various transverse and longitudinal sections of the six prepared mixtures are presented in (Fig.4.2). As the figure demonstrates, all cork-based concretes exhibited a uniform distribution of both mineral and vegetal particles across the different sections.

Furthermore, the longitudinal sections not only confirm the good distribution of components but also reveal the absence of segregation between the heavy phase (mineral particles) and the light phase (cork particles), despite the significant difference in their bulk densities. This indicates the effectiveness of the adopted mixing methodology for preparing the studied cork-based concrete mixtures.

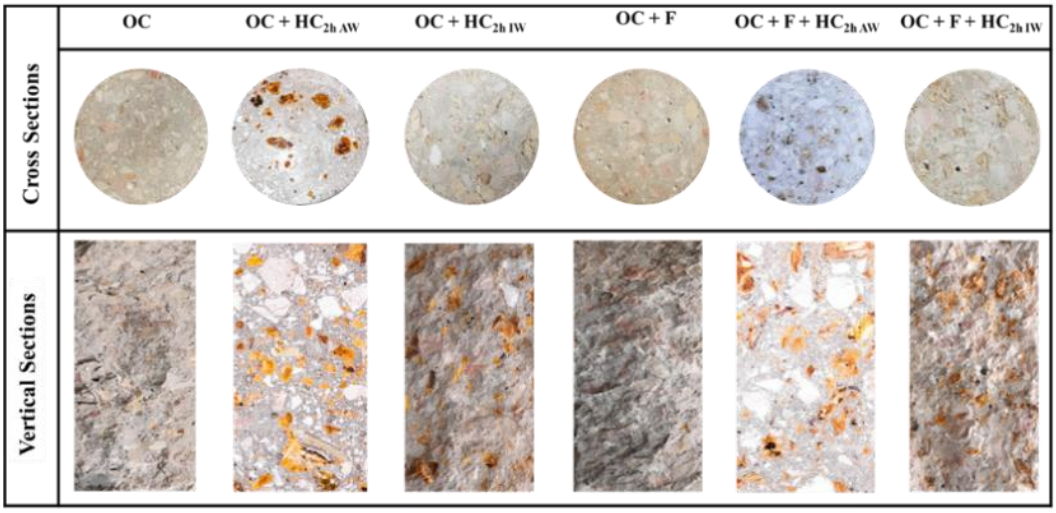


Fig. 4.2. Sections used to assess the homogeneity of concrete mixtures.

4.2. Workability

Fig. 4.3, when comparing the reference concrete (OC) with the mixture incorporating limestone filler (OC+F), an increase in slump from 5 to 8 cm was observed, indicating improved workability. This enhancement can be attributed to the beneficial influence of limestone filler on the rheological properties of fresh concrete, resulting in improved flowability and ease of handling (Sua iam et al., 2012). Moreover, limestone acts as a nucleation agent that accelerates cement hydration kinetics, thereby contributing to increased fluidity of the mixture (Li et al., 2018 & Rojo López et al., 2022). The slump response remained stable and consistent, corresponding to the S2 consistency class as defined by the NF EN 206/CN standard (NF EN 206/CN, 2003).

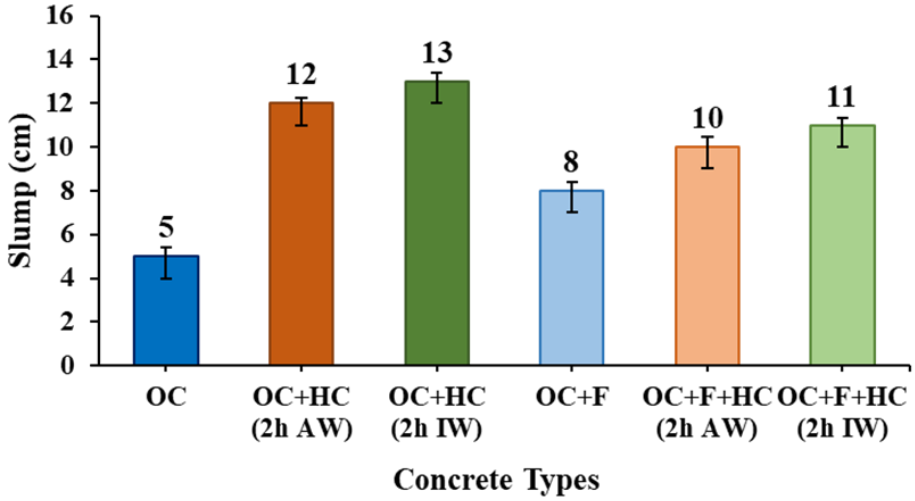


Fig. 4.3. Workability of the different mixtures.

A further improvement in workability was observed when comparing OC with the concrete containing cork (OC+HC), with a transition in consistency class from S2 to S3. This enhancement is primarily attributed to the incorporation of wet cork particles (2h AW or 2h IW). These particles reduce internal friction within the matrix and enhance deformability, thereby facilitating particle mobility within the cementitious system.

However, when comparing OC+HC with OC+HC+F, a slight decrease in slump was recorded, although the consistency class remained unchanged S3 (10–13 cm). This indicates that the combined incorporation of limestone filler and wet cork maintains a high level of workability without significantly altering the overall consistency classification (Hariz et al., 2025).

In conclusion, the synergistic interaction between limestone filler and wet cork particles contributes to a marked improvement in concrete flowability and fresh-state performance.

4.3. Viscosity

The viscosity results presented in Fig. 4.4 clearly indicate that the incorporation of both limestone filler and natural cork granules contributes to a reduction in the viscosity of concrete mixtures, in comparison with the reference composition (OC). More specifically, a significant reduction in viscosity—by approximately 46%—was recorded for the OC+HC mixture, while the greatest decrease, reaching 51%, was observed in the OC+F+HC formulation. It is noteworthy that the tested mixtures exhibited a high degree of internal uniformity throughout the testing process, with no signs of phase separation or segregation. Regarding the use of wet cork particles—either wetted (2h AW) or fully immersed in water for two hours (2h IW)—these materials possess unique properties that can positively influence the rheological behavior of concrete. One of the most distinctive characteristics of cork is its moderate coefficient of friction (Silva et al., 2005). The irregular geometry and surface roughness of cork granules induce a "spherical effect" that reduces direct frictional interactions inter-particle. The partial replacement of conventional mineral aggregates with cork granules can also improve particle size distribution within the concrete matrix. Moreover, the hygroscopic nature of cork enables it to gradually absorb and release moisture over time, thereby providing an internal curing mechanism that helps

maintain workability and enhances the overall flowability of the mixture. Accordingly, the integration of cork particles into concrete systems has the potential to significantly improve the rheological properties of the resulting composite. On the other hand, the inclusion of limestone filler in the OC+F+HC formulation resulted in a slight increase in viscous resistance compared to the cork-only mixture (OC+HC), as previously reported by Rojo López et al. (Rojo López et al., 2022). Nevertheless, this increase remains marginal when compared to the substantial impact exerted by cork particles on the viscosity of concrete.

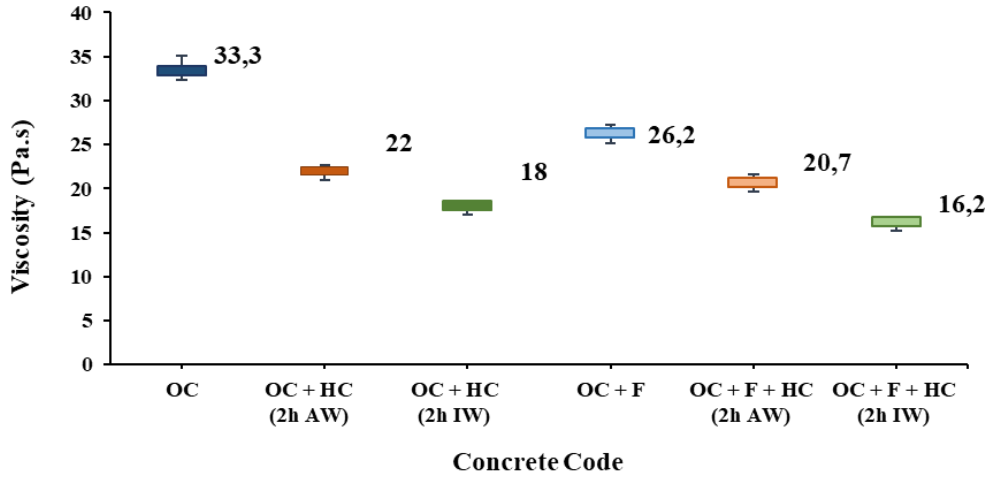


Fig. 4.4. Various concretes plastic viscosity.

4.4. Density

The experimental results shown in Fig. 4.5 indicate that the incorporation of virgin cork granules as a partial replacement in concrete mixtures led to a significant reduction in the overall density of the studied formulations (OC+HC and OC+F+HC).

This reduction in density is attributed not only to the inherently low bulk density of virgin cork—typically ranging from 120 to 200 kg/m³—but also to its highly porous cellular structure. Virgin cork consists of a three-dimensional network of closed, gas-filled cells, which substantially increases the internal void content of the composite material.

The inclusion of such a highly porous material results in an increase in the total porosity of the concrete matrix. As porosity rises, the solid fraction per unit volume decreases, leading to a corresponding reduction in bulk density. Therefore, the observed decrease in density is directly associated with the increased total pore volume induced by the presence of cork particles within the concrete system.

It is noteworthy that, in both experimental cases—whether in the presence or absence of limestone filler—the recorded densities of the cork-based concretes exceeded the 2000 kg/m³ threshold. This quantitative indicator confirms that these mixtures meet the standard criteria for normal-weight concrete (EN 206, 2013).

These experimental findings are consistent with existing trends in the scientific literature, where several studies have highlighted the ability of virgin cork to achieve a favorable balance between density reduction and the retention of acceptable mechanical performance (Ghernouti, 2023 & Pacheco Menor et al., 2024).

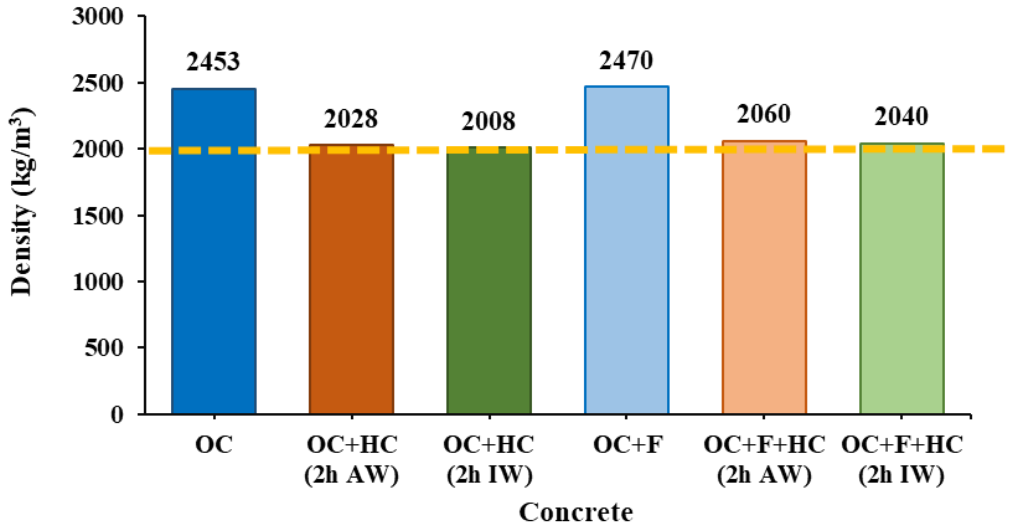


Fig. 4.5. Density of reference and virgin cork concretes.

4.5. Compressive strength

Experimental analysis Fig. 4.6 & Fig. 4.7 revealed that the incorporation of 25% wet virgin cork led to a significant reduction in the compressive strength of the OC+HC $_{(2h\ IW)}$ concrete mixture, with a decrease of 71% at 28 days and 73% at 90 days compared to the reference concrete (OC). These results are in agreement with findings reported by Ghernouti (Ghernouti, 2023) and Pacheco Menor et al. (Pacheco Menor et al., 2024), who noted that the addition of cork to concrete reduces both fresh and hardened density, compressive strength, and the modulus of elasticity. This decline in compressive performance is primarily attributed to the inherent physical properties of cork—namely, its high porosity, elevated water absorption capacity, and its tendency to increase pore volume within the cement matrix (De Larrard et al., 2002).

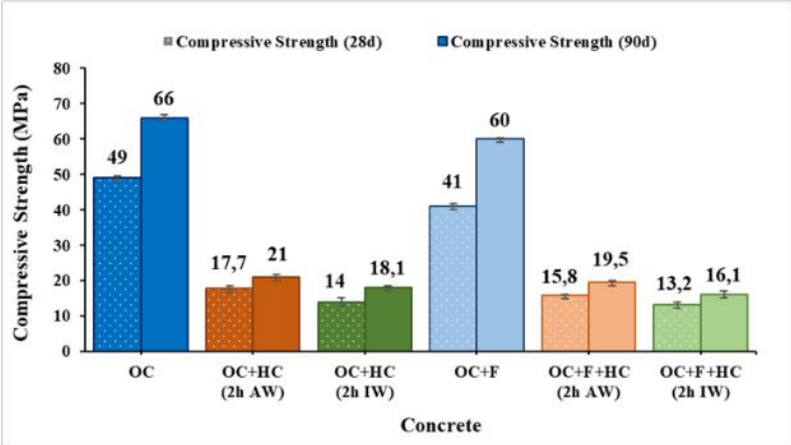


Fig. 4.6. Evaluating the compressive strength of concretes at 28 & 90 days.



Fig. 4.7. Compressive strength test.

It is worth noting that while the performance of concrete mixtures containing wet cork OC+HC $_{(2h\ AW)}$ and OC+HC $_{(2h\ IW)}$ was generally comparable, the use of wet cork OC+HC $_{(2h\ AW)}$ consistently yielded slightly superior compressive strength results, both in the presence and absence of limestone filler. Despite the implementation of pre-treatment procedures intended to enhance adhesion at the interfacial transition zone (ITZ), the bond between cork particles and the cementitious matrix remains relatively weak compared to traditional mineral aggregates. Furthermore, chemical interactions involving substances released by cork—such as tannins and polyphenolic compounds—may interfere with cement hydration processes, thereby compromising mechanical strength (Gil, 2015 & Moreira et al., 2014). Notably, the 28-day compressive strength of the OC+HC $_{(2h\ IW)}$ mixture showed a 67% improvement over the results obtained in earlier work by Tedjditi et al. (Tedjditi et al., 2022), who reported a strength of 6.2 MPa for concrete incorporating 25% wet cork aggregate.

This improvement indicates that the increase in cement content to 450 kg/m³, together with the mix design and preparation techniques adopted in this study, effectively enhanced the mechanical performance of wet cork concrete, making it more suitable for individual building applications. However, the addition of limestone filler in the OC+F and OC+F+HC mixture resulted in a slight reduction in compressive strength at both 28 and 90 days compared to OC and OC+HC respectively, despite initial expectations that the filler would increase binder volume and improve concrete density. This counterintuitive outcome is of particular interest, especially given that the limestone filler was introduced as an additive rather than a partial replacement.

The observed reduction in compressive strength of cork-based concrete containing limestone filler can be attributed to several interrelated factors. Firstly, the high breakage of fine particles (cement and limestone filler) and the weak bonding with cork aggregates reduce matrix cohesion, with the potential formation of localized microcracks at the cork–binder interface. Secondly, the presence of limestone or other mineral fillers may promote agglomeration of fine particles within the cement matrix, which can hinder the complete hydration of cement phases. This incomplete hydration reduces the formation of the cementitious gel responsible for strength development. Moreover, the simultaneous presence of cork and limestone filler appears to disrupt the pore structure, thereby impeding the formation of a dense and well-connected cementitious matrix. These observations underscore the critical importance of optimizing component proportions to enhance the mechanical performance of cork-based concrete. This explanation is consistent with findings reported in the literature, where excessive filler content has been shown to interfere with cement hydration kinetics and consequently reduce compressive strength (Scrivener et al., 2018).

4.6. Flexural strength

The variation in concrete flexural strength at 28 days is presented in Fig. 4.8 & Fig. 4.9. It was observed that the addition of limestone resulted in an 8% decrease in flexural strength compared to the reference concrete. The incorporation of virgin cork led to further reductions of approximately 22% and 29% in the OC+HC $_{(2h\ AW)}$ and OC+HC $_{(2h\ IW)}$ mixtures, respectively. When virgin cork was combined with limestone filler, the reductions were more pronounced, reaching 31% in OC+F+HC $_{(2h\ AW)}$ and 36% in OC+F+HC $_{(2h\ IW)}$.

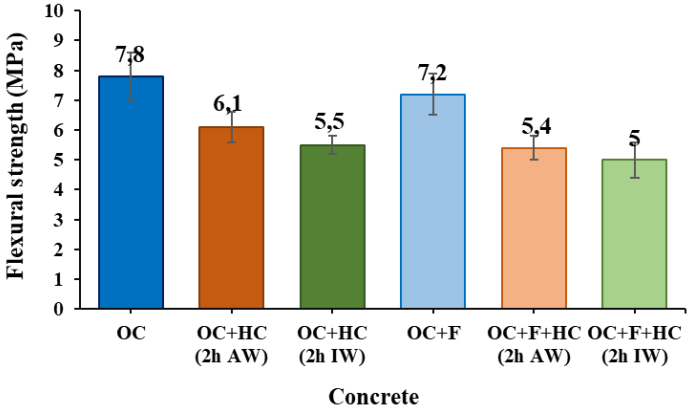


Fig. 4.8. Different concrete flexural strength.



Fig. 4.9. flexural strength analysis.

As previously discussed in the context of compressive strength. These reductions in flexural strength are primarily attributed to the intrinsic porosity of both virgin cork and limestone filler, in addition to the overall increase in concrete porosity, which negatively impacts mechanical performance. However, the most significant contributing factor appears to be the microstructural characteristics of the mixtures, particularly the quality of the interfacial transition zone (ITZ) between the virgin cork particles and the cement matrix.

Despite the reductions observed, the results of this study are consistent with findings reported in the literature. Diab et al. (Diab et al., 2016), in their long-term investigation on the mechanical performance, durability, and environmental impact of limestone cement concrete, reported a 10% decrease in 28-day cube tensile strength following the addition of 10% limestone. Similarly, Tedjditi et al. (Tedjditi et al., 2020) found that flexural strength decreases proportionally with increasing virgin cork content in concrete. Furthermore, Ortega et al. (Ortega et al., 2022) emphasized the significant influence of aggregate type on mechanical strength, noting that mortars incorporating natural cork exhibited lower flexural strength compared to both the reference mortar and those prepared with expanded clay.

4.7. Water porosity

Fig. 4.10 presents the measured water-accessible porosity values for the concrete samples tested at 28 days of age. These values were determined as the arithmetic mean of three independent measurements for each mixture. Experimental results showed that the addition of 10% limestone reduced the porosity by approximately 5% compared to the reference concrete OC.

The incorporation of cork as a substitute material in concrete formulations enhances entrained air content, total porosity, and water absorption capacity. This increase in porosity can be attributed to three primary factors: (i) the formation of air voids between adjacent cork granules; (ii) the intrinsic cellular structure of cork; and (iii) the characteristics of the interfacial transition zone (ITZ) formed between cork granules and the cement paste, which typically exhibits distinct microstructural properties (Tedjditi et al., 2020).

The results indicate that the addition of limestone fillers slightly mitigates this increase in porosity, although the overall effect remains limited. In general, the partial replacement of aggregates with 25% virgin cork results in a net increase in concrete porosity—even when the binder content is increased and limestone fillers are incorporated. Specifically, porosity values of 31%, 36%, 24%, and 27% were recorded for the OC+HC $_{(2h\ AW)}$, OC+HC $_{(2h\ IW)}$, OC+F+HC $_{(2h\ AW)}$, and OC+F+HC $_{(2h\ IW)}$ mixtures, respectively, compared to the reference concrete which reached 12.7%. These findings correspond with the observed reductions in bulk density and mechanical strength, with similar trends particularly noted in the OC+HC and OC+F+HC mixtures.

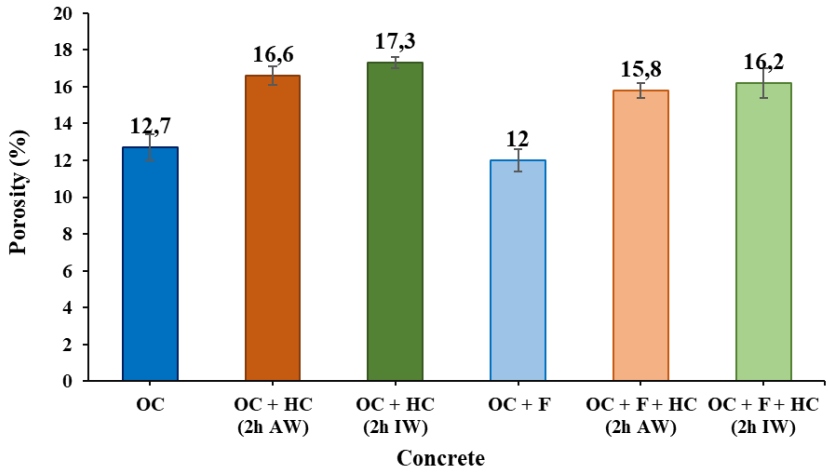


Fig. 4.10. Water accessible porosity of the different concretes.

These outcomes are consistent with the findings of Ortega et al. (Ortega et al., 2022), who investigated chloride ingress resistance, microstructure, and mechanical performance of lightweight mortar incorporating natural cork and expanded clay as aggregate replacements, using sustainable cementitious additives. Their study concluded that the lowest total porosity over the long term was observed in the reference mortar without lightweight aggregates. Additionally, the differences in porosity values between mortars containing natural cork and those with expanded clay were relatively minor, which further supports the findings of the present investigation.

4.8. Capillary water absorption

Fig. 4.11 illustrates the relationship between water uptake and the square root of time for the different concrete mixtures, revealing a characteristic absorption pattern. All plotted curves display a common trend consisting of two consecutive linear segments. The slope of the first segment represents the initial absorption coefficient, while the second segment corresponds to the secondary absorption coefficient (EN 13057, 2001).

Despite the general similarity among the curves, distinct convergence was observed between specific mixtures. The closest similarities were noted between the curves of ordinary concrete (OC) and concrete with limestone (OC+F), as well as between cork concrete (OC+HC), also between cork and limestone concrete (OC+F+HC).

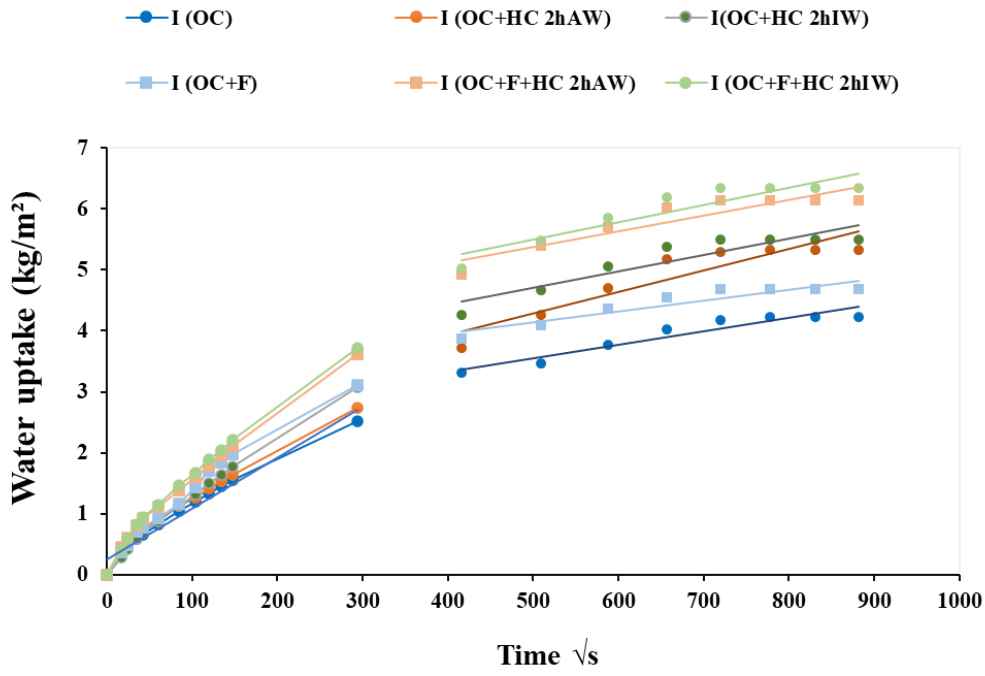


Fig. 4.11. Water uptake versus to square root of time.

By analyzing these curves, both the primary and secondary water absorption values were extracted and are detailed in Fig. 4.12 for all the concrete samples studied. The analysis focuses on the impact of incorporating limestone and virgin cork. Experimental results revealed differentiated effects of the additives on the absorption behavior. The incorporation of 10% limestone into the conventional concrete mix resulted in a 24% increase in the initial water absorption rate. When 25% virgin cork was added, the increase varied from 6% to 26%. The combination of limestone with cork resulted in a more significant rise in the initial absorption rate, which increased

from 8.3 in the reference concrete to 11.7 (g/m². √s * E^{-03}) for (OC+F+HC $_{2h\ AW}$) and 12.2 (g/m². √s * E^{-03}) for (OC+F+HC $_{2h\ IW}$), representing increases of 41% and 47%, respectively. In contrast, the secondary absorption coefficient exhibited only slight fluctuations, ranging narrowly between 3.4 and 6 (g/m². √s * E^{-03}).

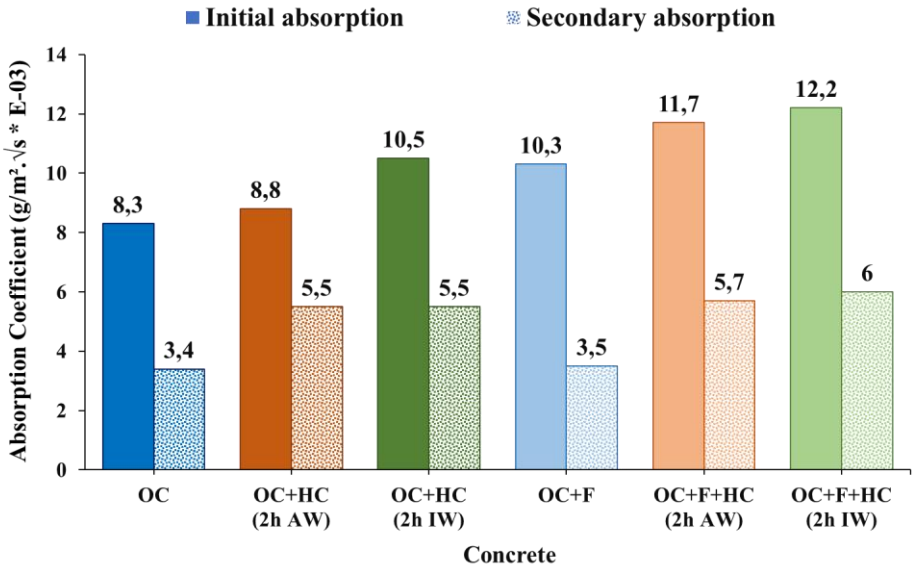


Fig. 4.12. Mixtures initial and secondary water absorption coefficient.

Concrete permeability is primarily governed by three factors: pore size, pore distribution, and pore continuity within the matrix (Neville, 2011). Although the addition of limestone does not significantly reduce the overall porosity of the concrete compared to the reference mixture, it does enhance water permeability. This is attributed to the extremely fine nature of limestone particles, which possess a high specific surface area of 5162 cm²/g. The increase in fine particle content necessitates additional mixing water to maintain workability, thereby increasing the final permeability of the concrete and facilitating water migration through its porous structure (Panesar et al., 2020).

The heightened water absorption observed with the addition of virgin cork can be explained by two key properties of the material. First is its high absorption capacity, which ranged between (54.2 - 154 %) in our experimental tests, effectively turning the cork into a natural water reservoir within the concrete matrix. Second—and more critically—is its unique cellular microstructure, resembling a honeycomb with interconnected voids. This complex porous system differs fundamentally from the internal structure of conventional mineral aggregates (Tedjditi, 2021), forming an

additional capillary network that promotes higher water retention and movement compared to traditional concrete.

This analytical study highlights the substantial impact of incorporating both limestone and virgin cork on the water absorption characteristics of concrete, albeit through different mechanisms. While limestone increases permeability through its fine particle size and greater water demand, cork exerts a more pronounced influence through its highly porous microstructure and superior absorption capacity.

4.9. Chloride diffusion coefficient

Fig. 4.13 presents the temporal evolution of the cumulative chloride ion concentration in the downstream compartment for the various concrete mixtures under investigation. As shown in this figure, chloride concentration increases progressively in all mixtures, with clear differences in both the rate of increase and the final values attained. The reference concrete (OC) and the filler-containing mixture (OC+F) exhibit the highest concentrations and steeper linear slopes, indicating a higher chloride transport rate. In contrast, the cork-based concrete (OC+HC), particularly under the 2hIW conditioning regime, demonstrates a slower concentration development and lower final values, reflecting improved resistance to chloride migration. The combined mixture (OC+F+HC) displays intermediate behavior depending on the conditioning regime, highlighting the influence of microstructural characteristics on ion transport kinetics.

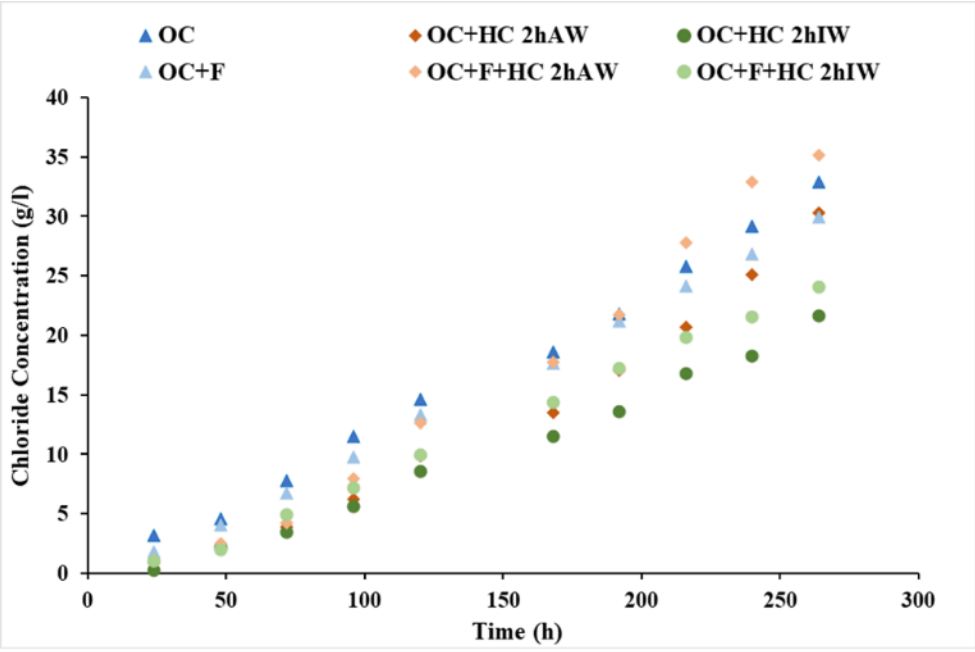


Fig. 4.13. Concrete cumulative chloride concentration in downstream cell.

The calculated values of the diffusion coefficients and lag times are summarized in Table 4.1.

Table 4.1. The diffusion coefficients and the lag times for all studied concrete types.

Concrete	Chloride diffusion coefficient D_e (E^{-12} m^2/s)	Lag time (Hours)
OC	21.62 ± 1.2	53.2
OC+F	26.2 ± 0.3	52.3
OC+HC_{2hAW}	30.6 ± 0.2	46.7
OC+HC_{2hIW}	15.60 ± 0.8	76.1
OC+F+HC_{2hAW}	36.3 ± 0.5	40.7
OC+F+HC_{2hIW}	17.43 ± 0.6	60

Overall, as indicated in Table 4.1, the chloride diffusion coefficients of all tested concrete mixtures were relatively close to that of the reference concrete (OC). The addition of limestone filler did not lead to a significant change in the diffusion coefficient. However, an increase of 41% and 68% was observed in the OC+HC_{2hAW} and OC+F+HC_{2hAW} mixtures, respectively. The results obtained are in line with the initial expectations of the study and can be explained by considering the microstructural characteristics of cork and the physical mechanisms governing the mixing process and the interaction between the various concrete constituents. Cork is characterized by a unique microstructure of closed cells, with air occupying approximately 90% of its volume. The walls, rich in suberin, provide partial resistance to water penetration, while the fine intercellular pores allow connectivity between adjacent cells. This structure results in a lightweight, highly porous material with a significant capacity for fluid absorption under prolonged exposure.

Concrete mixtures (OC+HC_{2hAW}) face significant challenges, particularly because the short mixing duration prevents full saturation of the dry cork particles. This leads the cork to absorb a substantial portion of the mixing water initially intended for cement hydration, resulting in a cascade of detrimental effects. In particular, the effective water-to-cement ratio (w/c) decreases below the design specification, and hydration reactions are delayed due to insufficient water availability (Miguel et al., 2021).

These adverse effects are substantially amplified by the concurrent incorporation of ultrafine limestone filler, which exhibits elevated water demand attributable to two primary factors: its extensive specific surface area necessitates additional water for surface saturation, and particle-level interactions with cement grains intensify internal friction, thereby requiring enhanced lubrication through increased water content. The simultaneous use of virgin cork aggregates and limestone filler (OC+F+HC $_{2hAW}$) generates a synergistic detrimental effect characterized by three principal manifestations. First, overall porosity increases dramatically through the superposition of cork's inherent porosity (approximately 90%), supplementary porosity arising from incomplete cement hydration, and void formation resulting from suboptimal particle packing. Second, an interconnected pore network develops, comprising voids surrounding cork particles, capillary channels forming continuous fluid transport pathways, and interstitial voids that enhance pore connectivity, thereby indicating an enhancement in the mass transport mechanism. Third, weak interfacial bonding emerges, characterized by poor adhesion between cork and the cementitious matrix, incomplete integration of limestone particles, and the formation of vulnerable zones that fundamentally compromise both mechanical performance and long-term durability of the composite material. These combined microstructural phenomena explain the increase in the chloride diffusion coefficient observed when virgin cork with 2hAW is used in conjunction with limestone filler. The highly porous, poorly bonded structure facilitates the transport of chloride ions through the concrete matrix, reducing its durability under aggressive environmental conditions. Notably, the mixtures containing cork aggregates pre-soaked in water for 2 hours (OC+HC $_{2hIW}$) demonstrated superior performance in reducing chloride diffusion. When virgin cork with (2hIW) was used, the diffusion coefficient decreased significantly. When combined with limestone filler (OC+F+HC $_{2hIW}$), the diffusion coefficient ranged between 15.6 and 17.4 $\times 10^{-12}$ m²/s, respectively (Ortega et al., 2022 & Miguel et al., 2020).

This enhanced performance in mixtures incorporating cork pretreated by two-hour water immersion (OC+HC $_{2hIW}$) is attributed to several microstructural changes. Pre-soaking the cork likely facilitates controlled water release during cement hydration and may activate chemical compounds that interact with the cement matrix. This interaction contributes to modifications in the pore structure and distribution, resulting in more tortuous and complex pathways for chloride ion ingress. These findings

suggest that parameters such as pore network tortuosity and connectivity play a crucial role in governing chloride transport. Greater tortuosity implies longer and more convoluted pathways, which reduce the effective diffusion rate. Similarly, limited pore connectivity restricts ion mobility, even when the total porosity is relatively high. Hence, the microstructural features of natural cork concrete substantially enhance its resistance to chloride penetration (Dhandapani et al., 2021).

The lag time is inversely proportional to the chloride diffusion coefficient; that is, the lower the diffusion coefficient, the longer the lag time. The maximum lag time, estimated at 76.1 hours, was recorded for the OC+HC $_{2hIW}$ mixture, whereas the minimum lag time, approximately 40.7 hours, was observed for OC+F+HC $_{2hAW}$. These results are consistent with previous studies, such as that of Touil et al. (Touil et al., 2017), which demonstrated that both the type and porosity of concrete have a significant influence on the diffusion coefficient. The lag time varies according to the degree of interaction between chloride ions and the concrete matrix, increasing as the diffusion coefficient decreases.

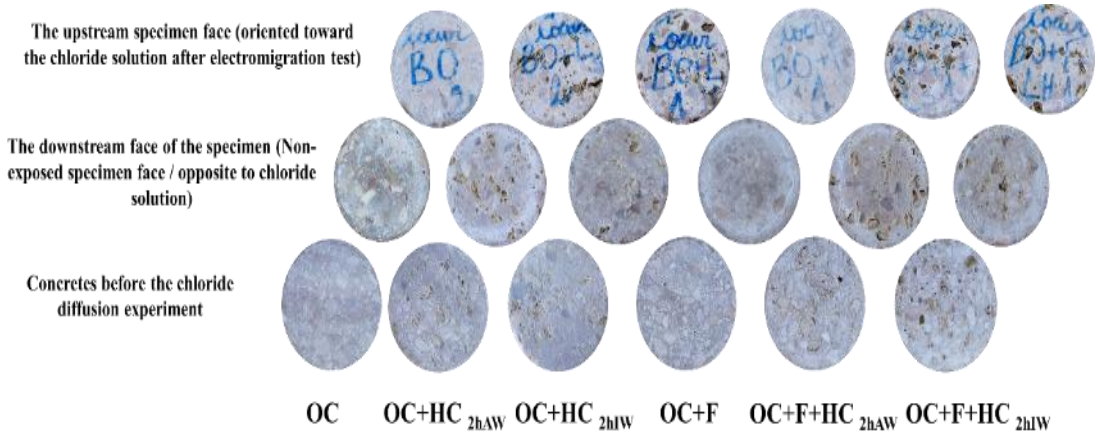
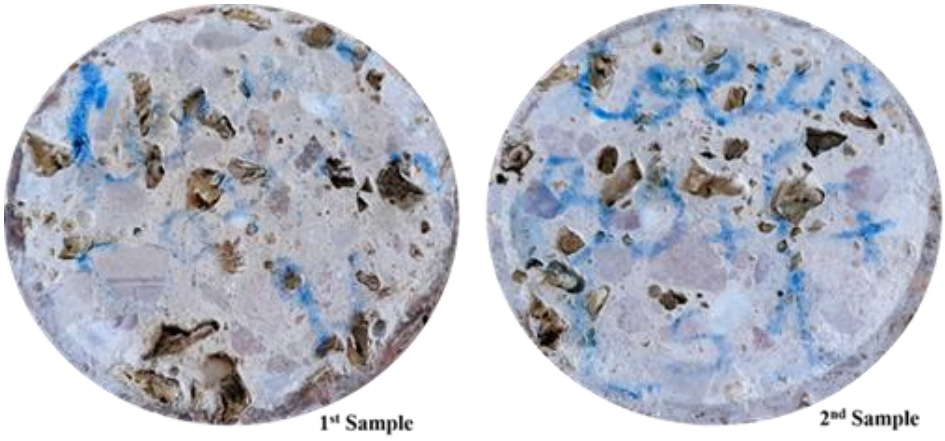


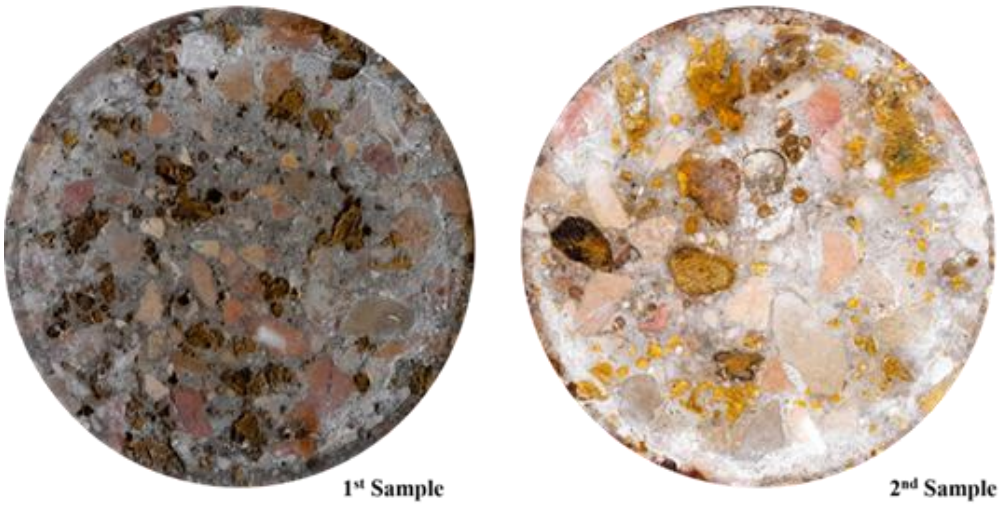
Fig. 4.14. Concrete samples before and after chloride diffusion tests.

As shown in Fig. 4.14, the degree and pattern of surface degradation on the specimen face exposed to the chloride solution varied depending on the concrete type. Both ordinary concrete and limestone concrete maintained similar external appearances, with no noticeable alterations observed on either the upper or lower surfaces of the tested specimens. In contrast, cork-based concretes (OC+HC$_{2hIW}$ & OC+F+HC$_{2hIW}$) exhibited visible deterioration, particularly in the form of erosion of cork particles on the specimen surfaces. The most severe damage was observed in the (OC+F+HC$_{2hAW}$) cork concrete specimens, which experienced significant surface degradation,

especially on the upper face directly exposed to the chloride solution. As illustrated in Fig.4.15, Severe surface degradation in the (OC+F+HC_{2hAW}) samples is attributed to cork porosity, weak matrix–cork bonding, chloride penetration, and partial cork disintegration, with accelerated damage on the exposed upper surface due to combined physical and chemical effects.



Exposed faces of the specimens directed toward chloride solution



The non-exposed faces of the specimens to the chloride solution

Fig. 4.15. The deterioration of the (OC+F+HC_{2HAW}) specimens.

The most significant finding was the superior resistance to chloride ion penetration exhibited by OC+HC_{2hIW} concrete. This result necessitated the completion and further development of the experimental framework. Accordingly, four concrete formulations were considered: reference concrete OC, limestone concrete OC+F, wet cork concrete with cork aggregate pre-soaked for two hours OC+HC_{2hIW}, hereafter referred to as OC+HC, and wet cork concrete with cork aggregate pre-soaked for two hours combined with limestone OC+F+HC_{2hIW}, designated as OC+F+HC.

4.10. Pore size distribution

Fig. 4.16 presents a detailed analysis of the pore size distributions of the various concretes investigated in this study, as determined using the advanced Mercury Intrusion Porosimetry (MIP) technique. The experimental data provide comprehensive insights into the porosity characteristics and internal structure of each concrete type examined.

The analytical results reveal a distinct bimodal pore size distribution in the ordinary reference concrete (OC), characterized by two clearly defined pore diameter classes representing different pore network types. The first class is centered around 0.095 µm and is primarily associated with medium-sized capillary pores formed during cement hydration and the generation of hydration products. The second class, centered around 0.432 µm, corresponds to larger pores and entrapped air voids introduced during mixing and casting.

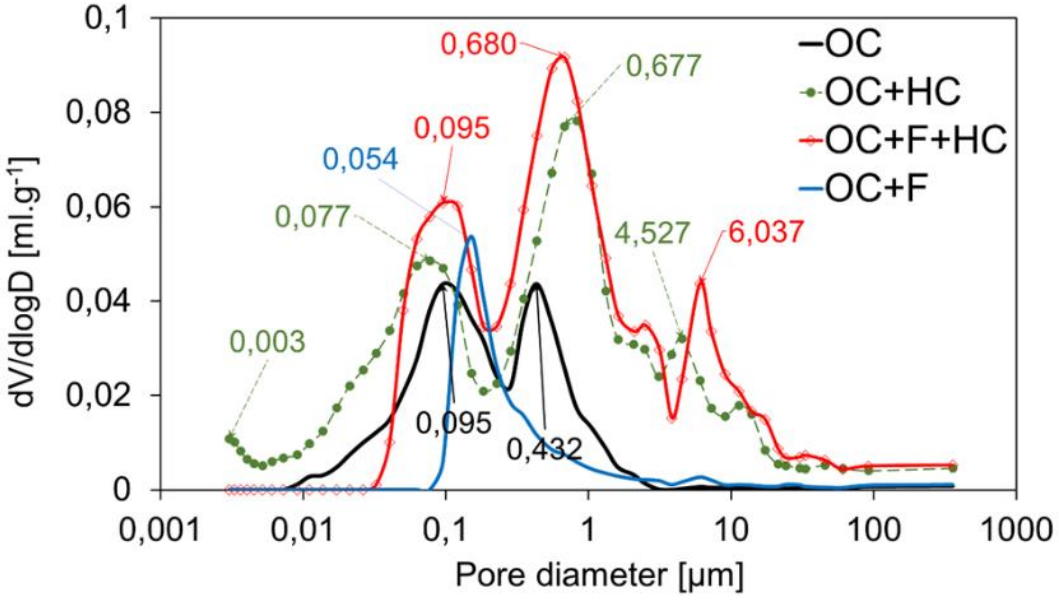


Fig. 4.16. The pore size distribution of the concrete tested.

In contrast, the incorporation of limestone filler resulted in a fundamental alteration of the pore structure, shifting the distribution from bimodal to a more uniform unimodal distribution in the limestone concrete (OC+F). This distribution is characterized by a single, prominent pore diameter of 0.054 µm, indicating the beneficial role of limestone filler in refining the pore structure through physical packing (filler effect) and nucleation mechanisms. These processes contribute to densifying the cementitious matrix and reducing the volume of interconnected pores.

The incorporation of virgin cork into the concrete (OC+HC) produced a markedly different outcome, generating a complex network of new pore families. This modification yielded a broad pore size spectrum encompassing finer and larger pores than those observed in the reference concrete (OC). The characteristic pore diameters in this case were 0.003 μm (ultrafine pores), 0.077 μm (fine pores), 0.677 μm (medium pores), and 4.527 μm (large pores). The presence of larger pores is primarily attributed to the relatively weak Interfacial Transition Zone (ITZ) formed between the organic cork particles and the inorganic cementitious matrix. This ITZ exhibits distinct physical and chemical properties, leading to imperfect interfacial bonding, as clearly illustrated in the high-resolution SEM images (see Figure 4.17), which reveal the microstructural details of these transitional regions.

A comparable trend was observed in the composite concrete containing both limestone filler and virgin cork (OC+F+HC), though with a notable difference: ultrafine pores (0.003 μm) were absent from the pore size distribution. The characteristic pore diameters for this mixture were 0.095 μm, 0.680 μm, and 6.037 μm. This alteration in pore structure and the reduction in fine pores is most likely due to the dual functional role of the limestone filler. The fine limestone particles penetrate and occupy the cork's intrinsic porosity, thereby limiting or preventing continued secondary hydration within these pores and reducing the formation of additional calcium silicate hydrate (C-S-H gel)—the primary phase responsible for concrete strength and cohesion. This mechanistic explanation accounts for the very limited change in the mechanical strength of the concrete containing both virgin cork and limestone filler compared to that containing virgin cork alone, as the potential performance gains from limestone filler addition are partially offset by the loss of internal curing benefits from additional hydration within the cork pores.

4.11. Scanning Electron Microscopy (SEM) Morphological Analysis

Fig. 4.17 presents the nanoscale spectroscopic analysis performed using Scanning Electron Microscopy (SEM) and Energy-Dispersive X-ray Spectroscopy (EDS) for the studied concrete mixtures, aiming to assess the morphological and chemical effects of incorporating virgin cork and limestone filler on the microstructure and phase composition of the cementitious matrix, with particular attention to the characteristics of the interfacial transition zone (ITZ) and structural defects.

Microscopic examinations revealed that the reference (OC) and limestone (OC+F) concrete mixture exhibits a homogeneous and densely packed microstructure, indicative of a well-hydrated cement matrix with a uniform distribution of crystalline phases, in contrast to the cork-containing mixtures (OC+HC and OC+F+HC), which displayed a reduced degree of structural uniformity. The reference mixtures demonstrated a compact nanostructure with strong surface bonding, reflecting the efficiency of hydration processes and crystallization mechanisms. In OC, average pore diameters of 1.1 μm and an ITZ width of up to 8 μm were recorded, consistent with mercury intrusion porosimetry (MIP) results showing pore size distributions in the range of (0.01–8) μm.

Cork-modified mixtures exhibited a progressive increase in both pore size and ITZ width, with the largest values recorded for (OC+F+HC). This suggests that partial replacement of natural aggregates with virgin cork particles promotes the development of a more open and interconnected pore network, with pore diameters reaching up to 50 μm, as confirmed by MIP analysis, while still maintaining acceptable mechanical interlocking and chemical bonding between the cement phase and aggregates. SEM images also revealed the characteristic honeycomb cellular structure of cork, with void diameters up to 35 μm. The ITZ in these mixtures displayed heterogeneous behavior, ranging from well-bonded interfaces to areas with microcracks and fissures; its width ranged from 16.4 μm in (OC+HC) to 50 μm in (OC+F+HC).

From a theoretical standpoint, the inclusion of limestone filler is expected to improve microstructural density and enhance ITZ cohesion through filler effects. However, the cumulative influence of cork particles increases porosity and entrained air content, which may counteract the densifying impact of mineral fillers and affect the composite’s mechanical performance. Conversely, the evolution of a closed pore network could enhance the thermo-physical and acoustic properties of the material.

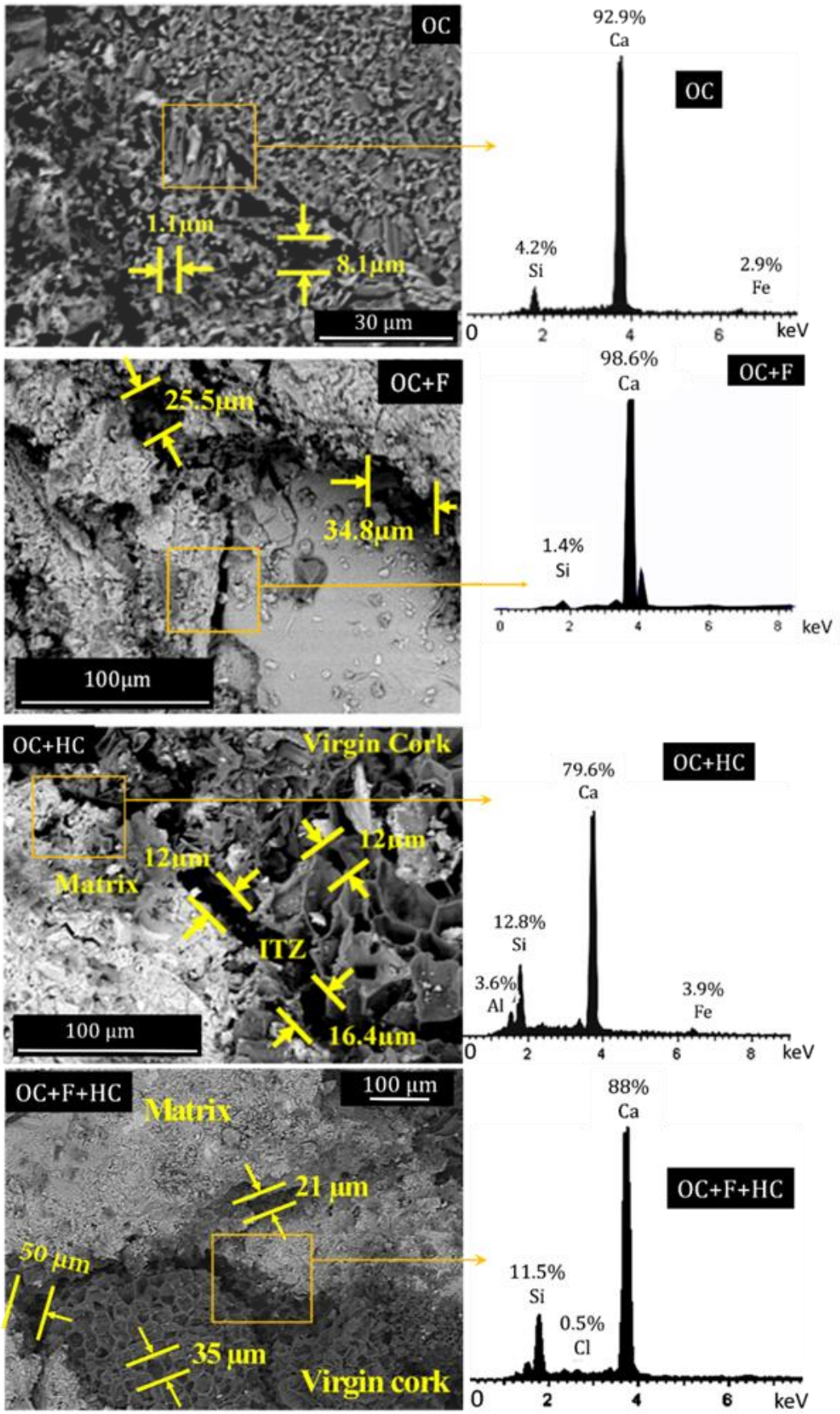


Fig. 4.17. SEM and EDS analysis for the studied concretes.

EDS analysis confirmed the anticipated elemental distribution of the major constituents-calcium (Ca), silicon (Si), iron (Fe), and aluminum (Al)-with trace amounts of chlorine (0.5%) detected in the (OC+F+HC) mixture, likely originating from mineral impurities in the limestone filler, as reported in Table 3.2.

4.12. Thermogravimetric Analysis (TGA)

This procedure yields a thermogravimetric curve that illustrates the mass evolution as a function of temperature Fig.4.18, providing valuable insights into the internal composition of the material, hydration products, and the mechanisms of different thermal decomposition processes. TGA enables the quantification of total weight loss and the identification of critical temperature ranges at which mass loss events occur. It is further employed to estimate moisture content, monitor dehydration of hydrates, detect the decomposition of calcium hydroxide, assess the loss of organic compounds, and capture a broad spectrum of other thermally induced phenomena that lead to measurable and quantifiable mass variations.

This analytical study aims to assess the comprehensive thermal behavior of ordinary concrete (OC), limestone concrete (OC+F), wet cork concrete (OC+HC), and (OC+F+HC) using thermogravimetric analysis (TGA) over the temperature range of 25–1000 °C. The objective is to investigate the effects of these additives on the thermal properties and stability of the base concrete. As shown in Fig.4.18, at the first stage of drying and moisture loss (25–200 °C), different mass losses were observed. OC exhibited ~1.5% mass loss corresponding to inherent moisture, whereas OC+F recorded a reduced value of ~1.2% due to the dry mineral nature of limestone. In contrast, OC+HC showed an increased value of ~4.0% as a result of the additional moisture content of cork, while OC+F+HC recorded ~3.5%, highlighting a synergistic effect in moisture management.

The second stage (200–450 °C) is characterized by the decomposition of cork's organic constituents. OC+HC exhibited an additional gradual mass loss (~3–4%) associated with the successive degradation of hemicellulose (200–280 °C), cellulose (280–350 °C), and lignin (350–450 °C). During the third stage of relative stability (450–700 °C), samples containing limestone demonstrated superior stability owing to the formation of a protective carbon $CaCO_3$ matrix. This composite acted as both a thermal reservoir and a physical barrier, in conjunction with the cork's residual carbon, while benefiting from evaporative cooling effects that delayed heat transfer.

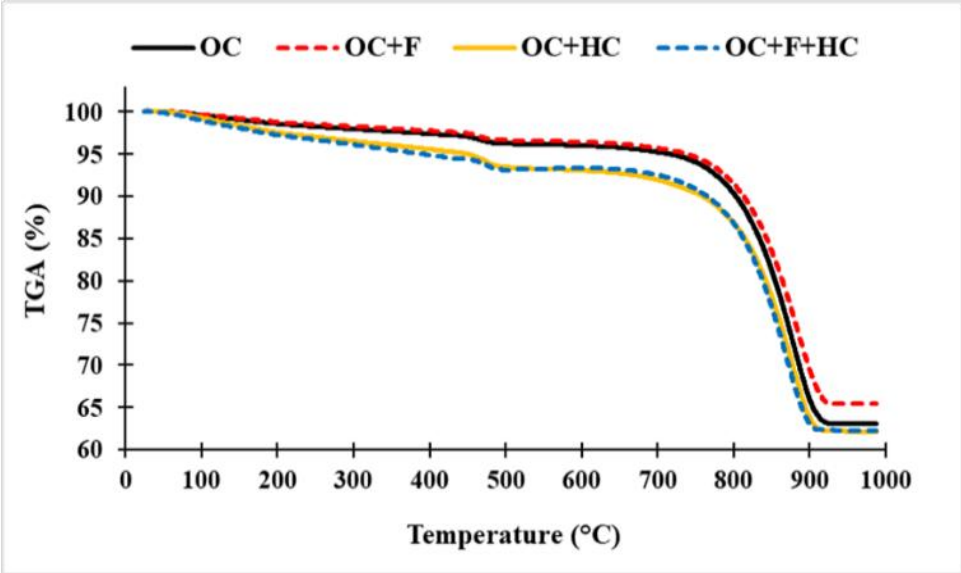


Fig. 4.18. TGA Results Analysis Diagram.

The significance of natural addition becomes particularly evident in the fourth stage (700–900 °C). OC exhibited sharp degradation at ~760 °C with a 35% mass loss, whereas OC+F delayed degradation to ~780 °C. This improvement is attributed to the endothermic decomposition of $CaCO_3$, the formation of a protective CaO layer, and the inert effect of the released CO_2, which together facilitated the development of a mixed CaO activated carbon layer with potential reactions that enhanced thermal cohesion.

In the final stage (900–1000 °C), quantitative analysis of the residues revealed higher stability in the limestone concrete, with residual masses of 62% for OC, 65% for OC+F, 63% for OC+HC, and 64% for OC+F+HC. These residues predominantly consisted of activated carbon, calcium oxide, un-decomposed calcium carbonate, and secondary mineral compounds.

Overall, the results confirm the effectiveness of limestone as a natural thermal stabilizer, primarily through its endothermic decomposition, the formation of a protective CaO layer, and the release of CO_2 as a diluting inert gas. Meanwhile, wet cork enhanced early-stage thermal insulation, contributed additional beneficial carbonaceous residues, and provided a graded thermal barrier. The combination of limestone and cork exhibited a limited but positive synergistic effect. leading to improved overall thermal stability without detrimental interactions, thus achieving an optimal balance between the distinct stabilizing contributions of limestone and cork.

4.13. The Derivative Thermogravimetric Analysis (DTG)

The derivative thermogravimetric analysis (DTG), conducted as a complementary approach to the thermogravimetric analysis (TGA), provides a deeper understanding of the dynamics of thermal decomposition and the associated mass loss rates (Fig. 4.19). This method enables more precise identification of critical decomposition points and underlying mechanisms.

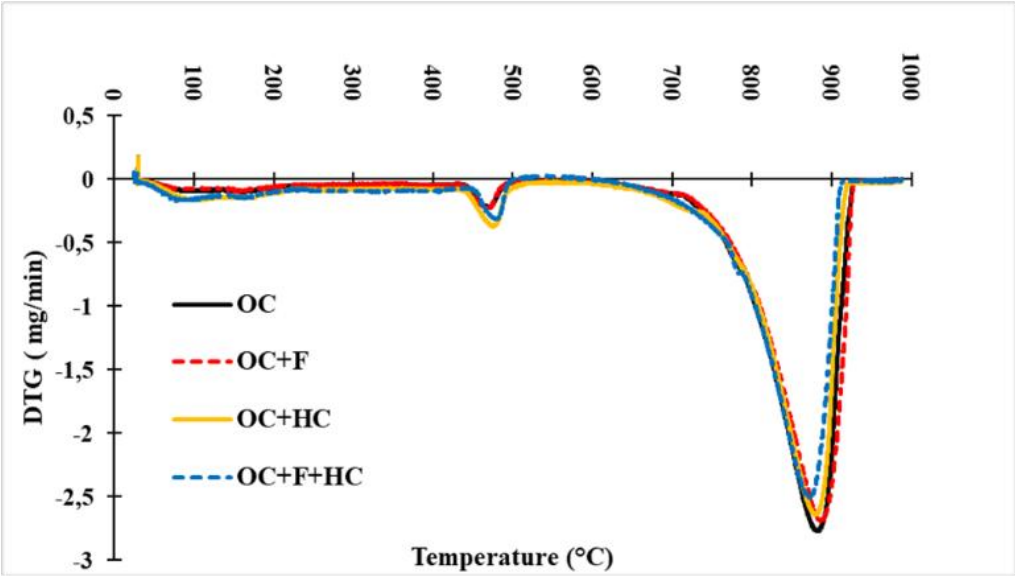


Fig. 4.19. DTG Results Analysis Diagram.

In the first stage, corresponding to the loss of moisture and volatile compounds (0-300 °C), all samples exhibit a minor peak at approximately 100 °C, which represents the evaporation of absorbed moisture. The OC+HC specimen shows an additional small peak (-0.15 mg/min) at around 150 °C, indicating the presence of supplementary moisture introduced by cork. Conversely, the OC+F specimen records a lower intensity peak (-0.08 mg/min), highlighting the drying effect of limestone, which contributes to maintaining a reduced decomposition rate. During the transitional stage of organic component degradation (300-700 °C), the OC+HC specimen exhibits a distinct medium-intensity peak at approximately 477 °C (-0.4 mg/min), corresponding to the decomposition of cellulose and hemicellulose in cork. In comparison, the OC+F+HC specimen displays the same peak, though with a mitigated intensity (-0.3 mg/min), confirming the inhibitory effect of limestone even at this early decomposition phase. The most critical stage corresponds to the main decomposition peak (700–1000 °C), where the DTG curves reveal a pronounced mass-loss event beginning around 750 °C, with marked variations across the samples. The OC

specimen records the highest mass-loss rate at 884 °C (–2.8 mg/min). In contrast, the OC+F specimen shows a delayed peak at 887 °C with reduced intensity (–2.6 mg/min). The OC+HC specimen demonstrates a similar trend to the ordinary concrete sample but with slightly lower intensity. Notably, the OC+F+HC specimen achieves the most favorable synergistic effect, with a delayed decomposition peak at 868 °C and the lowest intensity (–2.4 mg/min), underscoring the superior efficiency of the combined formulation in enhancing thermal degradation resistance.

Overall, this integrated study provides strong evidence supporting the development of thermally enhanced composites through the incorporation of natural and sustainable additives. The analytical results clearly demonstrate that the inclusion of limestone and wet cork does not adversely affect the thermal stability of the base material; rather, it imparts advanced functional characteristics that enhance the overall thermal performance. This combined thermal and functional compatibility positions these natural additives as highly suitable candidates for advanced thermal applications, while simultaneously meeting environmental sustainability requirements.

Calcium hydroxide (CH) The measurement of mass loss enables the determination of chemically bound water content and the concentration of free calcium hydroxide (CH) within the cementitious matrix. Chemically bound water is a fundamental component in the development of mechanical strength and the formation of cement hydrates, whereas free CH contributes to the enhancement of pozzolanic reactions and the generation of additional C–S–H gel, thereby improving the mechanical properties and sustaining the alkaline environment necessary for reinforcing steel passivation. A quantitative assessment of these two parameters provides valuable insight into predicting the long-term performance of concrete and its resistance to environmental degradation (Pandiaraj et al., 2024).

The content of chemically bound water in the sample can be determined using the following equation (Pandiaraj et al., 2024):

$$W_B = L_{dh} + L_{dx} + 0.41\, L_{dc} \quad (10)$$

The free CH present in the sample is calculated according to this equation (Pandiaraj et al., 2024):

$$\text{Free CH content} = 4.11 L_{dx} + 1.68\, L_{dc} \quad (11)$$

Where: W_B is the chemically bound water (%). L_{dh} is the mass loss between105 and 440 °C due to dehydration of the hydrates (%). L_{dx} is the mass loss between 440 and 580 °C due to dehydroxylation of calcium hydroxide (%). L_{dc} is the mass loss between 580 and 1000 °C due to decarbonation of calcite and the anhydrous material (%).

The amount of $CaCO_3$ in the sample is determined using the following equation:

$$CaCO_3(mg) = \Delta W \times \frac{MCaCO_3}{MCO_2} \quad (12)$$

Where: ΔW: mass loss between (600–900 °C) (mg). M_{caco_3}: molar mass of calcium carbonate (100 g/mol). M_{co_2}: molar mass of carbon dioxide (44 g/mol).

Table 4.2. Chemical Composition and $CaCO_3$ Content of Concrete Mixtures.

Concrete	L_{dh}	L_{dx}	L_{dc}	Mass Loss (600-900°C) (mg)	W_B (%)	Free CH (%)	$CaCO_3$ (mg)
OC	2,36	1,11	33,03	24,87	17,02	60,07	56,52
OC+F	2,07	1,08	31,06	23,32	15,89	56,64	53,01
OC+HC	4,04	2,02	31,08	23,99	18,81	60,53	54,53
OC+F+HC	4,41	1,14	31,07	23,29	18,30	56,91	52,93

The analytical results demonstrate that the influence of limestone and wet cork on the internal chemical interactions of concrete is distinct, yet becomes complementary when both are combined. The reference concrete (OC) exhibited relatively high contents of chemically bound water (W_B = 17.02%) and free calcium hydroxide (CH = 60.07%), along with elevated values of calcium carbonate ($CaCO_3$ = 56.52 mg). The incorporation of limestone (OC+F) resulted in a marked decrease in W_B (-6.7%) and CH (-5.7%), which was reflected in a reduction of $CaCO_3$ content (-6.2%) and. This behavior suggests that limestone consumes part of the available CH through secondary reactions but does not effectively promote carbonation when used in isolation. In contrast, wet cork (OC+HC) significantly increased W_B (+10.5%) while maintaining CH at a level comparable to the reference (+0.76%), with only a slight decrease in $CaCO_3$ content (-3.5%). This indicates that wet cork enhances moisture retention within the matrix. The combined system (OC+F+HC) exhibited a clear synergistic effect, as $CaCO_3$ content decreased to 52,93 mg. This finding confirms that the concurrent action of limestone and wet cork has little influence on carbonate formation within the cementitious structure.

4.14. Thermo-Diffusive Investigation

Fig. 4.20 illustrates the chloride concentration at a temperature of 5 °C over a period of 250 hours for the four concrete mixtures. The results reveal clear differences in chloride release rates among the studied samples. The OC+F mixture exhibited the highest chloride accumulation, reaching approximately 15 g/L at the end of the test period, followed by the OC mixture with about 12 g/L. In contrast, the OC+HC and OC+F+HC mixtures showed lower concentrations, around 7 g/L and 9 g/L, respectively. All samples exhibited a similar trend in chloride release, characterized by a slow rate during the first 100 hours, followed by a gradual acceleration thereafter. These findings indicate that the addition of limestone significantly enhances chloride release, primarily by increasing the pH of the medium and creating an alkaline environment that promotes dissolution, hydrolysis, and ion-exchange processes leading to chloride liberation. Conversely, the presence of wet cork considerably reduces chloride release, highlighting its effective role as a physical barrier that decreases permeability or as an adsorptive material capable of retaining chloride ions, even to a limited extent. The low temperature (5 °C) influenced the overall reaction kinetics, resulting in relatively slower release rates during the initial stage of the experiment. Our results are consistent with those reported by Touil et al. (Touil et al., 2017) as the lowest chloride diffusion coefficients for both ordinary concrete (OC) and 10% pozzolan concrete were recorded at 5°C. The migration coefficient decreased by approximately 58–60% compared to 20°C, accompanied by an increase in the time lag (T_{lag}), reflecting reduced ionic mobility and improved resistance to chloride penetration at low temperature. Nevertheless, pozzolan concrete remained less permeable than ordinary concrete.

Fig. 4.22 presents the variation of chloride concentration at a temperature of 50 °C, over a 250-hour period for four concrete mixtures. The results demonstrate substantial differences in chloride release rates among the studied concretes, with a pronounced influence of elevated temperature compared to the previous test conducted at 5 °C. The OC+F mixture exhibited the highest chloride accumulation, reaching approximately 36 g/L at the end of the experiment, followed by the OC mixture with about 35 g/L. In contrast, the OC+F+HC and OC+HC mixtures showed lower concentrations of around 23 g/L and 21 g/L, respectively. It is observed that chloride release rates were considerably faster from the beginning of the test, showing an immediate onset followed by an almost linear increase throughout the entire

experimental period. These findings indicate that raising the temperature to 50 °C significantly enhanced the kinetics of chloride release in all mixtures, resulting in approximately double the final concentrations compared to those observed at 5 °C. Furthermore, the inhibitory effect of wet cork remains evident even under elevated thermal conditions, confirming its efficiency as a physical and/or chemical barrier that reduces chloride permeability within the concrete matrix. Our findings are in agreement with those reported by Touil et al. (Touil et al., 2017), as the highest chloride diffusion coefficients were recorded at 50°C. The migration coefficient increased by approximately 64–66% compared to 20°C, reaching nearly three times the reference value, with a marked decrease in the time lag (T_{lag}). This behavior reflects a significant acceleration in chloride penetration kinetics, particularly at temperatures above 30°C. Despite this pronounced increase in diffusivity, pozzolan concrete exhibited greater resistance and lower chloride transport than ordinary concrete at the same temperature level.

A comparison of the three profiles obtained at 5 °C, 20 °C, and 50 °C (Fig. 4.20, 21, 22) clearly demonstrates the progressive influence of temperature on the kinetics of chloride release from all studied concrete mixtures. The final chloride concentrations increased markedly with temperature, ranging for the OC mixture from approximately 12 g/L at 5 °C to 32 g/L at 20 °C, and reaching 35 g/L at 50 °C. This trend indicates that higher temperatures significantly accelerate the chemical reactions responsible for chloride liberation.

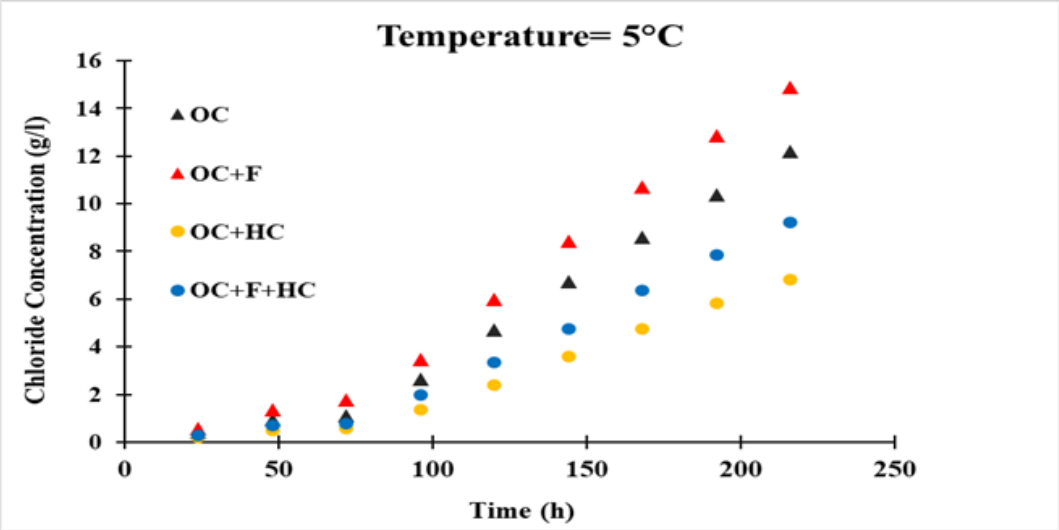


Fig. 4.20. Cumulative chloride content in the downstream compartment of concrete at 5°C.

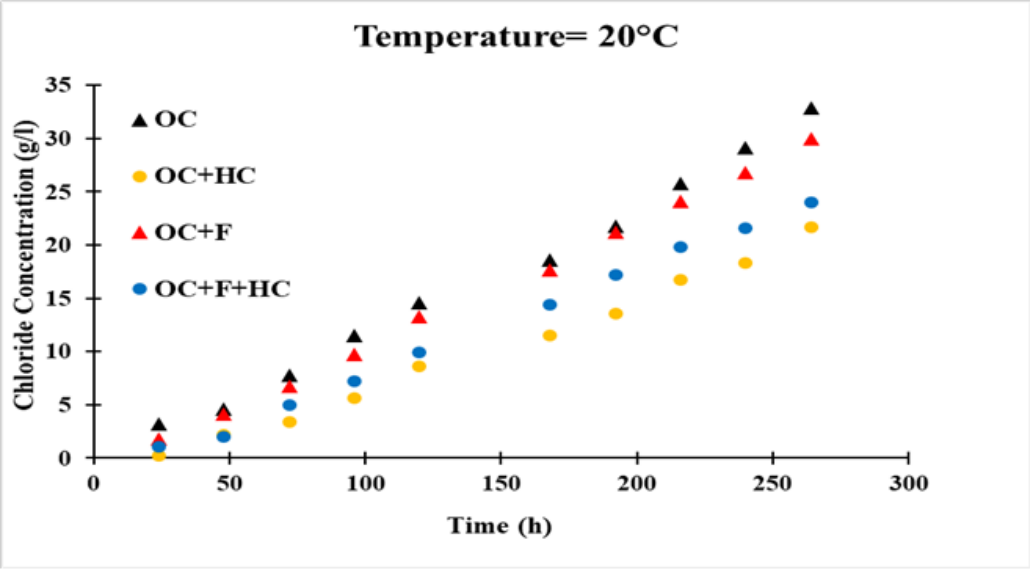


Fig. 4.21. Total chloride accumulation within the downstream cell of concrete at 20°C.

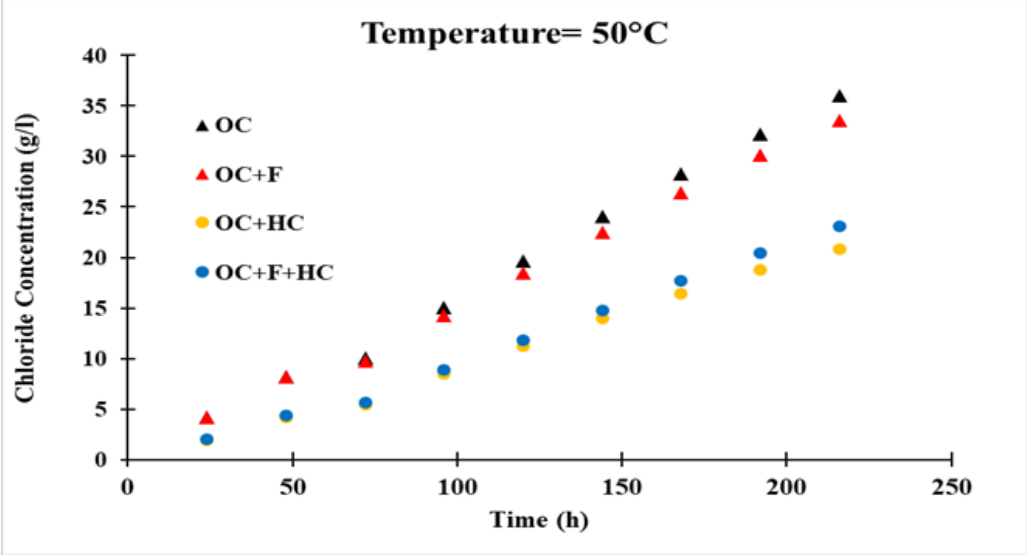


Fig. 4.22. Total chloride accumulation within the downstream cell of concrete at 50°C.

It is also observed that the initial induction period-during which chloride release was slow-was evident at 5 °C (approximately 100 hours) but progressively shortened as the temperature increased, leading to an immediate and rapid release at 50 °C. The OC+F mixture consistently exhibited the highest chloride concentrations across all tested temperatures, confirming the catalytic role of limestone in promoting chloride release by increasing the pH of the medium and facilitating ion-exchange reactions.

Conversely, the mixtures containing wet cork (OC+HC and OC+F+HC) consistently displayed a 30-40% reduction in released chloride concentrations compared with those without cork, regardless of temperature. This finding highlights the effectiveness of wet cork as a physical and/or chemical barrier that reduces chloride

permeability and release, even under harsh thermal conditions. Taken together, these results emphasize that both temperature control and the selection of suitable additives are critical factors in regulating chloride release from the studied systems.

Table 4.3 results clearly demonstrate the combined influence of temperature and concrete type on the chloride diffusion coefficient (De), lag time through the concrete. The diffusion coefficient exhibited a consistent increase with rising temperature across all samples.

Table 4.3. Diffusion coefficients, lag times of all studied concrete mixtures.

Concrete	Chloride diffusion coefficient D_e (E^{-12} m^2/s)			Lag time (Hours)		
	5°C	20°C	50°C	5°C	20°C	50°C
OC	15.75 ± 0.5	21.62 ± 1.2	30 ± 0.6	64.7	53.2	13.74
OC+F	17.66 ± 0.7	26.2 ± 0.3	31,1 ± 0.5	62.14	52.3	13,47
OC+HC	10.2 ± 0.4	15.60 ± 0.8	20.36 ± 0.9	68.64	76.1	21.65
OC+F+HC	12.38 ± 0.2	17.43 ± 0.6	22.06 ± 0.7	62.2	60	21.7

Among the studied mixtures, OC+F concrete showed the highest diffusion coefficients values at all temperatures (17.66, 26.2, and 31.1 $\times 10^{-12}$ m^2/s at 5°C, 20°C, and 50°C, respectively), followed by OC concrete. In contrast, mixtures incorporating wet cork OC+HC & OC+F+HC presented the lowest diffusion coefficients, indicating the cork's ability to reduce chloride permeability by approximately 28–35%.

Regarding lag time, a sharp decrease was observed with increasing temperature, ranging from 62–68 hours at 5°C and 52–76 hours at 20°C, before dropping substantially to 13–21 hours at 50°C. This confirms that elevated temperatures accelerate the onset of chloride diffusion processes. Overall, these findings indicate that the inclusion of limestone tends to reduce the concrete's resistance to chloride diffusion, whereas the incorporation of wet cork effectively enhances its barrier properties across all tested temperatures.

4.15. Chloride–Concrete Interactions

The study of chloride adsorption behavior in this research is based on the Langmuir Isotherm model. This mathematical model describes the equilibrium relationship between the concentration of free chlorides (Cf) in the pore solution and the bound

chlorides (Cb) within the cementitious matrix. This model operates on the assumption that adsorption occurs on a homogeneous surface through a single layer (monolayer) at specific, well-defined binding sites. The fundamental equation is expressed as:

$$C_b = \frac{K_L \times C_{b,max} \times C_f}{1 + K_L \times C_f} \qquad (13)$$

Where:

C_b (Bound Chlorides): quantity of chloride ions chemically or physically sequestered by the concrete matrix, expressed in (g/g).

C_f (Free Chlorides): Denotes the concentration of free chloride ions remaining in the pore solution at equilibrium, measured in (**g/L**).

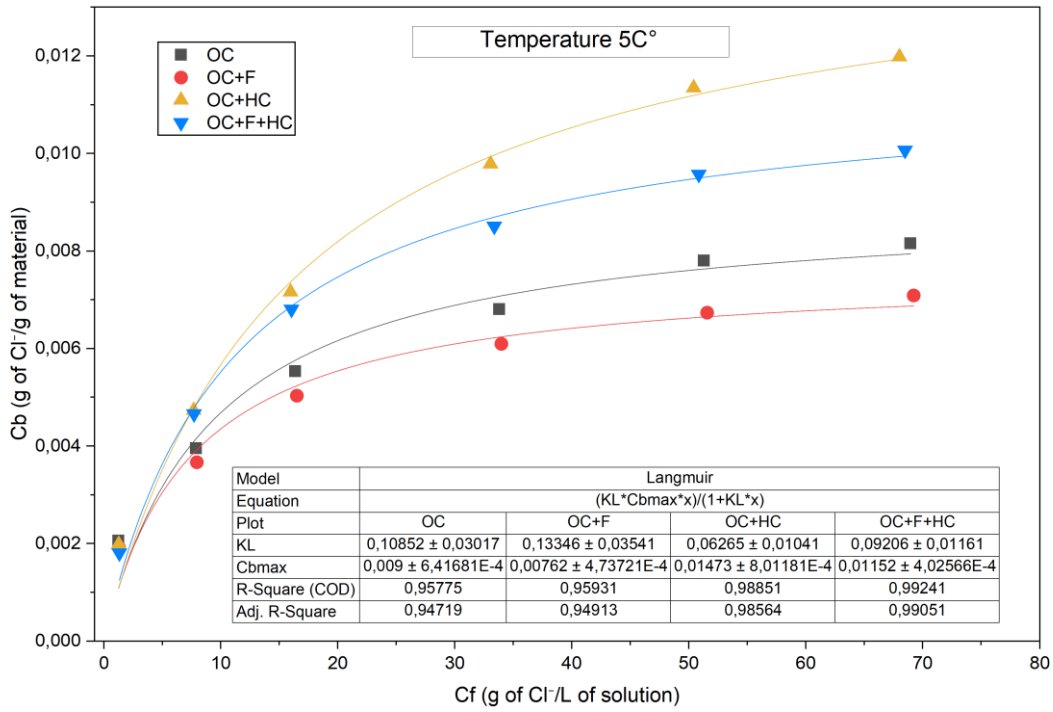
$C_{b,\,max}$ (Maximum Binding Capacity): Defines the theoretical maximum adsorption capacity, representing the total number of active binding sites available for chloride sequestration within the matrix.

K_L (Langmuir Equilibrium Constant): An equilibrium constant that reflects the binding affinity between chloride ions and the adsorbent surface; higher values indicate a stronger and more stable interaction at the binding sites.

The results demonstrated that the Langmuir model provided an accurate representation of the adsorption isotherms, with its curves fitting most of the experimental data points across the different temperature conditions, indicating its high suitability for describing chloride binding behavior in all the studied cases.

The results presented in the Fig. 4.23 illustrate the chloride binding isotherms for chloride ions in various types of concrete at a constant temperature of 5°C. These isotherms describe the relationship between the concentration of free chlorides (C_f) in the pore solution and the bound chlorides (C_b) within the cementitious matrix, as it is a key parameter for assessing the concrete's resistance to chloride ingress and the protection of steel reinforcement against corrosion.

The data indicate that all concrete mixtures characterized by a rapid increase in chloride binding at low concentrations (0–20 g Cl^-/L), followed by a gradual decline in the binding rate as the free chloride concentration increases. This trend suggests that the available binding sites approach saturation, which is consistent with the limited chemical and physical binding mechanisms inherent to the cement matrix.



Model	Langmuir			
Equation	(KL*Cbmax*x)/(1+KL*x)			
Plot	OC	OC+F	OC+HC	OC+F+HC
KL	0,10852 ± 0,03017	0,13346 ± 0,03541	0,06265 ± 0,01041	0,09206 ± 0,01161
Cbmax	0,009 ± 6,41681E-4	0,00762 ± 4,73721E-4	0,01473 ± 8,01181E-4	0,01152 ± 4,02566E-4
R-Square (COD)	0,95775	0,95931	0,98851	0,99241
Adj. R-Square	0,94719	0,94913	0,98564	0,99051

Fig. 4.23. Chloride binding isotherms of concretes at 5°C.

The OC+HC concrete mixture exhibited the highest chloride binding capacity, with a $C_{b,max}$ value of 0.01473 g Cl^-/g, exceeding that of the reference concrete (OC) (0.009 g Cl^-/g) and the limestone-based mixture (OC+F) (0.00762 g Cl^-/g).

In contrast, the OC+F mixture showed the lowest chloride binding capacity (0.00762 g Cl^-/g), raising questions regarding the effectiveness of limestone in enhancing chloride adsorption.

The results clearly show that the wet cork concrete (OC+HC) achieved the highest chloride binding capacity (≈0.012 g Cl^-/g of material) at higher concentrations, outperforming all other mixtures. This unexpectedly superior performance can be attributed to a combination of interrelated mechanisms operating at both microstructural and chemical levels. Firstly, cork incorporation induces microstructural modifications by enhancing the porous architecture of concrete through the generation of additional pores upon moisture evaporation or degradation of organic constituents, consequently expanding the available surface area for physical adsorption processes. Secondly, the chemical functionality inherent in cork's organic components, particularly the presence of carboxyl and hydroxyl functional groups, facilitates interaction with chloride ions via hydrogen bonding mechanisms.

Thirdly, the elevated moisture content characteristic of wet cork may exert a retarding effect on cement hydration kinetics, thereby promoting the formation of modified AFm phases with enhanced chloride binding capacity. Collectively, these synergistic mechanisms contribute to the observed improvement in chloride resistance performance.

In contrast, the limestone-modified concrete (OC+F) exhibited the lowest binding capacity (≈0.007 g Cl^-/g), even lower than the reference concrete (OC), which reached approximately 0.008 g Cl^-/g. This finding contradicts conventional expectations that limestone enhances chloride binding through the formation of carboaluminate phases. The deterioration in performance can be attributed to several interrelated factors operating within the cementitious matrix. Primarily, the reduction may stem from diminished availability of reactive aluminates essential for the formation of AFm phases, which constitute the principal chloride-binding compounds in concrete. Additionally, the consumption of potential binding sites through carboaluminate formation may competitively inhibit chloride uptake mechanisms. Furthermore, densification of the pore structure may impose constraints on both chloride ion mobility and accessibility to adsorption sites, thereby limiting the overall binding capacity. Collectively, these factors contribute to the observed decline in chloride resistance performance of the modified concrete systems.

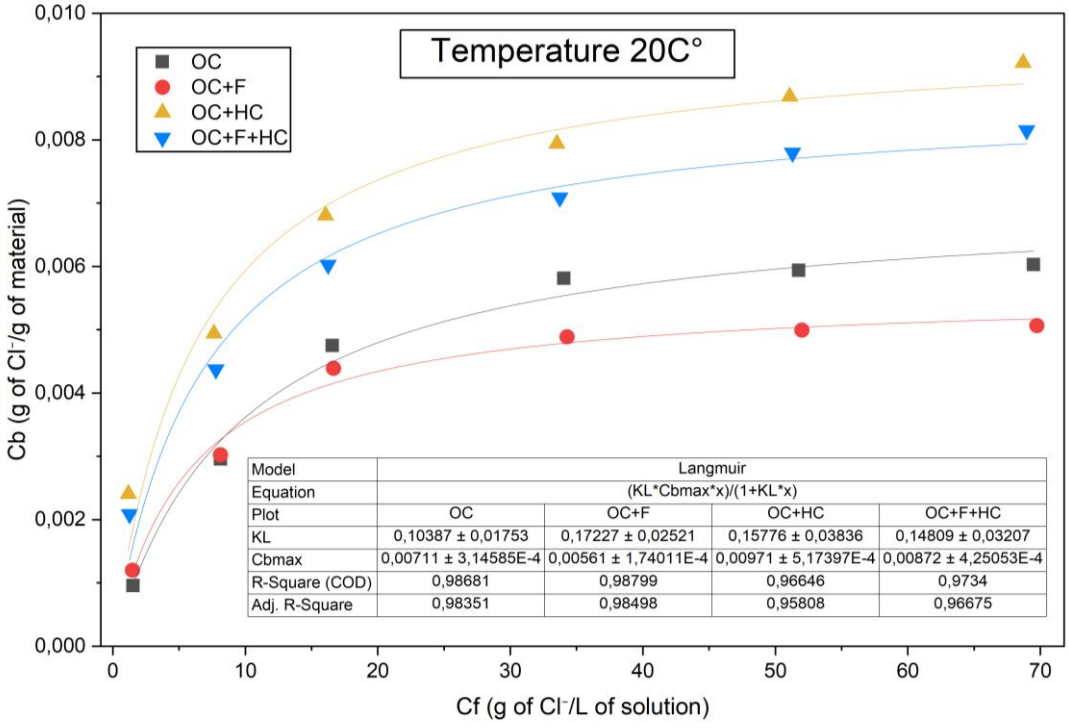
The composite mixture (OC+F+HC) exhibited an intermediate behavior (≈0.010 g Cl^-/g), falling between that of the reference concrete and the wet cork concrete. This suggests that the addition of limestone partially counteracts the strong positive effect of wet cork, implying a complex interaction between the mineral and organic components that affects both chemical and physical chloride binding mechanisms.

It is important to note that the low temperature (5°C) plays a crucial role in these observations. Temperature influences the kinetics of hydration reactions, solution viscosity, and ion diffusion dynamics. At lower temperatures, hydration processes slowdown, which may alter the formation of hydration products responsible for chloride binding and, consequently, the overall binding capacity of the material.

The results presented in Fig. 4.24 depict the chloride binding isotherms for chloride ions in various concrete types at a constant temperature of 20°C.

At 20°C, the results exhibited a behavior similar to that observed at 5°C; however, a slight reduction in chloride binding capacity was noted. The OC+HC mixture recorded the highest value (0.00971 g Cl^-/g), whereas the OC+F mixture remained the least efficient in chloride binding.

The results demonstrate that the wet cork concrete (OC+HC) exhibited the highest chloride binding capacity, reaching approximately 0.0092 g Cl^-/g of material at the highest studied concentration (75 g Cl^-/L). This represents a significant improvement of nearly 53% compared to the reference concrete. In contrast, the limestone-modified concrete (OC+F) showed the lowest binding capacity (≈0.0051 g Cl^-/g), which is even lower than that of the reference mixture (OC), measured at about 0.006 g Cl^-/g, corresponding to a 15% reduction.



Model	Langmuir			
Equation	(KL*Cbmax*x)/(1+KL*x)			
Plot	OC	OC+F	OC+HC	OC+F+HC
KL	0,10387 ± 0,01753	0,17227 ± 0,02521	0,15776 ± 0,03836	0,14809 ± 0,03207
Cbmax	0,00711 ± 3,14585E-4	0,00561 ± 1,74011E-4	0,00971 ± 5,17397E-4	0,00872 ± 4,25053E-4
R-Square (COD)	0,98681	0,98799	0,96646	0,9734
Adj. R-Square	0,98351	0,98498	0,95808	0,96675

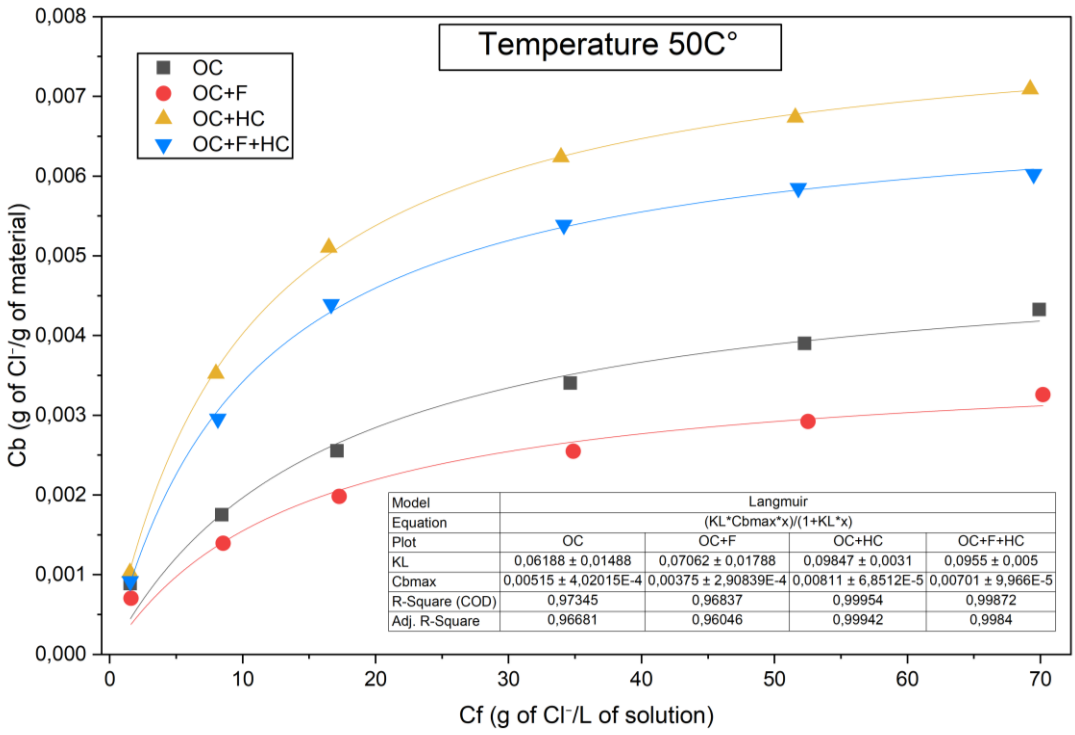
Fig. 4.24. Chloride binding isotherms of concretes at 20°C.

The composite mixture (OC+F+HC) displayed an intermediate performance (≈0.0082 g Cl^-/g), positioned between that of the wet cork mixture and the reference concrete, with an improvement of approximately 37% relative to the plain concrete. This outcome suggests a partial synergistic interaction between the two components: the wet cork appears to partially compensate for the negative influence of limestone, although it does not fully achieve the performance observed when cork is used alone.

This behavior may be attributed to competitive interactions between the two additives affecting distinct binding mechanisms, or to microstructural adjustments that limit the full utilization of each material's individual properties.

It is also noteworthy that the binding capacities recorded at 20°C are generally lower than those observed at 5°C in the preceding experiment. This finding aligns with thermodynamic principles, which state that adsorption processes are typically exothermic in nature, and therefore favored at lower temperatures. At 20°C, the increased ionic mobility and solubility may reduce the stability of bound chlorides, enhancing their tendency to remain in the free solution phase.

The results presented in Fig.4.25 illustrate the chloride binding isotherms for chloride ions in various concrete mixtures at an elevated temperature of 50°C.



Model	Langmuir			
Equation	(KL*Cbmax*x)/(1+KL*x)			
Plot	OC	OC+F	OC+HC	OC+F+HC
KL	0,06188 ± 0,01488	0,07062 ± 0,01788	0,09847 ± 0,0031	0,0955 ± 0,005
Cbmax	0,00515 ± 4,02015E-4	0,00375 ± 2,90839E-4	0,00811 ± 6,8512E-5	0,00701 ± 9,966E-5
R-Square (COD)	0,97345	0,96837	0,99954	0,99872
Adj. R-Square	0,96681	0,96046	0,99942	0,9984

Fig. 4.25. Chloride binding isotherms of concretes at 50°C.

The most significant observation is the reduction in chloride binding capacity $C_{b,\,max}$ across all mixtures at 50°C compared with those at lower temperatures (5°C and 20°C). Nevertheless, OC+HC remained the best performing, followed by OC+F+HC. The binding values decreased by approximately 40–60% for all types of concrete. The decline in chloride binding performance can be explained through

several interconnected thermodynamic and kinetic phenomena associated with temperature elevation. The enhancement of ionic mobility resulting from increased thermal energy destabilizes the physically adsorbed chloride species, promoting their release into the pore solution as free ions. Concurrently, elevated temperatures may induce structural alterations in hydration products, particularly the thermally labile AFm phases that serve as primary chemical binding agents, through decomposition or phase transformation mechanisms. Moreover, the temperature-dependent increase in chloride solubility coupled with accelerated desorption rates drives the system toward a thermodynamic state favoring unbound chloride ions. These synergistic thermal effects collectively account for the observed deterioration in chloride immobilization capacity within the cementitious matrix under high-temperature exposure conditions.

Despite the overall decline, the wet cork concrete (OC+HC) maintained the highest chloride binding capacity (≈0.0071 g Cl^-/g), representing an improvement of about 66% relative to the reference concrete (OC), which exhibited ≈0.0043 g Cl^-/g. This consistent performance across all temperatures indicates that the chloride-binding mechanisms associated with wet cork possess superior thermal stability compared to those in conventional concrete. This may be linked to the thermally stable porous structure of cork, which remains relatively unaffected by temperature fluctuations.

The composite mixture (OC+F+HC) also demonstrated good performance (≈0.006 g Cl^-/g), ranking second with a 40% improvement over the reference concrete. The synergistic interaction between cork and limestone appears to become more pronounced at higher temperatures: limestone may enhance the thermal stability of the cementitious matrix, while cork provides additional, stable binding sites. Conversely, the limestone-modified concrete (OC+F) continued to show the lowest binding capacity (≈0.0033 g Cl^-/g), representing a 23% reduction compared to the reference mixture. This persistently poor performance across all temperatures reinforces the adverse influence of limestone on chloride-binding capacity under the studied conditions.

These findings have significant implications for engineering applications in hot climates or structures exposed to high operational temperatures. The reduction in chloride-binding capacity at 50°C implies a higher concentration of free chlorides within the pore solution, thereby increasing the risk of steel reinforcement corrosion and reducing the expected service life of concrete structures. It is also noteworthy that

the rate of decline in chloride binding capacity with increasing temperature varies among mixtures. While the reference concrete lost approximately 46% of its binding ability (from ≈0.008 g Cl^-/g at 5°C to ≈0.0043 g Cl^-/g at 50°C), the wet cork concrete experienced a smaller reduction of about 41% (from ≈0.012 to ≈0.0071 g Cl^-/g). This indicates a relatively higher thermal stability of the chloride-binding mechanisms in cork-modified concrete.

- **Comprehensive Comparison: Temperature Effect on the Chloride Binding Capacity of Concrete**

A comprehensive comparison of the results obtained at 5°C, 20°C, and 50°C reveals a clear and consistent inverse relationship between temperature and chloride binding capacity across all studied concrete types, confirming the exothermic nature of the adsorption processes. At the lowest temperature (5°C), all mixtures exhibited their highest chloride binding capacities. Wet cork concrete (OC+HC) achieved the maximum value of approximately 0.012 g Cl^-/g, which decreased to 0.0092 g Cl^-/g at 20°C and further to 0.0071 g Cl^-/g at 50°C-representing a cumulative reduction of about 41% across the studied thermal range.

The most notable observation is that wet cork concrete consistently maintained superior chloride binding performance at all temperatures, indicating enhanced thermal stability of its binding mechanisms, likely associated with its porous structure and the functional organic groups inherent to cork. Conversely, limestone-modified concrete (OC+F) exhibited the weakest performance under all thermal conditions, with its binding capacity dropping from 0.007 g Cl^-/g at 5°C to 0.0051 g Cl^-/g at 20°C and reaching 0.0033 g Cl^-/g at 50°C—a total decline of approximately 53%, the highest among all mixtures.

The reference concrete (OC) showed an intermediate trend, with values decreasing from 0.008 g Cl^-/g at 5°C to 0.006 g Cl^-/g at 20°C and to 0.0043 g Cl^-/g at 50°C. The composite mixture (OC+F+HC) demonstrated relatively balanced performance across temperatures, decreasing from 0.010 g Cl^-/g to 0.0082 g Cl^-/g and finally to 0.006 g Cl^-/g. This behavior suggests that wet cork partially compensates for the adverse influence of limestone, enhancing the thermal stability of the overall mixture.

These findings have significant practical implications for designing chloride-resistant concrete. The expected service temperature should be carefully considered: in cold or temperate environments, all mixtures perform more effectively in chloride binding,

whereas in hot climates (e.g., tropical or industrial settings), the inclusion of thermally stable modifiers such as wet cork becomes essential to maintain an acceptable level of chloride protection. The main conclusion drawn from this comparison is that wet cork represents a promising and sustainable additive for improving concrete's resistance to chloride ingress across a wide range of temperatures.

4.16. Cork Interactions with Saline Solutions

Three categories of virgin cork specimens underwent prolonged immersion—four months—in an artificially prepared saline solution that replicates seawater conditions. Upon completion, the solution was titrated with silver nitrate to verify the fixation of chloride ions within the cork's porous structure (Fig. 4.26).

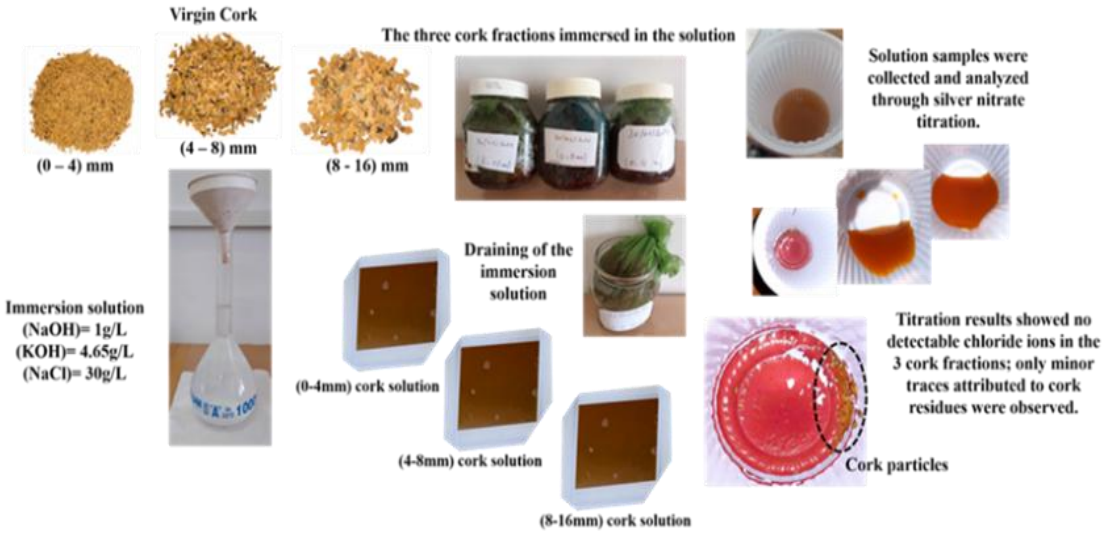


Fig. 4.26. Virgin Cork Interaction with Saline Solutions.

Table 4.4. Effect of particle size on the efficiency of chloride ion adsorption by cork.

Cork	Free Chlorides	Fixed Chloride Quantity		Concentration reduction
	Cf (g/l)	(g)[Cl] /(g)[Cork]	(%)	(%)
0-4 mm	35,358	0,001136	0,1136	0,4
4-8 mm	35,3935	0,000852	0,0852	0,3
8-16 mm	35,455625	0,000355	0,0355	0,125

Table 4.4 summarizes the results of a chloride ion adsorption experiment using natural cork samples of varying particle sizes (0–4 mm, 4–8 mm, and 8–16 mm). The samples were immersed in a 1 M sodium chloride solution for a duration of four months. A

fixed mass of 50 g of cork was used for each sample in 400 mL of solution. The data reveal a clear and consistent trend linking adsorption capacity to particle size: smaller particles (0–4 mm) exhibited the highest adsorption efficiency, reaching 0.1136, followed by medium-sized particles (4–8 mm) at 0.0852, and the largest particles (8–16 mm) at 0.0355. This represents a 25% reduction in efficiency when shifting from the smallest to the medium-sized category, and a 58% reduction when moving to the largest size class.

This performance variation is primarily attributed to the specific surface area principle, as smaller particles possess a higher surface area-to-volume ratio, offering more potential binding sites for chloride ions. Additionally, differences in porosity characteristics among the particle size classes influence their chloride retention capacity. As particle size decreases, the probability of chemical and physical interactions increases due to enhanced surface exposure and structural openings induced during cutting. The internal porous structure of cork plays a crucial role in this process by facilitating mass transport and internal ion diffusion, thereby enhancing physical adsorption through weak electrostatic forces and van der Waals interactions, as well as potential ion exchange with hydroxyl groups (OH-) present on the cork surface.

Although the adsorption values reported are modest compared to synthetic adsorbents, they are consistent with the behavior of cork as a physical (rather than chemical) adsorbent and align with reference studies that report similar uptake levels for natural porous materials (Pintor et al., 2012). These findings provide compelling experimental evidence that optimizing particle size can significantly improve cork's performance as a natural adsorbent, making it a promising candidate for use in primary treatment systems or as part of multi-stage water purification processes, particularly as a sustainable and environmentally friendly material.

Previous works have demonstrated the potential of cork-based materials to adsorb ions from aqueous solutions. For instance, cork waste removed up to 97% of Cr ions under acidic conditions (Sfaksi, 2014), while cork-derived biochar and magnetic cork powders have been shown recently to effectively uptake heavy metal ions in batch experiments (Abenojar et al., 2024 & Pertile et al., 2025).

The findings of the present study are consistent with the trends reported in the scientific literature regarding the adsorption behavior of cork toward inorganic species. Pintor et al. (Pintor et al., 2012) demonstrated that cork powder and granules exhibit limited yet stable adsorption capacities, attributable to their finely porous cellular structure, the presence of suberin, and the abundance of active functional groups on their surface. These characteristics render cork a low-capacity adsorbent for dissolved inorganic ions, which aligns with the low chloride uptake measured in this study. This agreement indicates that cork behaves as a bio-based material with predictable and stable adsorption performance, even when exposed to saline or chloride-rich environments, thereby reinforcing the reliability of the results obtained in the present investigation. Similarly, the work of Olivella et al. (Olivella et al., 2011) on alternative porous media documented adsorption efficiencies ranging from 0.08% to 0.12%, demonstrating consistency with the findings of the current research. This convergence validates the reliability of the methodology employed in the present study and substantiates the accuracy of the obtained results, particularly when benchmarked against established literature in the field.

Extensive literature reviews also indicate that cork is used as a natural adsorbent for various pollutants via physical adsorption mechanisms such as electrostatic interactions and hydrogen bonding. Thanks to its porous structure and active surface, cork has demonstrated the ability to remove heavy metals and oils from water. The study by Ortega et al. (Ortega et al., 2022) on mortar incorporating natural cork revealed that the chloride diffusion coefficient was similar to-or slightly higher than-that of reference mortar, suggesting that cork does not chemically bind chloride but instead contributes to internal complexity and delays ion transport, yielding modest positive effects. Furthermore, Sergi et al. (Sergi et al., 2022) study highlighted the influence of cork density and water type on absorption rates: low-density cork showed a 36.7–46.5% higher absorption rate compared to high-density cork, while seawater absorption was 21.8–44.4% lower than distilled water due to the presence of salts. Regarding compressive behavior, cork exhibited a softening effect when wet, with partial recovery upon drying, likely due to salt crystal deposition within the structure. These findings confirm that low-density cork enhances absorption but may reduce mechanical strength, and that salts negatively impact absorption while partially aiding the recovery of mechanical properties after drying.

Fig. 4.27 illustrates the formation of a thin, viscous green layer on the surface of raw cork samples after being stored in water for four years. This is a natural phenomenon attributed to the biological growth of algae and microorganisms under favorable environmental conditions. Several factors contribute to this development, including the highly porous structure of raw cork, which facilitates water absorption and maintains persistent moisture, as well as the extended exposure time that allows the establishment of a mature biological community. Additional contributing factors include the availability of light, oxygen, and dissolved nutrients in the water or those released through the degradation of organic matter in the cork.



Fig. 4.27. Alterations in cork after 40 months of immersion.

The viscous layer is composed of a biofilm that includes microscopic algae-such as green algae and cyanobacteria-responsible for the green pigmentation, as well as specific bacteria, particularly cyanobacteria, and extracellular polymeric substances (EPS) secreted by the microorganisms to anchor the biofilm. Other microbial organisms, such as fungi, may also be present.

This phenomenon is further reinforced by the absence of antimicrobial treatments, which allows unhindered microbial growth, along with warm temperatures and the emission of unpleasant odors-an indication of anaerobic bacterial activity producing sulfur- or nitrogen-containing compounds (Toledo et al., 2025). Collectively, this makes the phenomenon a natural model for understanding the long-term interactions between organic materials and moist environments. It also provides valuable insight into the preservation of natural materials and the development of more efficient storage methods.

4.17. Conclusion

In this chapter, a comprehensive experimental study was conducted to evaluate the potential for enhancing the mechanical properties and durability characteristics of concrete incorporating virgin cork as a partial aggregate replacement and limestone as an additive to conventional constituents, with the aim of developing formulations suitable for specialized construction applications. The results demonstrated a notable improvement in workability and a reduction in plastic viscosity upon the addition of cork and limestone, while the density remained within the typical range for ordinary concrete (2008–2470 kg/m³). Limestone contributed to a reduction in total porosity and improved the uniformity of the pore structure, whereas cork increased porosity and expanded the interfacial transition zone, resulting in a decrease in mechanical strength.

From a durability perspective, the findings indicated that cork-containing concrete, particularly when pre-soaked, exhibited enhanced resistance to chloride ion penetration, with a reduction in permeability of up to 35% compared to the reference mixtures, whereas limestone alone led to increased diffusion rates. Microscopic and thermal analyses (TGA/DTG) revealed that limestone acts as an effective thermal stabilizer through endothermic decomposition and the formation of a protective CaO layer, while wet cork enhanced thermal insulation during the initial stages by retaining moisture. The composite mixture (OC+F+HC) achieved the best thermal performance, exhibiting the highest residual mass and the lowest heat flux.

Chloride diffusion tests showed that the diffusion coefficient and lag time were influenced by temperature, with diffusion mechanisms accelerating at higher temperatures; nevertheless, concrete containing wet cork maintained the best overall performance, underscoring its role in improving concrete resistance to chloride ingress, especially under hot climatic conditions.

Overall, the results confirm that a balanced incorporation of limestone and natural cork enables the development of sustainable concrete with competitive mechanical performance, improved thermal behavior, and effective resistance to aggressive agents, making it suitable for a wide range of structural and insulating applications, while also providing clear environmental benefits through the use of natural and renewable materials.

General Conclusion

This research endeavored to develop sustainable concrete systems through the strategic partial substitution of conventional mineral aggregates with natural raw cork, with the objective of enhancing thermal and environmental performance while preserving adequate mechanical properties for both structural and insulating applications. The investigation was prompted by the substantial environmental burdens associated with conventional concrete production, encompassing elevated carbon emissions, intensive energy consumption, water and atmospheric pollution, and significant solid waste generation. Within this framework, natural cork emerged as a viable alternative material owing to its superior thermal and acoustic insulation properties, reduced density, and regional availability in Algeria.

Laboratory characterization revealed that male cork aggregate exhibits distinctive properties that differentiate it from conventional mineral aggregates. The particle size distribution demonstrated compliance with standard specifications for the 4–8 mm and 8–16 mm fractions, whereas the 0–4 mm fraction displayed a deficiency in fine constituents relative to natural sand. Microstructural examination revealed a complex cellular architecture characterized by an extensive network of voids and internal pores, which directly influences the material's apparent density. Furthermore, cork demonstrated exceptional water absorption capacity, exceeding 100% of its dry mass and achieving complete saturation after nine days, thereby necessitating meticulous adjustment of water content during mixture proportioning.

The comprehensive experimental program yielded substantial findings concerning the performance characteristics of cork- and limestone-modified concretes. In terms of fresh and hardened properties, the incorporation of cork and limestone enhanced workability and flowability while reducing plastic viscosity. Cork addition resulted in moderate reductions in dry density ranging from 2008 to 2470 kg/m³, whereas limestone induced marginal density increases, with all mixtures maintaining classification as normal-weight concrete. Regarding porosity and capillary transport, limestone reduced total porosity while cork caused slight increases, with composite mixtures exhibiting elevated capillary absorption rates. Although mechanical strength was diminished relative to reference concrete, cork-modified mixtures maintained acceptable performance levels suitable for structural and thermal insulation

applications. Notably, significant enhancement in chloride ion resistance was observed in mixtures containing cork pre-saturated for two hours combined with limestone, demonstrating improved durability under aggressive environmental exposure.

Microstructural and thermal investigations revealed distinct pore structure modifications and thermal response characteristics. Reference concrete exhibited bimodal pore size distribution, whereas limestone refined the microstructure toward a unimodal distribution with finer pores. Cork incorporation produced a multi-scale pore network attributed to weak interfacial bonding with the cementitious matrix. Thermal analyses demonstrated that limestone functioned as an effective thermal stabilizer through endothermic decomposition reactions and formation of a protective calcium oxide layer, while wet cork enhanced early-stage thermal insulation through moisture retention mechanisms. The composite mixture incorporating both additives achieved optimal thermal stability.

Temperature-dependent chloride diffusion studies demonstrated increasing diffusion coefficients with elevated temperature, with limestone-modified concrete exhibiting the highest diffusion rates. Conversely, wet cork reduced permeability by 28–35%, with cork-modified concrete maintaining superior overall performance, particularly under elevated temperature conditions representative of hot climatic zones.

In conclusion, this dissertation establishes the technical viability of developing sustainable concrete through natural raw cork incorporation as a partial aggregate replacement. The developed systems offer substantial environmental advantages through utilization of renewable, locally sourced materials, enhanced resistance to chloride ingress, and competitive mechanical performance. The optimal preparation methodology involves either two-hour pre-saturation of cork or direct addition of water equivalent to cork's two-hour absorption capacity, with both approaches yielding comparable performance and marginal superiority of pre-saturated cork in chloride resistance. These findings provide valuable insights for integrating sustainable natural materials into concrete technology, contributing toward more resource-efficient and environmentally responsible construction practices for future infrastructure development.

Future Perspectives

Despite the comprehensive nature of this research, which aimed to encompass various aspects of cork-based concrete incorporated with limestone powder—ranging from mechanical properties, durability, and diffusion coefficients to adsorption isotherm behavior under varying temperatures—scientific inquiry remains a continuous process. No study, regardless of its depth, can claim absolute finality.

Based on the findings, it was observed that while limestone powder played a pivotal role as a filler material, enhancing the microstructural density of the concrete, its impact on mechanical strength remained limited and did not yield a significant improvement compared to the reference concrete. Consequently, we aspire to extend this research path through the following prospective axes:

1. Integration of Active Pozzolanic Admixtures

Rather than relying solely on inert materials like limestone, we propose the incorporation of Silica Fume or Ground Granulated Blast-Furnace Slag (GGBS). These supplementary cementitious materials do not merely function as fillers; they react chemically with the calcium hydroxide resulting from cement hydration to form additional Calcium Silicate Hydrate (C-S-H) bonds. This secondary reaction is expected to substantially enhance the mechanical strength and refine the pore structure of the cork-based concrete.

2. Enhancing Sustainability via Cement Clinker Reduction

Given the study's focus on sustainable cork-based concrete, a logical progression involves further reducing the cement content. By substituting cement with high proportions of mineral admixtures (reaching levels of 30% to 50%), future research could investigate the feasibility of developing a Green Concrete with a significantly lower carbon footprint, while maintaining the requisite thermal and mechanical performance.

3. Investigation of Long-term Durability and Carbonation

We suggest expanding the scope to evaluate the long-term durability of this material over time. Specifically, assessing its resistance to carbonation and freeze-thaw cycles is crucial to ensure its structural viability under harsh environmental conditions, moving beyond controlled laboratory settings.

References

Articles

Abenojar, J., López, S., Juan, D.A., Miguel, R. & Martinez, A., 2024. Magnetic cork as adsorbent to remove hexavalent chromium from aqueous solution. Applied Water Science, 14(12), pp.1–17. https://doi.org/10.1007/s13201-024-02322-z.

Acikel, H., 2011. The use of Miscanthus gigantheus as a plant fiber in concrete production. Scientific Research and Essays, 6(13), pp.2660 2667. https://doi.org/10.5897/SRE10.1139.

Ahmed, Y.H., Babikir, K.S.E., 2021. Effects of limestone powder on self-compacting concrete properties. FES Journal of Engineering Sciences 9(2), 14–20. https://doi.org/10.52981/fjes.v9i2.671 (journal.oiu.edu.sd).

Akhtar, A., Sarmah, A.K., 2018. Construction and demolition waste generation and properties of recycled aggregate concrete: A global perspective. Journal of Cleaner Production 186, 262–281. https://doi.org/10.1016/j.jclepro.2018.03.085.

Aït-Mokhtar, A., Amiri, O. Dumargue, P. & Sammartino, S., 2002. A new model to calculate water permeability of cement-based materials from MIP results. Advances in Cement Research, 14(2), pp.43–49. https://doi.org/10.1680/adcr.14.2.43.39549.

Amin, A.M.N., Ahmad, W. and Khan, K., 2022. A comprehensive review of types, properties, treatment methods and application of plant fibers in construction and building materials. Materials, 15(12), 4362. https://doi.org/10.3390/ma15124362.

Andrade, C., 1993. Calculation of chloride diffusion coefficients in concrete from ionic migration measurements. Cement and Concrete Research, 23(3), pp.724–742. https://doi.org/10.1016/0008-8846(93)90023-3.

Antony, M.R., Santhappan, J.S., Al Kindi, Z.H.S., Shahulhameed, B. & Annamal, L.A.W., 2024. Date palm fibre: a sustainable reinforcement material for thermal insulation concrete. AIP Conference Proceedings, AIP Publishing, p.20022. https://doi.org/10.1063/5.0193702.

Ashraf, W., 2016. Carbonation of Cement-Based Materials: Challenges and Opportunities. Construction and Building Materials, 120, pp. 558–570. https://doi.org/10.1016/j.conbuildmat.2016.05.080.

Barco Tocto, E.K., Agüero Hualcas, D.S. & Farfán Córdova, M., 2025. Nopal extract and aloe vera to improve structural concrete exposed to saline environments. Revista de Ingeniería, 115, pp.62 74. https://doi.org/10.17533/udea.redin.20240514.

Barnat-Hunek, D., Widomski, M.K., Szafraniec, M. & Łag, G., 2018. Impact of Different Binders on the Roughness, Adhesion Strength, and Other Properties of Mortars with Expanded Cork. Materials, 11(3), 364. https://doi.org/10.3390/ma11030364.

Bazan, P., Mierzwiński, D. & Bogucki, R., 2020. Bio based polyethylene composites with natural fibers. Materials (Basel), 13(11), p.25. https://doi.org/10.3390/ma13112595.

Benhalima, Y. & Dehane, B., 2020. Characterization of flammability parameters of cork by the mass loss calorimeter technique. IOBC WPRS Bulletin, 152, pp.22 25.

Branco, F.G. & Godinho, L., 2013. On the use of lightweight mortars for the minimization of impact sound transmission. Building and Environment, 45, pp. 184–191. https://doi.org/10.1016/j.buildenv.2009.08.014.

Chaitanya, M.S.K., Nagaraju, T.V., Gadhiraju, L., Madepalli, V.R. & Raju, J.N.S.S.N., 2023. Strength and micro structural performance of geopolymer concrete using highly burned rice husk ash. Materials Today: Proceedings. https://doi.org/10.1016/j.matpr.2023.04.617.

Chang, X., He, T., Niu, M., Zhao, L., Wang, L. & Wang, Y., 2024. Influence of Limestone Powder Mixing Method on Properties of Manufactured Sand Concrete. Case Studies in Construction Materials, 20, e02996. https://doi.org/10.1016/j.cscm.2024.e02996.

Cherif, R., Hamami, A.E.A., Aït-Mokhtar, A. & Siddique, R., 2020. Chemical properties of pore solution of hardened cement pastes with mineral additions.

Advances in Cement Research, 33(8), pp.331–341. https://doi.org/10.1680/jadcr.19.00037.

Chorana, A., Dehane, B. & Beltrán, R.S., 2019. Characterization of the cork growth and quality of cork oak woodlands, North West Algeria. International Journal of Environmental Studies, 76(10), pp.1 16. https://doi.org/10.1080/00207233.2019.1594290.

Costa, A., Barbosa, I., Miguel, C. & Graça, J., 2021. Variation of cork porosity along the stem in harvested cork oak (Quercus suber L.) trees. Annals of Forest Science, 78:52. https://doi.org/10.1007/s13595 021 01068 x.

Costa, R., Lourenço, A., Oliveira, V. & Pereira, H., 2019. Chemical characterization of cork, phloem and wood from different Quercus suber provenances and trees. Heliyon, 5(October), p.e02910. https://doi.org/10.1016/j.heliyon.2019.e02910.

Cunha, M., Lourenço, A., Barreiros, S., Paiva, A. & Sim, P., 2020. Valorization of cork using subcritical water. Molecules, 25(20), p.46. https://doi.org/10.3390/molecules25204695.

Damtoft, J.S., Lukasik, J., Herfort, D., Sorrentino, D. & Gartner, E.M., 2008. Sustainable development and climate change initiatives. Cement and Concrete Research 38(2), 115–127. https://doi.org/10.1016/j.cemconres.2007.09.008.

Dehane, B., Benrahou, A., Bouhraoua, R., Hamani, F. Z. & Belhoucine L., 2014. Chemical composition of Algerian cork according the origin and the quality. IJRES 1 (2014) 17-25.

De Larrard, F. & Sedran, T., 2002. Mixture proportioning of high-performance concrete. Cement and Concrete Research, 32(11), pp.1699–1704. https://doi.org/10.1016/S0008-8846(02)00861-X.

Dhandapani, Y., Santhanam, M., Kaladharan, G. & Ramanathan, S., 2021. Towards ternary binders involving limestone additions — A review. Cement and Concrete Research, 143, p.106396. https://doi.org/10.1016/j.cemconres.2021.106396.

Diab, A.M., Elmoaty, A., Elmoaty, M.A. & Aly, A.A., 2016. Long term study of mechanical properties, durability and environmental impact of limestone cement concrete. Alexandria Engineering Journal. https://doi.org/10.1016/j.aej.2016.01.031.

Estellé, P., Lanos, C. & Perrot, A., 2008. Processing the Couette viscometry data using a Bingham approximation in shear rate calculation. Journal of Non-Newtonian Fluid Mechanics, 154(1), pp.31–38. https://doi.org/10.1016/j.jnnfm.2008.01.006.

Evangelista, L. & de Brito, J., 2005. Mechanical Behaviour of Concrete Made with Fine Recycled Concrete Aggregates. INCOS05 - International Conference on Concrete for Structures, FCTUC, Coimbra, Portugal, July. DOI:10.13140/RG.2.1.5110.0884.

Flores-Nicolás, A., Flores-Nicolás, M., Menchaca-Campos, E.C. and Uruchurtu-Chavarín, J., 2025. Mechanical behavior of concrete reinforced with natural palm and mango fibers. Journal of Engineering and Technological Sciences, 57(1), pp.48–65. https://doi.org/10.5614/j.eng.technol.sci.2025.57.1.4.

Frigione, M., 2010. Recycling of PET bottles as fine aggregate in concrete. Waste Management, 30(6), pp.1101–1106. https://doi.org/10.1016/j.wasman.2010.01.030.

Gartner, E., Hirao, H., 2015. A review of alternative approaches to the reduction of CO_2 emissions associated with the manufacture of the binder phase in concrete. Cement and Concrete Research 78, 126–142. https://doi.org/10.1016/j.cemconres.2015.04.012

Ghernouti, Y., 2023. Potential Use of Recycled Cork as Aggregates for Lightweight Self-Compacting Concrete. Environmental Research, 214, 114024. https://doi.org/10.1016/j.envres.2022.114024.

Habert, G., Miller, S.A. and John, V.M., 2020. Environmental impacts and decarbonization strategies in the cement and concrete industries. Nature Reviews Earth & Environment, 1(11), pp.559–573. https://doi.org/10.1038/s43017-020-0093-3.

Hamza, M., Al-Marzouqi, A.H. and Ahmed, W., 2023. The potential of adopting natural fibers reinforcements for fused deposition modeling: Characterization and implications. Heliyon, 9(4), e15023. https://doi.org/10.1016/j.heliyon.2023.e15023.

Hariz, S., Ghomari, F. & Touil, B., 2022. Characterization of a bio-based concrete using virgin cork aggregate. Journal of Building Materials and Structures, 9, pp.141–149. https://doi.org/10.34118/jbms.v9i2.2780.

Hariz, S., Touil, B., Cherif, R. Ghomari, F. & Aït Mokhtar, A., 2025. Development of a cork-based concrete as a structural material for lightweight construction. European Journal of Environmental and Civil Engineering. https://doi.org/10.1080/19648189.2025.2573812.

Hasanbeigi, A., Morrow, W., Masanet, E., Sathaye, J., Xu, T., 2013. Energy efficiency improvement and CO_2 emission reduction opportunities in the cement industry in China. Energy Policy 57, 287–297. https://doi.org/10.1016/j.enpol.2013.01.053.

Hossain, M.S., Madlool, N.A., Rahim, N.A., Selvaraj, J., Pandey, A.K. and Faheem, A., 2016. Role of smart grid in renewable energy: An overview. Renewable and Sustainable Energy Reviews, 60, pp.1168–1184. https://doi.org/10.1016/j.rser.2015.09.098.

Ismail, M., 2014. Assessment of green inhibitor on the crystal structures of carbonated materials. Jurnal Teknologi, 3, pp.1 9.

Jahami, A., Zeaiter, N. & Cheaib, M., 2024. Reviewing the potential: a comprehensive review of natural fibers (NFs) in structural concrete and their multifaceted influences. Springer International Publishing. Doi: 10.1007/s41062-024-01384-x.

Jové, P. & Olivella, L.M., 2011. Study of the variability in chemical composition of bark layers of cork from different production areas. BioResources, 6(2), pp.1806 1815. https://doi.org/10.15376/biores.6.2.1806 1815.

Kim, Y., Van Leeuwen, R., Cho, B., Sriraman, V., 2018. Evaluation of the efficiency of limestone powder in concrete and the effects on the environment. Sustainability 10(2), 550. https://doi.org/10.3390/su10020550.

Kolour, H.M., Rajendran, R., Selvaraj, M., Sivakumar, T. & Siddiqui, M.F., 2024. Property investigation of nanocellulose I and II from different non wood fibers using chemical acid hydrolysis method. Industrial Crops and Products, 222, p.117013. https://doi.org/10.1016/j.indcrop.2024.117013.

Kumar, S., Kumar, D. & Rud, Ž., 2022. A review on sustainable use of agricultural straw and husk biomass ashes: transitioning towards low carbon economy. Science of the Total Environment, 838, pp.1 21. https://doi.org/10.1016/j.scitotenv.2022.156728.

Kuramochi, T., Ramírez, A., Turkenburg, W. and Faaij, A., 2012. Comparative assessment of CO_2 capture technologies for carbon-intensive industrial processes. Progress in Energy and Combustion Science, 38(1), pp.87–112. https://doi.org/10.1016/j.pecs.2011.05.001.

Leeson, D., Mac Dowell, N., Shah, N., Petit, C. and Fennell, P.S., 2017. A techno-economic analysis and systematic review of carbon capture and storage (CCS) applied to the iron and steel, cement, oil refining and pulp and paper industries. International Journal of Greenhouse Gas Control, 61, pp.71–84. https://doi.org/10.1016/j.ijggc.2017.03.020.

Li, C., Jiang, L., Xu, N. & Jiang, S., 2018. Pore structure and permeability of concrete with high volume of limestone powder addition. Powder Technology, 338, pp.416–424. https://doi.org/10.1016/j.powtec.2018.07.054.

Lopes, M.H., Gil, A.M., Silvestre, A.J.D. & Neto, C.P., 2000. Composition of suberin extracted upon gradual alkaline methanolysis of Quercus suber L. cork. Polymer Degradation and Stability, pp.383 391.

Machado, S. & Pereira, H., 2016. Cork as a building material: a review. Construction and Building Materials, 2010. https://doi.org/10.1007/s00107 016 1076 4.

Madlool, N.A., Saidur, R., Hossain, M.S., Rahim, N.A., 2011. A critical review on energy use and savings in the cement industries. Renewable and Sustainable Energy Reviews 15(4), 2042–2060. https://doi.org/10.1016/j.rser.2011.01.005.

Marcos, J. & Branco, F.G., 2023. Long-Term Behavior Related to Water Ingress in Mortars Which Combine Expanded and Natural Cork Lightweight Aggregates and

Eco-Friendly Cements. Buildings, 13(7), 165. https://doi.org/10.3390/buildings13071651.

Meddour, R., Sahar, O. & Médail, F., 2021. Checklist of the native tree flora of Algeria: diversity, distribution, and conservation. Plant Ecology and Evolution, 154(3), pp.405 418. https://doi.org/10.5091/plecevo.2021.1868.

Merabti, S., Kenai, S., Belarbi, R. & Khatib, J., 2021. Thermo-Mechanical and Physical Properties of Waste Granular Cork Composite with Slag Cement. Construction and Building Materials, 272, 121923. https://doi.org/10.1016/j.conbuildmat.2020.121923.

Miguel, J., Montes, D., Rosendo, V., Maderuelo Sanz, R., Gozalo, G.R. & Moraga, P.A., 2021. Virgin natural cork characterization as a sustainable material for use in acoustic solutions. Wood Research, 66(6), pp.1025 1030. https://doi.org/10.37763/wr.1336 4561/66.6.1025 1030.

Miguel, J., Morillas, B. & Maderuelo Sanz, R., 2020. Virgin cork, a possible environmentally friendly by product of the cork with acoustic properties for its use inside dwellings? Wood Research, 65(6), pp.1025–1030. https://doi.org/10.37763/wr.1336-4561/65.6.10251030.

Miller, S.A., Horvath, A. and Monteiro, P.J.M., 2018. Impacts of booming concrete production on water resources worldwide. Nature Sustainability, 1(1), pp.69–76. https://www.nature.com/articles/s41893-017-0009-5.

Mohanraj, R. & Krishnasamy, R., 2024. Enhancing concrete flexural behaviour with Euphorbia tortilis cactus: sustainable additive for improved load carrying capacity and ductility. Indian Journal of Engineering and Materials Science, 31, pp.388 396. https://doi.org/10.56042/ijems.v31i3.6667.

Monteiro, P.J., Miller, S.A. & Horvath, A., 2017. Towards sustainable concrete. *Nature Materials*, 16(7), pp.698-699. Doi :10.1038/nmat4930.

Moreira, A., António, J. & Tadeu, A., 2014. Lightweight screed containing cork granules: Mechanical and hygrothermal characterization. Cement and Concrete Composites, 49, pp.1–8. https://doi.org/10.1016/j.cemconcomp.2014.01.012.

Novais, R.M., Carvalheiras, J., Senff, L., Lacasta Palacio, A.M., Rodríguez Cantalapiedra, I., Giró Paloma, J., Seabra, M.P. & Labrincha Batista, J.A., 2020. Multifunctional cork–alkali activated fly ash composites: a sustainable material to enhance buildings' energy and acoustic performance. Energy & Buildings, 210, p.109739. https://doi.org/10.1016/j.enbuild.2019.109739.

Oettel, V., 2024. Experimental investigations on the application of natural plant fibers in ultra-high-performance concrete. Materials, 17(14), 3519. https://doi.org/10.3390/ma17143519.

Olivella, M. À., Jové, P., Şen, A., Pereira, H., Villaescusa, I. and Fiol, N., 2011. Sorption performance of Quercus cerris cork with polycyclic aromatic hydrocarbons and toxicity testing. BioResources, 6(3), pp.3363–3375.

Ortega, J.M., Branco, F.G. & Pereira, L., 2022. Chloride Ingress Resistance, Microstructure and Mechanical Properties of Lightweight Mortars with Natural Cork and Expanded Clay Prepared Using Sustainable Blended Cements. Journal of Marine Science and Engineering, 10(9), 1174. https://doi.org/10.3390/jmse10091174.

Ortega, J.M., Branco, F.G. & Pereira, L., 2023. Long-Term Behavior Related to Water Ingress in Mortars Which Combine Expanded and Natural Cork Lightweight Aggregates and Eco-Friendly Cements. Buildings, 13(7), 1651; https://doi.org/10.3390/buildings13071651.

Ozel, M., 2014. Effect of insulation location on dynamic heat-transfer characteristics of building external walls and optimization of insulation thickness. Energy and Buildings 72, 288–295. https://doi.org/10.1016/j.enbuild.2013.11.015.

Pacheco Menor, C.M., José, M., Caballero, A., García, A.M. & Ros, P.S., 2024. Multiproperty characterization of non-structural concrete for block made with granulated cork with bark. Construction and Building Materials, 418, 135404. https://doi.org/10.1016/j.conbuildmat.2024.135404.

Pandiaraj, K.P. & Sankararajan, V., 2024. Experimental analysis on lightweight concrete utilizing compost and Ground Granulated Blast Furnace Slag (GGBS): Insights into elevated temperature properties through TGA. International Review of Applied Sciences and Engineering, 15(2), pp.252–259. https://doi.org/10.1556/1848.2023.00724.

Panesar, D.K. & Zhang, R., 2020. Performance comparison of cement replacing materials in concrete: Limestone fillers and supplementary cementing materials – A review. Construction and Building Materials, 251, p.118866. https://doi.org/10.1016/j.conbuildmat.2020.118866.

Pereira, H., 2015. The rationale behind cork properties: a review of structure and chemistry. BioResources, 10(3), pp.1 12. https://doi.org/10.15376/biores.10.3.Pereira.

Pereira, H., Rosa, M.E. & Fortes, M.A., 1987. The cellular structure of cork from Quercus suber L. Wood Science and Technology, 8(3), pp.213 218. DOI:10.1163/22941932-90001048.

Pertile, E., Dvorsk, T., Berkyová, L. & Balvín, P., 2025. Removal of hexavalent chromium from water using cork based biochars obtained via slow and microwave pyrolysis. Molecules, 30(23), p.4501. https://doi.org/10.3390/molecules30234501.

Petlitckaia, S., Barboni, T., Santoni, P. A. & Quilichini, Y., 2024. Valorization of virgin cork by the design of cork plaster composites. Inorganic Chemistry Communications, 161, p.111782. https://doi.org/10.1016/j.inoche.2023.111782.

Pintor, A.M.A. et al., 2012. Use of cork powder and granules for the adsorption of pollutants: A review. Water Research, 46(10), pp.3152–3166. https://doi.org/10.1016/j.watres.2012.03.048.

Ramadan, A., Jahami, A., Khatib, J., El-Hassan, H. & Elkordi, A., 2023. Improving structural performance of reinforced concrete beams with Phragmites australis fiber and waste glass additives. Applied Sciences, 13(7), p.420. https://doi.org/10.3390/app13074206.

Rojo López, G., González Fonteboa, F., Martínez Abella, B. & González Taboada, I., 2022. Rheology, durability, and mechanical performance of sustainable self-compacting concrete with metakaolin and limestone filler. Case Studies in Construction Materials, 17, p.e01143. https://doi.org/10.1016/j.cscm.2022.e01143.

Sadineni, S.B., Madala, S., Boehm, R.F., 2011. Passive building energy savings: A review of building envelope components. Renewable and Sustainable Energy Reviews 15(8), 3617–3631. https://doi.org/10.1016/j.rser.2011.07.014.

Saikia, N. and De Brito, J., 2012. Use of plastic waste as aggregate in cement mortar and concrete preparation: A review. Construction and Building Materials, 34, pp.385–401. https://doi.org/10.1016/j.conbuildmat.2012.02.066.

Sergi, C., Sarasini, F., Fiore, V., Barbero, E. & Sánchez Sáez, J., 2022. The effects of water absorption and salt fog exposure on agglomerated cork compressive response. European Journal of Wood and Wood Products, 80(1), pp.101–114. https://doi.org/10.1007/s00107-021-01754-7.

Sfaksi, Z., 2014. Removal of Cr (VI) from water by cork waste. Arabian Journal of Chemistry, 7(1), pp.37–42. https://doi.org/10.1016/j.arabjc.2013.05.031.

Siddique, R. and Naik, T.R., 2004. Properties of concrete containing scrap-tire rubber – An overview. Waste Management, 24(6), pp.563–569. https://doi.org/10.1016/j.wasman.2004.01.006.

Silva, S.P., Sabino, M.A., Fernandes, E.M., Correlo, V.M., Boesel, L.F. & Reis, R.L., 2005. Cork: properties, capabilities and applications. Journal of Materials Science, 50(6), pp.345 365. https://doi.org/10.1179/174328005X41168.

Soares, B., Gama, N., Freire, C., Barros-Timmons, A., Neto, C.P. & Ferreira, A., 2014. Ecopolyol Production from Industrial Cork Powder via Acid Liquefaction Using Polyhydric Alcohols. Journal of Renewable Materials, 2(1), pp. 1–9. https://doi.org/10.7569/JRM.2014.634117.

Sua iam, G. & Makul, N., 2012. Use of limestone powder to improve the properties of self-compacting concrete produced using cathode ray tube waste as fine aggregate. Applied Mechanics and Materials, 194, pp.472–476. https://doi.org/10.4028/www.scientific.net/AMM.193-194.472.

Tam, V.W.Y. and Tam, C.M., 2008. Diversifying two-stage mixing approach (TSMA) for recycled aggregate concrete: TSMA and TSMA-SC. Construction and

Building Materials, 22(10), pp.2068–2077. https://doi.org/10.1016/j.conbuildmat.2007.07.024.

Tam, V.W., Soomro, M. & Evangelista, A.C.J., 2018. A review of recycled aggregate in concrete applications (2000–2017). Construction and Building Materials, 172, pp.272-292. https://doi.org/10.1016/j.conbuildmat.2018.03.240.

Tang, L. & Nilsson, L. O., 1993. Chloride binding capacity and binding isotherms of OPC pastes and mortars. Cement and Concrete Research, 23(2), pp.247–253. https://doi.org/10.1016/0008-8846(93)90089-R.

Tedjditi, A.K., Ghomari, F., Belarbi, R., Cherif, R. & Boukhelf, F., 2022. Towards Understanding Cork Concrete Behaviour: Impact of Considering Cork Absorption During Mixing Process. Construction and Building Materials, 317, 125905. https://doi.org/10.1016/j.conbuildmat.2021.125905.

Tedjditi, A.K., Ghomari, F., Taleb, O., Belarbi, R. & Tarik, R., 2020. Potential of Using Virgin Cork as Aggregates in Development of New Lightweight Concrete. Construction and Building Materials, 265, 120734. https://doi.org/10.1016/j.conbuildmat.2020.120734.

Teti, A.J., Rodriguez, D.E. & Federici, J.F., 2011. Non-Destructive Measurement of Water Diffusion in Natural Cork Enclosures Using Terahertz Spectroscopy and Imaging. Journal of Infrared, Millimeter, Terahertz Waves, pp. 513–527. https://doi.org/10.1007/s10762-011-9769-6.

Theodosiou, T.G., Papadopoulos, A.M., 2008. The impact of thermal bridges on the energy demand of buildings with double brick wall constructions. Energy and Buildings 40(11), 2083–2089. https://doi.org/10.1016/j.enbuild.2008.06.006.

Toledo, M. & Muñoz., R., Odour prevention strategies in wastewater treatment and composting plants: A review. Journal of Environmental Management, 375, 2025. https://doi.org/10.1016/j.jenvman.2025.124402.

Touil, B., Ghomari, F., Bezzar, A., Khelidj, A. & Bonnet, S., 2017. Effect of temperature on chloride diffusion in saturated concrete. Materials Journal, 114(5), pp.713–721. https://doi.org/10.14359/51688929.

Truc, O. & Ollivier, J.P., 2000. A new way for determining the chloride diffusion coefficient in concrete from steady state migration test. Cement and Concrete Research, 30, pp.217–226. https://doi.org/10.1016/S0008-8846(99)00232-X.

Turk, K., Kina, C. & Nehdi, M.L., 2022. Durability of Engineered Cementitious Composites Incorporating High-Volume Fly Ash and Limestone Powder. Sustainability, 14(16), 10388. https://doi.org/10.3390/su141610388.

Scrivener, K.L., John, V.M. & Gartner, E.M., Eco efficient cements: Potential economically viable solutions for a low CO_2 cement-based materials industry. Cement and Concrete Research, (March 2018). https://doi.org/10.1016/j.cemconres.2018.03.015.

Xiao zhou, S., Lingyan, Z., Shiqian, W. & Yafang, L., 2017. Structural and mechanical properties of cork cell walls from Quercus variabilis Blume. Wood Research, 62(6), pp.873 882.

Younes, A., Elbeltagi, E., Diab, A., Tarsi, G., Saeed, F. and Sangiorgi, C., 2024. Incorporating coarse and fine recycled aggregates into concrete mixes: Mechanical characterization and environmental impact life cycle inventory. Journal of Material Cycles and Waste Management, 26(1), pp.654–668. https://doi.org/10.1007/s10163-023-01834-1.

Zareei, S.A., Ameri, F., Dorostkar, F. & Shahriar S., 2017. Partial Replacement of Limestone and Silica Powder as a Substitution of Cement in Lightweight Aggregate Concrete. Civil Engineering Journal, 3(9), pp. 727–740. https://doi.org/10.21859/cej-03099.

Zhang, M., Yang, Y., Wu, Y., Yu, J., Pang, H., Lv, H., 2025. Effect of limestone powder fineness on the physical and mechanical performance of concrete. Materials 18(4), 835. https://doi.org/10.3390/ma18040835 (MDPI).

Ziregue, A., Krobba, B., Khenfer, M.M., Dheilly, R.-M., Houessou, J. & Queneudec-T'kint, M., 2022. Study of the Physicochemical and Mechanical Compatibility of Expanded Cork with a Cement Matrix Based on Limestone Sand. Epitoanyag-Journal of Silicate Based and Composite Materials, 74(2), pp. 71–76. https://doi.org/10.14382/epitoanyag-jsbcm.2022.12.

Books

Amziane, S. and Collet, F., 2017. Bio-aggregates Based Building Materials: State-of-the-Art Report of the RILEM Technical Committee 236-BBM. Dordrecht: Springer Netherlands. https://doi.org/10.1007/978-94-024-1031-0.

Khan, R.S. and Monteiro, P.J.M., 2011. Supplementary Cementing Materials. Springer Berlin Heidelberg. https://doi.org/10.1007/978-3-642-17866-5.

Mehta, P.K. and Monteiro, P.J.M., 2014. Concrete: Microstructure, Properties, and Materials, 4th ed. McGraw-Hill Education.

Neville, A.M., 2011. Properties of Concrete, 5th ed. Essex, UK: Pearson Education Limited.

Pereira, H., 2007. Cork: Biology, Production and Uses. Elsevier. https://doi.org/10.1016/B978-0-444-52967-1.X5000-6.

Szokolay, S.V., 2004. Introduction to Architectural Science: The Basis of Sustainable Design, 1st ed. Oxford: Architectural Press.

Thesis

Alexandre Ricardo, R.C., 2019. Chemical composition of cork, phloem and xylem of Quercus suber L. from different provenances. Mestre em Engenharia Florestal e dos Recursos Naturais, Instituto Superior d'Agronomia, Universidad de Lisboa, Portugal.

Arsenault, R., 1999. Electrochemical chloride extraction and migration tests for concrete structures. PhD thesis - Université de Sherbrooke, Sherbrooke, QC, Canada.

Gomes, R.F.S.L., 2016. Chemical Characterization and Biological Activity of Cork Sub-Products. Thèse de doctorat - Universidade de Lisboa, Lisbonne, Portugal.

Taleb, O., 2017. Etude du comportement rhéologique des bétons autoplaçants locaux. Thèse de doctorat - Université Aboubakr Belkaïd, Tlemcen, Algérie.

Tedjditi, A.K., 2021. Le béton de liège : Optimisation de la formulation et des performances thermiques. Thèse de doctorat - Université Aboubakr Belkaïd, Tlemcen, Algérie.

Touil, B., 2017. Study the durability of concrete in a marine environment: performant and predictive approach based on durability indicators. Thèse de doctorat - Université Aboubakr Belkaïd, Tlemcen, Algérie.

Standards & Norms

AFNOR NF P 18-598, 1991. Aggregates: Sand Equivalent Test Method. Paris, France : Association Française de Normalisation (AFNOR).

AFPC–AFREM (1997) Durabilité des bétons : méthodes recommandées pour la mesure des grandeurs associées à la durabilité ; compte rendu des journées techniques AFPC-AFREM, Laboratoire matériaux et durabilité des constructions, Institut National des Sciences Appliquées, Université Paul Sabatier, Toulouse. ISBN 2876490226.

AFREM, 1997. Recommendations for Determining the Chloride Diffusion Coefficient of Concrete by the Migration Test. Paris, France: Association Française pour la Recherche et les Essais sur les Matériaux et les Constructions.

ASTM C1585-04, 2004. Standard Test Method for Measurement of Rate of Absorption of Water by Hydraulic-Cement Concretes. West Conshohocken, PA, USA: ASTM International.

ASTM C618-19, 2019. Standard Specification for Coal Fly Ash and Raw or Calcined Natural Pozzolan for Use in Concrete. West Conshohocken, PA: ASTM International.

BS EN 1008, 2002. Mixing Water for Concrete — Specification for Sampling, Testing and Assessing the Suitability of Water, Including Water Recovered from Processes in the Concrete Industry, as Mixing Water for Concrete. London, United Kingdom: British Standards Institution (BSI).

BS EN 1097-3, 1998. Tests for Mechanical and Physical Properties of Aggregates — Part 3: Determination of Loose Bulk Density and Voids. London, United Kingdom: British Standards Institution (BSI).

BS EN 1097-6, 2013. Tests for Mechanical and Physical Properties of Aggregates — Determination of Particle Density and Water Absorption. London, United Kingdom: British Standards Institution (BSI).

BS EN 12350-2, 2009. Testing Fresh Concrete — Part 2: Slump-Test. London, United Kingdom: British Standards Institution (BSI).

BS EN 12390-3, 2009. Testing Hardened Concrete — Part 3: Compressive Strength of Test Specimens. London, United Kingdom: British Standards Institution (BSI).

BS EN 12390-5, 2009. Testing Hardened Concrete — Part 5: Flexural Strength of Test Specimens. London, United Kingdom: British Standards Institution (BSI).

BS EN 12390-7, 2009. Testing Hardened Concrete — Part 7: Density of Hardened Concrete. London, United Kingdom: British Standards Institution (BSI).

BS EN 932-1, 2012. Tests for Geometrical Properties of Aggregates — Part 1: Determination of Particle Size Distribution (Sieving Method). London, United Kingdom: British Standards Institution (BSI).

BS EN 933-1, 2012. Tests for Geometrical Properties of Aggregates — Part 1: Determination of Particle Size Distribution (Sieving Method). London, United Kingdom: British Standards Institution (BSI).

EN 12390-2, 2021. Testing Hardened Concrete — Making and Curing Specimens. Brussels, Belgium: European Committee for Standardization (CEN).

EN 13057, 2001. Products and Systems for the Protection and Repair of Concrete Structures — Test Methods — Determination of Resistance of Concrete to Capillary Absorption. Brussels, Belgium: European Committee for Standardization (CEN).

EN 196-6, 2010. Methods of Testing Cement — Part 6: Determination of Fineness. Brussels, Belgium: European Committee for Standardization (CEN).

EN 197-1:2011, 2011. Cement — Part 1: Composition, Specifications and Conformity Criteria for Common Cements. Brussels: European Committee for Standardization (CEN).

EN 206, 2013. Concrete — Specification, Performance, Production and Conformity. Brussels, Belgium: European Committee for Standardization (CEN).

NA 442, 2013. Composition, Specifications and Conformity Criteria for Common Cements. Algiers, Algeria : Institut Algérien de Normalisation (IANOR).

NF EN 206/CN, 2003. Concrete — Specification, Performance, Production and Conformity — French National Annex. Paris, France : Association Française de Normalisation (AFNOR).

Online sources, reports & institutional publications

ASHRAE, 2021. ASHRAE Handbook—Fundamentals. Atlanta, GA: American Society of Heating, Refrigerating and Air-Conditioning Engineers. Available at: https://www.ashrae.org/technical-resources/ashrae-handbook/description-2021-ashrae-handbook-fundamentals.

APCOR (Associação Portuguesa da Cortiça), 2015. Boletim Estatístico 2015. Santa Maria de Lamas, Portugal. Available at : https://apcor.pt/pt/pesquisa?p=Boletim+Estat%C3%ADstico+2015

CSI (Cement Sustainability Initiative), 2018. Global Cement Database on CO_2 and Energy Information. Available at: https://www.wbcsd.org/Sector-Projects/Cement-Sustainability-Initiative/Resources/Global-Cement-Database-on-CO2-and-Energy-Information.

Environmental Protection Agency (EPA), 2021. Portland Cement Manufacturing Industry Profile. Washington, U.S. Available at: https://www.epa.gov/stationary-sources-air-pollution/portland-cement-manufacturing-industry-national-emission-standards.

European Commission, 2020. EU Construction and Demolition Waste Management Protocol. Brussels: European Commission. Available at: https://ec.europa.eu/docsroom/documents/20509.

Gibson, L.J., 2016. Cork: Structure, Properties, Applications. Arnold Arboretum, Harvard University. Available at: https://arboretum.harvard.edu/stories/cork-structure-properties-applications/.

Global Cement and Concrete Association (GCCA), 2021. Concrete Future: The GCCA 2050 Roadmap for Net Zero Concrete. London: Global Cement and Concrete Association. https://gccassociation.org/concretefuture/

Hammond, G.P. & Jones, C.I., 2011. Inventory of Carbon & Energy (ICE) database, Sustainable Energy Research Team, Department of Mechanical Engineering, University of Bath, UK. Available at: https://kps.fsv.cvut.cz/upload/files/icev2.0summarytables.pdf.

IEA (International Energy Agency), 2018. Technology Roadmap: Low-Carbon Transition in the Cement Industry. Available at: https://www.iea.org/reports/technology-roadmap-low-carbon-transition-in-the-cement-industry.

International Energy Agency (IEA), 2020. Energy Technology Perspectives 2020: Special Report on CCUS. Paris: IEA. Available at: https://www.iea.org/reports/energy-technology-perspectives-2020-special-report-on-ccus.

MECD, 2025. Matériaux biosourcés : innovations et perspectives pour la construction durable – Replay webinaire MECD du 6 novembre. Available at: https://www.youtube.com/watch?v=MUCDqpc-qd4.

Portland Cement Association (PCA), 2021. Design and Control of Concrete Mixtures. 17th ed. Skokie, Illinois: Portland Cement Association. https://www.cement.org/intelligence-resources/store/design-control-of-concrete-mixtures/?utm.

RE2020, Decret No. 2021-19 of January 11, 2021 relating to the environmental regulation RE2020, French Republic. Available at: https://www.ecologie.gouv.fr/reglementation-environnementale-re2020.

Reddit, 2021. Cork production/distribution of cork oak (thread). Available at: https://www.reddit.com/r/MapPorn/comments/gjygvr/cork_production_distribution_of_cork_oak/.

SPHERE Project, 2021. Integrated Life Cycle Assessment of Concrete Structures. Available at: https://sphere-project.eu/integrated-life-cycle-assessment-of-concrete-structures/.

Volume Concrete, 2025. Worldwide cement consumption: An in-depth survey. Available at: https://volumeconcrete.com/worldwide-cement-consumption/

WBCSD (World Business Council for Sustainable Development) – Cement Sustainability Initiative (CSI), 2018. Low-Carbon Transition in the Cement Industry. https://doi.org/10.1787/9789264300248-en.